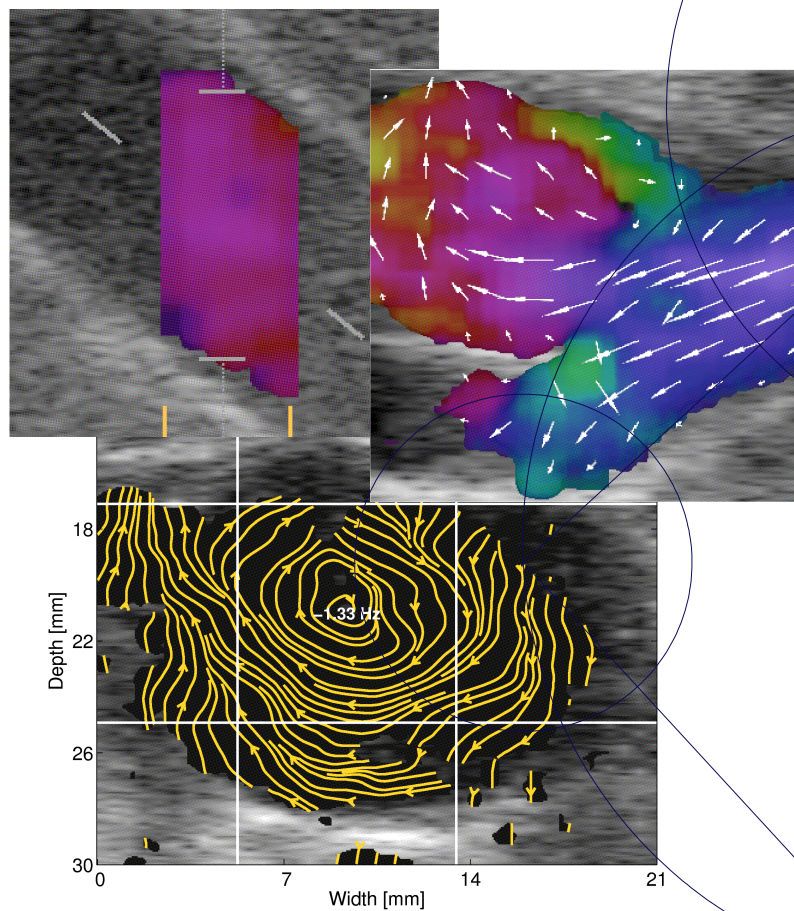


Quantification of *In Vivo* 2D Vector Flow Ultrasound



Ph.D. thesis
Mads Møller Pedersen, M.D.
Department of Radiology
Copenhagen University Hospital, Rigshospitalet
Denmark

© **Mads Møller Pedersen, 2011**

All rights reserved. No part of this publication may be reproduced or transmitted, in any form or by any means, without permission.

Copenhagen University Hospital, Rigshospitalet
Department of Radiology
DK-2100 Copenhagen
Denmark

Submitted in partial fulfillment of the requirements for the degree of Doctor of Philosophy at
Copenhagen University, Denmark.

Main supervisor

Michael Bachmann Nielsen, M.D., Ph.D., Dr.Med, Professor
Department of Radiology
Copenhagen University Hospital, Rigshospitalet, Denmark

Project supervisor

Jørgen Arendt Jensen, M.Sc., Ph.D., Dr.Techn., Professor
DTU Elektro, Building 349, Room 222
Technical University of Denmark, Denmark.

Evaluating committeeChairman

Liselotte Højgaard, M.D., Dr.Med., Professor
Department of Clinical Physiology and Nuclear Medicine and PET
Copenhagen University Hospital, Rigshospitalet, Denmark

External examiner

Patrick Segers, Civ Eng, PhD, Professor
The Institute for Biomedical Technology
Ghent University, Gent, Belgium.

External examiner

Ola Björgell, M.D., Dr.Med., Docent
Department of Radiology
Universitetssjukhuset MAS, 205 02 Malmö, Sweeden

Front page illustration: Simultaneous spectral and vector data acquisition (top left), the complex flow pattern of the carotid bulb (right), and the secondary flow pattern in the cross-sectional plane of the abdominal aorta (bottom).

Preface

This Ph.D. dissertation has been submitted to University of Copenhagen, Denmark to achieve the degree of Doctor of Philosophy.

The work was carried out from June 1st, 2009 to November, 2011 at the Department of Radiology at Copenhagen University Hospital, Rigshospital and the Center for Fast Ultrasound Imaging at the Technical University of Denmark in Lyngby. It resulted in three journal papers, three conference papers, five oral presentations, and two poster presentations.

The work has given me the opportunity to add a new, technical dimension to my existing medical experience resulting in new abilities to process and image ultrasound data.

During the past three years the projects have brought me around the world including Beijing, Rome, Vienna, Vallencia, San Diego, and Orlando. I have enjoyed working with engineers and physicists and have had great help in their enthusiasm to teach me how to process and plot data.

I also got the opportunity to teach students in medicine, medico technology, and human biology about the basic principles in medical ultrasound and X-ray computed tomography. As reviewer, chairman and webmaster, I have also been involved in other areas of ultrasound science. Furthermore, I have been able to assist three other phd-students with access and data processing of magnetic resonance scanning. These projects are present in the data processing phase and are expected to result in several journal papers within the next year.

Mads Møller Pedersen
Copenhagen, October 2011

Acknowledgements

I would like to thank my supervisors, Professor Michael Bachmann Nielsen from Copenhagen University and Professor Jørgen Arendt Jensen from the Technical University of Denmark for giving me the opportunity to collaborate with engineers and physicists and learn about the new techniques within ultrasound. Without my supervisors patience and the collaboration with DTU, this dissertation would not have been possible. From the beginning of the project I was helped by Kristoffer Lindskov Hansen whos creative mind has influenced most of my work. At DTU I have enjoyed the support from Michael Johannes Pihl, Marie Sand Enevoldsen, Jens Munk Hansen, and Henrik Laursen.

A great thanks to Paul Nilsson, Head of the Department of Radiology at Copenhagen University Hospital, for his support from the second I entered the department. I would also like to thank Linda Schumann and Elna Sørensen and all volunteers at both departments for their help. At B-K Medical A/S Per Haugaard has provided essential knowledge on the scanner setup and data processing and at the Department of Biostatistics, University of Copenhagen, Denmark, Theis Lange provided statistical assistance. All post processing has been performed with the program Matlab, which the colleagues at DTU kindly have tough me to use.

Dansk resumé

Denne phd har undersøgt nye anvendelser af en ny metode til at måle blodets bevægelser. Metoden, der tidligere kun har været tilgængelig på eksperimentelle skannere på DTU, er blevet implementeret i en kommerciel ultralydskanner, som er bygget til anvendelse i hospitalsmiljøet. Grundlæggende kan vektormetoden måle blodets bevægelser i et 2D vektor felt - også når det løber vinkelret på ultralydsbølgen. Det er konventionelle metoder ikke i stand til.

Afhandlingen omfatter tre studier med vector flow målinger på raske frivillige. Med studie I blev *a. carotis communis* på 16 raske frivillige personer skannet med simultan måling af blodets hastighed med vektor teknikken og den konventionelle teknik, spektral estimation. Studiet sammenlignede de følgende kliniske parametre: Peak systole hastigheder, slut diastoliske hastigheder, resistive index og blodets retning. Studiet viste, at hastighederne samt resistive index var signifikant forskellige. Den gennemsnitlige retning af blodet stemte overens for de to metoder. Da den konventionelle teknik anvender operatørens manuelle indstilling af vinklen, er det primære budskab med studiet, at det med vector flow vil være muligt at erstatte den manuelle vinkel indstilling med en automatisk vinkelberegning ved hjælp af vector flow metoden.

I studie II blev 8 frivillige raske personer skannet over carotis bifurkaturen, herunder *bulbus caroticus* og *a. carotis communis*. I samtlige optagelser blev *bulbus caroticus* og *carotis communis* indtegnet. Hvert billede blev forevist ialt 5 erfarne radiologer individuelt for at evaluere tilstedeværelsen af et komplekst flowmønster. Vektor data fra de samme områder blev anvendt til at beregne kompleksiteten i form af vektor koncentrationen, der er præsenteret inden for cirkulær statistik. Denne beregning blev sammenholdt med den visuelle evaluering. Resultatet viste, at den visuelle evaluering stemte statistisk overens med den beregnede værdi for kompleksitet. Således har studiet præsenteret en ny metode til at kvantitere komplekst flow med vector flow ultralyd.

Med studie III blev det roterende flowmønster i tre arterier visualiseret og kvantiteret med vektor data for første gang. Fem raske frivillige blev alle skannet på tre arterier: *Carotis communis*, *aorta abdominalis* og *a. iliaca communis*. Vektorerne for ni op-

tagelser blev anvendt til at tegne flowlinjer, der viser blodets mønster og retning. Desuden blev rotations frekvensen af synlige rotationer beregnet og vist. Resultaterne viste, at rotationsregningen i diastolen er ensartet for hver af de tre arterier. Udvidede målinger på aorta abdominalis viste desuden at blodet under systolen roterer mod uret, hvorefter det i diastolen skifter til at rotere med uret. Observationer, der tidligere har krævet magnetisk resonans eller eksperimentel ultralydskanning for at kunne måles.

Denne afhandling viser med de tre studier, at vektor metodens implementering i en kommerciel ultralydskanner er i stand til at måle og kvantitere blodets bevægelser, som ikke er vist tidligere.

Abstract

This PhD thesis has investigated the use of a new ultrasound technique that to measure the movement of blood. The technique was developed at the Center for Fast Ultrasound Imaging at the Technical University of Denmark and has previously only been available with experimental ultrasound scanners. Now, the method has been implemented into a commercial ultrasound scanner made for hospital use. In real-time, the technique measures movements in all directions as 2D vector fields, including movements perpendicular to the ultrasound beam. This is not available with conventional ultrasound scanners today.

The thesis consists of three studies that uses vector flow ultrasound measurements on healthy volunteers. In study I the common carotid artery of 16 healthy volunteers were scanned simultaneously with the vector technique and the conventional, spectral estimation method. The study compared the clinical parameters: peak systole velocity, end diastole velocity, resistive index, and the flow direction. The results showed significant difference on the velocities and the resistive index. However, no significant difference on the manually defined flow angle and the calculated mean flow angle by the vector technique. With the conventional technique, the manual setting of the angle is operator dependent. With the calculated vector angle, this operator is relieved from the angle setting and the measurement is angle corrected by the identical method every time.

With study II the carotid bifurcation including the carotid bulb and the common carotid artery were scanned on 8 healthy volunteers. The flow patterns of the two structures were outlined and presented to each of 5 experienced radiologists. The complexity of the identical areas were calculated by the vector concentration and compared to the visual evaluations. No significant difference was found between the two methods which were equally good at discriminating the laminar flow of the common carotid artery from the complex flow in the carotid bulb. Thus, a new method was presented to quantify complex flow patterns with vector flow.

The final study III presented the rotational flow patterns in the cross-sectional plane of three arteries: The common carotid artery, the abdominal aorta, and the common iliac

artery. Five healthy volunteers were included in the study and nine datasets visualized the flow patterns during the diastole. The rotational frequency was calculated and the results indicate a constant direction of the rotation for each artery. Extended measurements on the abdominal aorta showed a two-directional rotation during the cardiac cycle. An observation that corresponds to previous MR and Doppler studies.

With the three studies, this thesis presents new methods that quantifies *in vivo* vector flow obtained in real-time with a new implementation.

List of papers

Comparison of real-time in-vivo spectral and vector velocity estimation

Mads Møller Pedersen, Michael Johannes Pihl, Per Haugaard, Jens Munk Hansen, Kristoffer Lindskov Hansen, Michael Bachmann Nielsen and Jørgen Arendt Jensen.

Ultrasound in Med. Biol., Vol. 38, No. 1, pp. 145–151, 2012

Included in appendix 1.

Novel flow quantification of the carotid bulb and the common carotid artery with vector flow ultrasound

Mads Møller Pedersen, Michael Johannes Pihl, Per Haugaard, Kristoffer Lindskov Hansen, Theis Lange, Lars Lönn, Michael Bachmann Nielsen and Jørgen Arendt Jensen.

Submitted

Included in appendix 2.

Rotational flow patterns in the arterial blood stream with vector flow ultrasound

Mads Møller Pedersen, Michael Johannes Pihl, Jens Munk Hansen, Peter Møller Hansen, Per Haugaard, Michael Bachmann Nielsen and Jørgen Arendt Jensen.

Submitted

Included in appendix 3.

Abbreviations

AA	Abdominal aorta
AVI	Audio Video Interleaved
CCA	Common carotid artery
CFD	Computational fluid dynamics
CFU	Center for Fast Ultrasound Imaging, Department of Electrical Engineering, DTU
CIA	Common iliac artery
DTU	Technical University of Denmark
ED	End diastole
MRI	Magnetic Resonance Imaging
PIV	Particle-image velocimetry
PRF	Pulse Repetition Frequency
PS	Peak systole
PW	Plane wave
RASMUS	Remotely Accessible Software configurable Multi-channel Ultrasound Sampling
RI	Resistive index
TO	Transverse Oscillation
WSS	Wall-shear-stress

CONTENTS

Preface

Acknowledgement

Dansk resumé

Abstract

List of papers

Abbreviations

1	Introduction and background	1
1.1	Velocity estimation	3
1.2	Complex flow	6
1.3	Secondary flow	9
2	Study aims	11
3	Materials, methods and results	13
3.1	Study I	15
3.2	Study II	18
3.3	Study III	22
4	Discussion	27
4.1	Study I - blood velocity estimation	28
4.2	Study II - complex flow patterns	31
4.3	Study III - rotational flow patterns	34
5	Conclusion	37
6	Perspectives	39
	Bibliography	41
	Appendix 1: Journal paper I	47
	Appendix 2: Journal paper II	57
	Appendix 3: Journal paper III	77

Introduction and background

This thesis is the result of the collaboration between the Department of Radiology at Copenhagen University Hospital, Rigshospitalet, and the Center for Fast Ultrasound Imaging (CFU) at the Technical University of Denmark (DTU).

The thesis consists of three studies based on measurements by the vector technique, Transverse Oscillation (TO), implemented in a new commercial ultrasound scanner. The technique was developed at CFU [1–5] and has been tested in simulation [6], by in-vivo studies with the experimental ultrasound scanner RASMUS [7], and in comparison with magnetic resonance (MR) angiography [8].

With the new implementation it was possible to perform faster, real-time measurements in a hospital environment for the first time. All scannings were performed on healthy, young volunteers, all colleagues and friends, after informed consent. The movements of the blood in the human arteries were measured as vectors and compared to conventional techniques. The conventional Doppler based techniques can only measure movements towards and away from the surface of the ultrasound transducer thus, only obtain the data as a scalar, not a vector.

Blood velocity and flow direction of the common carotid artery have been measured with the new method and compared to the conventional spectral estimation method [9]. The disturbed flow patterns in the carotid bulb (CB) have been compared to the laminar flow patterns in the common carotid artery (CCA) with visual and quantitative measures [10]. Finally the secondary flow patterns in the transverse plane of three main arteries have been visualised and quantified by angular frequencies [11].

Along with the primary studies, I have enjoyed to participate in the following studies:
Hansen KL, Pedersen MM, Jensen JA, Nielsen MB. Praktisk guide til Doppler ultralydskanning med eksempler fra abdomen, *Danish Medical bulletin*, 2011, Accepted for publication, august 2011.

Hemmsen MC, Svetoslav N, Pedersen MM, Pihl MJ, Enevoldsen MS, Hansen JM, Jensen JA. Implementation of a versatile research data acquisition system using a commercially available medical ultrasound scanner, *Transactions on Ultrasonics, Ferroelectrics, and Frequency Control*, Accepted for publication, 2011.

Hansen PM, Pedersen MM, Hansen KL, Nielsen MB, Jensen JA. Demonstration of a Vector Velocity Technique, *Ultraschall in der Medizin*, vol: 32(2), p. 213-215 (2011).

Hansen KL, Gran F, Pedersen MM, Holfort IK, Jensen JA, Nielsen MB. In-vivo Validation of Fast Spectral Velocity Estimation Techniques, *Ultrasonics*, vol: 50(1), p. 52-59 (2010).

Andresen H, Nikolov S, Pedersen MM, Buckton D, Jensen JA. Three-Dimensional Synthetic Aperture Focusing Using a Rocking Convex Array Transducer, *IEEE Transactions on Ultrasonics, Ferroelectrics and Frequency Control*, vol: 57(5), p. 1051-1063 (2010).

Vector flow ultrasound

The vector flow technique, Transverse Oscillation (TO), has been investigated thoroughly since the first presentations in 1996 [1–3, 5]. The method has been tested in simulation [6], by *in vivo* studies with the experimental scanner, RASMUS [7], and in comparison with magnetic resonance (MR) angiography [8]. In contrast to conventional Doppler techniques, TO directly provides the absolute velocities and flow angles of blood at any angle in a 2D vector field. The method is non-invasive, as it does not require contrast agents. The main purpose of this thesis is to investigate how to use the vector method in a clinical setting and how to quantify the vector data.

1.1 Velocity estimation

Spectral velocity estimation

Measurements of the blood velocities are widely used clinically [12, 13]. With the conventional method, spectral velocity estimation, the axial velocity in the direction along the ultrasound beams, v_z , is obtained [14, 15].



Figure 1.1: *Triplex mode combines b-mode imaging, color Doppler, and spectral estimation. (a) The portal vein including real-time calculations of peak systole and end diastole with an angle correction of 45°. (b) Peak systole, end diastole, and resistive index calculations on an interlobar artery in the right kidney. The triplex mode decreases the frame rate compared to simple b-mode imaging.*

The peak systole (PS) velocity, end diastole (ED) velocity, and the resistive index (RI) are used to diagnose several haemodynamic diseases. In renal artery stenosis, both PS and RI are increased and the spectrogram waveform is changed [16, 17]. Two examples

of clinical measurements of the portal vein in the liver and an interlobar artery in the kidney are shown in Fig. 1.1. The spectral estimation is also used to diagnose pulmonary hypertension [18], restrictive liver conditions [19, 20], pressure gradients of the aortic valve [21, 22], increased resistance in the umbilical artery [23] etc. Most clinical measurements are performed on blood vessels where the blood is not flowing at an angle of zero, directly along the ultrasound beam [24]. Thus, the estimated axial velocity, v_z , does not represent the true velocity, v , and the direction of the true flow must be accounted for with angle correction:

$$|v| = \frac{v_z}{\cos \theta} = \frac{f_p c}{2f_0 \cos \theta}, \quad (1.1)$$

where θ is the flow angle between the ultrasound beam and the blood velocity direction, f_p is the estimated frequency, f_0 is the center frequency of the emitted ultrasound pulse, and c is the speed of sound [14]. The axial velocity is obtained in the range gate area, and it is assumed that the blood in this area flows in one direction all the time. Thus, no spatial velocity details are available. For clinical use, a flow angle of $[0\ 60]^\circ$ is accepted, whereas the error of the angle corrected velocity is too large $>60^\circ$ [25] and at an angle of 90° the velocity is not available as $\cos(90) = 0$. This is illustrated in Fig. 1.2, where no signal is obtained in the central part of the abdominal aorta.

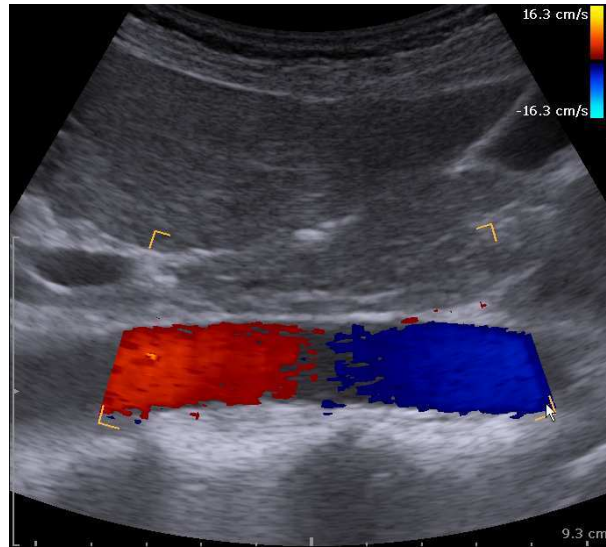


Figure 1.2: *Conventional color Doppler ultrasound imposed on a b-mode image of the abdominal aorta in the longitudinal plane. There is no signal from the area in the center where the flow is directed perpendicular to the ultrasound beam ($\theta=90^\circ$).*

This angle limitation of 60° restricts the clinical use of the spectral velocity estimation [26]. To compensate for this limitation the transducer and the ultrasound beam can be

tilted. However, this requires that the blood flows in one direction and is not disturbed or rotating.

In many clinical settings the blood vessel of interest is not directed at an angle of [0 60] towards the surface of the skin but rather runs along the skin surface. Tilting of the transducer and tilting of the ultrasound beam can compensate sufficiently in many situations. With vector flow the axial and transverse vector velocity components are directly

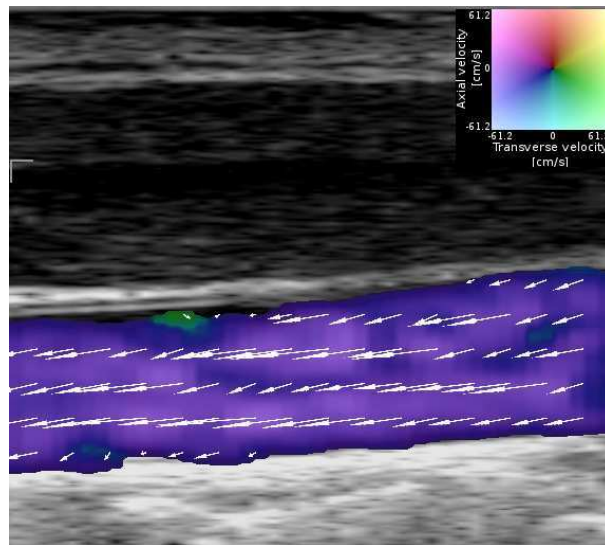


Figure 1.3: *Vector flow imaging of the common carotid artery with no tilting of the beam or the transducer at 90°. The vector information is clearly measuring the velocity and direction of the blood through the entire diameter, providing both spatial and temporal vector information in real-time.*

available and thus, detailed velocity and flow angle information can be measured at any angle as illustrated in Fig. 1.3. Thus, no angle correction is needed and new spatial information over the entire vessel lumen is available.

1.2 Complex flow

Atherosclerosis is a leading cause of health problems worldwide and changes in the carotid arteries are associated with an increased risk of stroke. The changes are primarily found at bends and bifurcations and during the initial plaque development the artery is enlarged to maintain the flow [27]. Disturbed blood flow has also been shown to initiate the arterial inflammatory response [28] and the development of atherosclerosis has been related to the vortex formation in the carotid bifurcation [29–32]. Thus, the morphology and classification of stenosis in the carotid bulb has been investigated to predict the risk of a future stroke. Kassam et al. found that the peak Doppler frequency and spectral broadening index is correlated to the degree of carotid stenosis [33] and complex flow changes analyzed with Doppler have been found at the carotid bulb [34]. The stenosis classification uses velocity estimates of the common carotid artery [35]. However, no conventional method is able to quantify the complex flow in the carotid bulb. In this thesis a disturbed flow pattern is defined as a more than 90 degree change

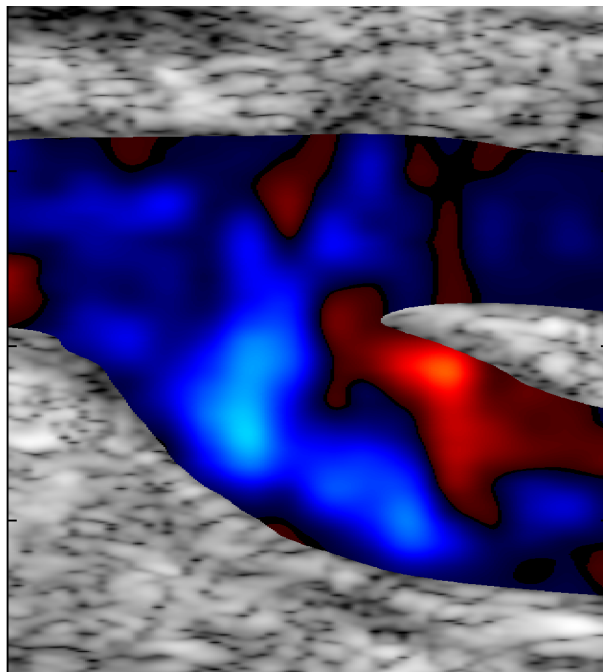


Figure 1.4: *Ultrasound scanning with conventional color flow mapping of the carotid bifurcation. The complex flow in the carotid bulb (bottom right) is visible, however, not quantified.*

in vector angle in part of the cardiac cycle. With conventional ultrasound methods these complex flow patterns are visible but not quantifiable. Complex flow patterns are visible with color flow mapping where a mixture of colors indicate a mixture of velocities and

directions as illustrated in Fig. 1.4. The flow patterns of the common carotid artery and the carotid bulb have long been investigated as the bifurcation is one of the most frequent sites for cerebrovascular disease occurrence [36–39]. The carotid artery intima media thickness measured by ultrasound has proven to be a risk marker for preclinical atherosclerosis and can identify incident cardiovascular disease. Especially areas with low shear stress compared to areas of high shear stress [40].

Conventional ultrasound measurements of complex flow patterns are not able to obtain all velocities, because velocities at flow directions around 90° are not obtained. Thus, visualization and quantification of the flow complexity are not available with conventional ultrasound systems and therefore, the complexity is not used for clinical diagnosis or prognosis. Previous studies with the vector flow ultrasound technique have demon-

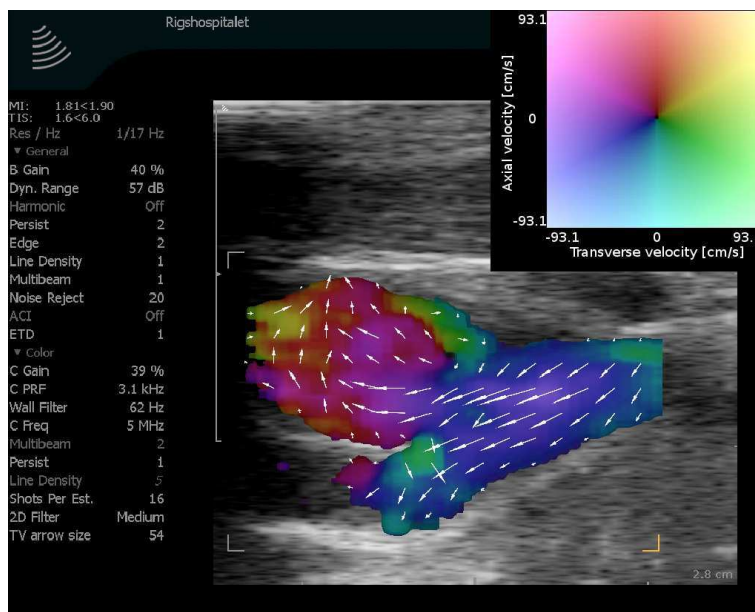


Figure 1.5: *Ultrasound scanning with vector flow of the carotid bifurcation. The complex flow in the carotid bulb (top left) is visible and detailed vector information can be used to quantify the complexity of the flow.*

strated the vortex formation in CB during systole [7, 8, 41, 42] and this was also demonstrated with the experimental ultrasound vector method, Plane Wave [43].

The new implementation of the TO visualizes the complex flow with white vectors indicating the velocity magnitude and direction during the cardiac cycle in real-time. Thus, the laminar flow pattern of the common carotid artery, and the complex flow pattern of the carotid bulb can be visualised in real-time. The data is also available as 2D vector fields, and post processing of the flow complexity can be performed. Visual evaluation of the flow patterns can be performed and compared to a simple calculation of the

flow complexity and a threshold value that separates the flow patterns of the common carotid artery from the carotid bulb can be found. With such quantitative method, further development of an objective measure of complexity in correlation with the degree of cardiovascular disease is possible.

1.3 Secondary flow

The blood movements in the arteries during the cardiac cycle can be described as a simple, parabolic shape. However, as the arteries bend and twist, minor flow patterns in different directions occur. These secondary flow patterns have previously been investigated with the Doppler based technique [44–47], magnetic resonance (MR) [48–50] and with particle-image velocimetry (PIV) using micro bubbles as contrast agent [51–53]. However, the Doppler method does not obtain the flow data perpendicular to the ultrasound beam, the MR technique requires several minutes of data acquisition, and the PIV technique is not yet implemented for in-hospital use.

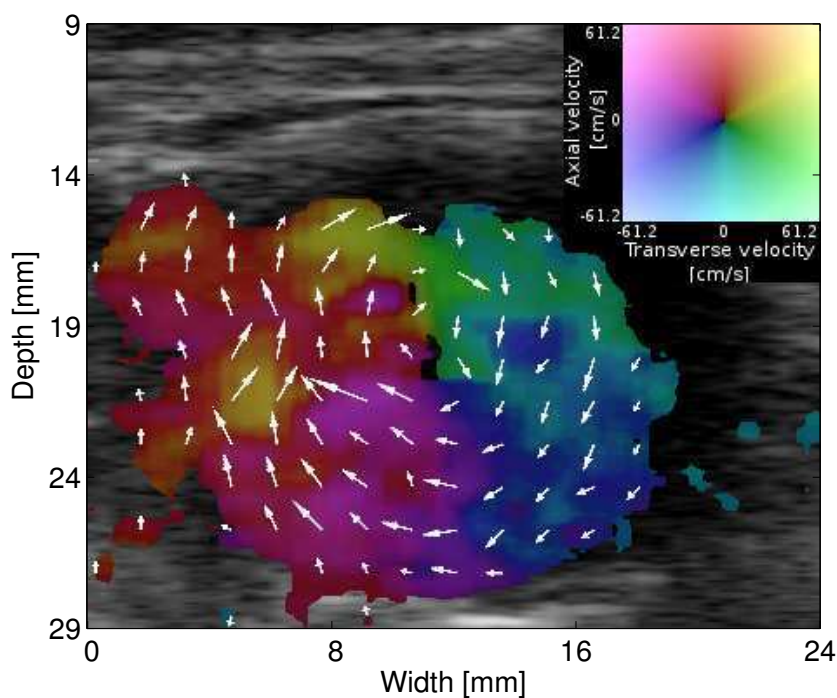


Figure 1.6: *Real-time, in vivo vector flow ultrasound image of the abdominal aorta in the cross-sectional plane. The vector velocity color map is shown in the upper right corner.*

Previous studies have indicated that rotational flow patterns may play a role in the pathogenesis of atherosclerosis [39, 54, 55] and with the vector flow ultrasound scanner it is possible to visualize these flow patterns. The blood velocities of all directions are obtained and result in 2D vector fields, that can be used to quantify the flow pattern. Such method has the potential of a new diagnostic and prognostic cardiovascular tool for the aorta aneurysms, hypertension etc. The calculation of the rotational frequency [56] and the wall shear stress [57–60] are examples of physical forces that are possible to calcu-

late for a 2D vector field. With streamlines the flow can be visualized and the rotational frequencies can be calculated from real-time *in vivo* vector flow data as shown in Fig. 1.7.

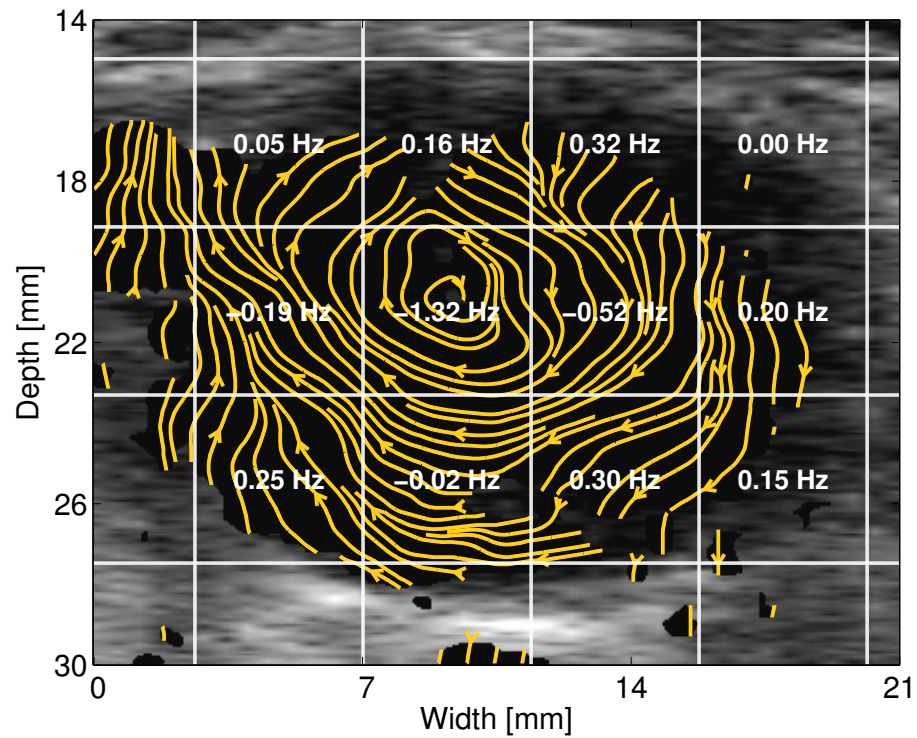


Figure 1.7: *Cross-sectional vector ultrasound of the abdominal aorta where the flow pattern is visualized with streamlines and the rotational frequencies are calculated in a grid centered over the rotation center.*

Study aims

In study I the velocity and direction of blood in the common carotid arteries were measured with spectral velocity estimation and vector flow ultrasound. The scanner was able to obtain the data for both methods simultaneously. The widely used clinical parameters, peak systole velocity, end diastole velocity, resistive index, and the flow angle were compared. The aim of this study was to validate the vector method with the conventional spectral approach.

Study II investigated the vector methods ability to visualize the laminar flow pattern of the common carotid artery and the complex flow pattern in the carotid bulb. The flow patterns were visually evaluated for the presence of disturbed flow by expert radiologists. With the expert evaluations as reference, a quantitative vector method, the vector concentration, was calculated. The aim of the study was to validate the quantitative calculation with the visual evaluation.

With study III the secondary flow patterns in the cross-sectional plane of three main arteries were measured with the vector flow method. The rotational flow patterns were visualized with streamlines and the rotational frequency of the flow was calculated in subareas of the vessel lumen. The results were imposed on the streamline plot and suggested as a useful visualization for clinical use in future scanner editions. The aim of the study was to introduce the rotational frequency calculation in combination with streamline visualization.

Materials, methods and results

This thesis includes three studies using a new vector flow ultrasound scanner. For all studies presented in appendices I-III the new vector flow ultrasound scanner was used (Profocus Ultraview, BK Medical, Denmark) with a 5 MHz linear array (type: 8670, BK Medical, Denmark) and prototype scanner software. These studies were the first to present data from the new scanner.

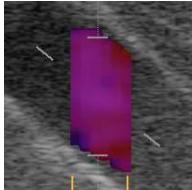
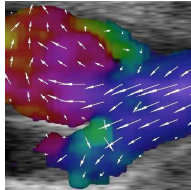
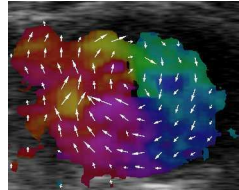
Study no.	I	II	III
Volunteers	N=16	N=8	N=9
			
Anatomical area	Common carotid artery	Carotid bifurcation	Three main arteries
Target of evaluation	Velocity and angle	Complex flow	Rotational flow
Reference method	Spectral estimation	Visual evaluation	MR, Doppler, PIV

Table 3.1: Overview of the main content of the three studies.

For study I the common carotid artery of 16 healthy volunteers were scanned in the longitudinal plane in a scanner mode allowing interleaved data acquisition of the conventional spectral method and the new vector method. In study II the common carotid artery and the carotid bulb were imaged in the same data set and the different flow patterns of the two anatomical areas were analyzed visually and quantitatively. In study III the cross-sectional plane of three arteries were scanned with vector flow to visualize and quantify the secondary, rotational flow pattern during the cardiac cycle. Earlier work with Doppler ultrasound [44], MR[48, 59, 60], and PIV [53, 61, 62] describing the flow patterns were used for comparison.

Vector data conversion

Vector data was obtained as AVI files where the vector data was color encoded using a circular color map as illustrated in Fig. 3.1.

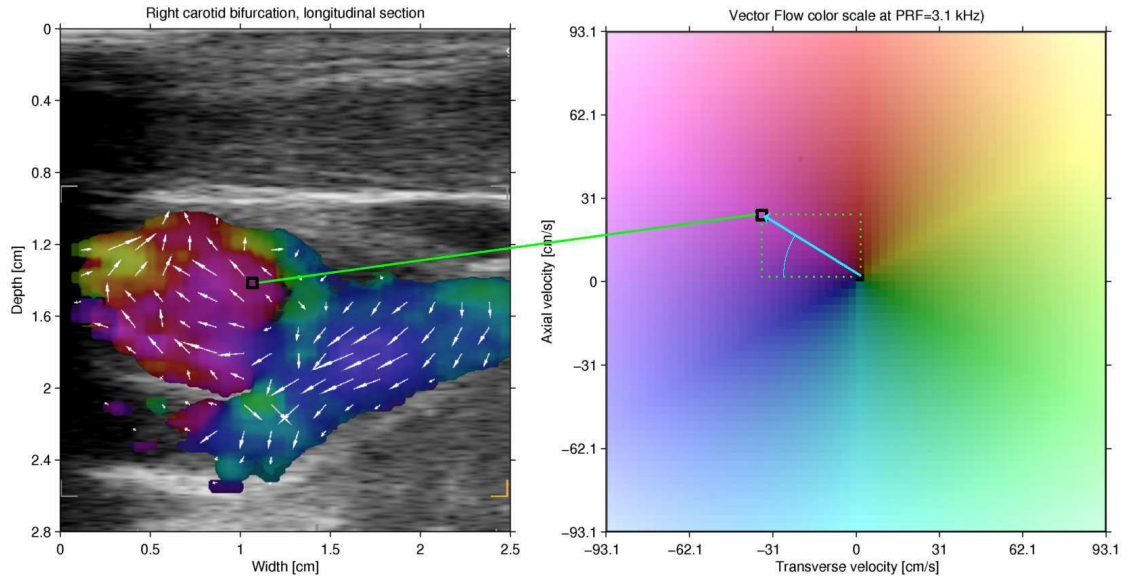


Figure 3.1: *Vector color image frame of the carotid bifurcation (left), and the circular color map used for decoding the vector data.*

With an in-house Matlab (Mathworks, Natick, MA, USA) script, the vector information of each pixel in a vector image frame was decoded into vector data in a 2D vector field consisting of the axial velocities, v_z , and transverse velocities, v_x . Using Pythagoras' theorem, the true velocity magnitude, $|v|$, and the flow direction, θ , were calculated for each colored pixel in every frame by:

$$|v| = \sqrt{v_x^2 + v_z^2}. \quad (3.1)$$

$$\theta = \arctan(v_x, v_z) \quad (3.2)$$

3.1 Study I

Comparison of real-time in-vivo spectral and vector velocity estimation

Further details are found in appendix 1

Aim

The aim of the study was to investigate whether the flow angle, velocity estimations and resistive index are estimated equally well for two methods: Conventional spectral velocity estimation and vector flow.

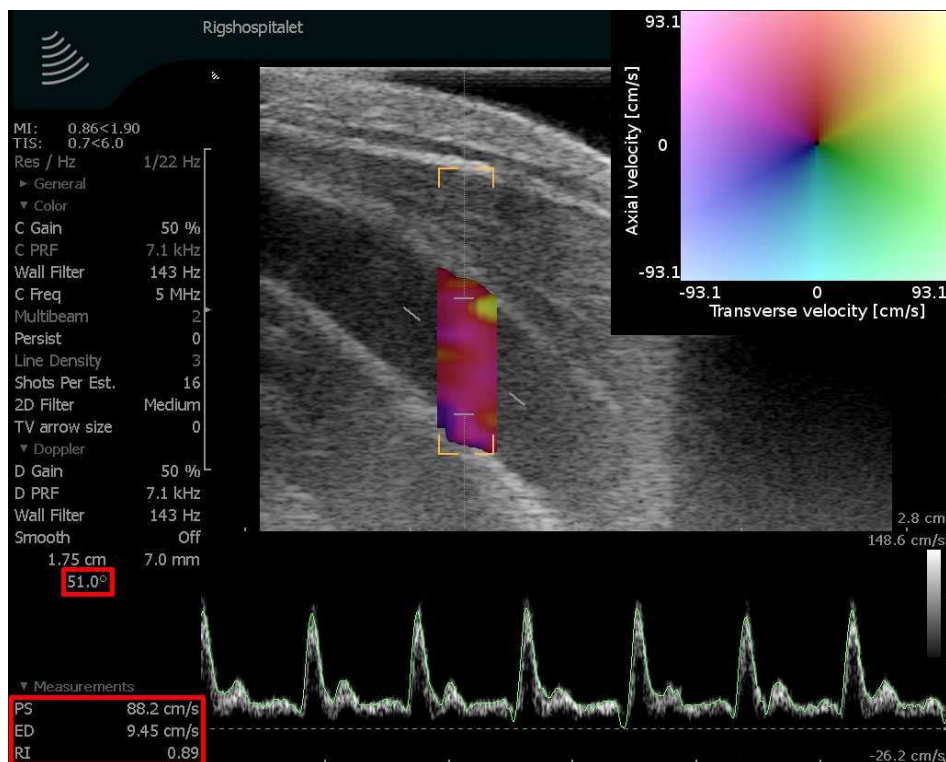


Figure 3.2: *Ultrasound image frame showing the longitudinal ultrasound scanning of the right common carotid artery with interleaved spectral velocity estimation and vector flow.*

Materials and methods

For this study the common carotid artery was scanned at an angle $<60^\circ$ by tilting the transducer. The setting allowed interleaved measurements of spectral velocity estima-

tion and vector flow data as shown in Fig. 3.2. With the optimal setting for the conventional method, 16 healthy volunteers were scanned on the right common carotid arteries. For each volunteer 11.2 s of data was obtained with a frame rate of 14.8 frames per second.

The vector information provided the axial velocity component and the transverse velocity component for each pixel in the image and the flow angle and 'true' velocity was calculated. For each image frame a 2D vector field was produced for the central half of the range gate area and for each vector field, the maximum velocity was calculated. With in-house software the peak systole and the end diastole was tracked as shown in Fig. 3.3 and the resistive index was calculated using PS and ED [63].

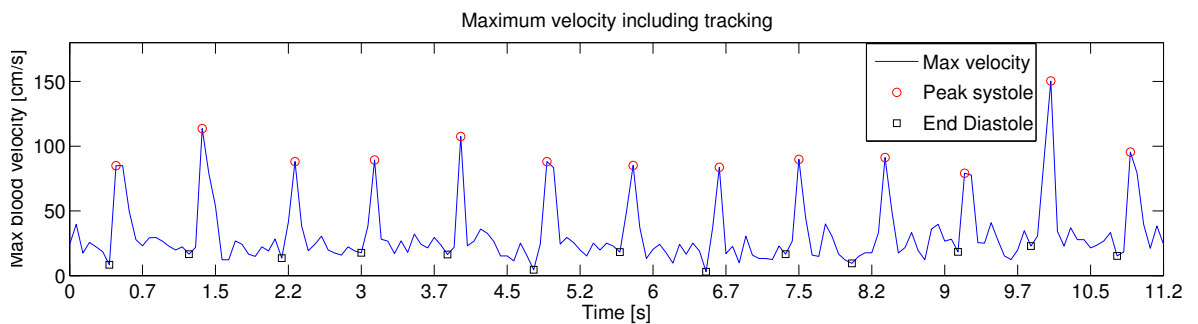


Figure 3.3: One data set showing the maximum velocities as a function of time. The peak velocities and the lowest velocities prior a peak was tracked with in-house software.

The following parameters were calculated for each volunteer:

- mean peak systole vector velocity
- mean end diastole vector velocity
- resistive index
- mean vector flow angle

These parameters were compared to the spectral estimation parameters: peak systole, end diastole, resistive index and the manually set flow angle.

Statistical analysis

Using a paired t -test, and Bland-Altman plots [64], the spectral estimation method and the vector method were compared for each parameter. The null-hypothesis tested with the paired t -test states that the mean difference between the two methods does not differ from a normal distribution with a mean of zero. For each parameter the

p-value, the confidence interval at 95% significance level, and the standard deviation were calculated. $p < 0.05$ was considered significant, meaning that the two methods differ significantly. The deviation between the two methods, the vector difference, were calculated for each parameter as

$$dif_{vector} = \left(1 - \frac{v_{vector}}{v_{spectral}}\right) \cdot 100, \quad (3.3)$$

where v_{vector} is the vector velocity, and $v_{spectral}$ is the spectral velocity.

Results

Parameter	Angle	PS	ED	RI
p	0.658	0.034*	0.0004*	< 0.0001*
Confidence interval	[-0.2 4.4]°	[0.6 13.3] cm/s	[-4.9 -1.7] cm/s	[0.06 0.12]
Std of the difference	6.26°	17.64 cm/s	4.55 cm/s	0.07

Table 3.2: Paired *t*-test of the hypothesis that the spectral and vector data came from the same distribution. Each parameter was tested and a $p < 0.05$ was considered significant and marked with *.

The flow angle did not differ significantly for the two methods ($p=0.66$), whereas the peak systole velocities ($p=0.03$), the end diastole velocities ($p=0.0004$), and the resistive indexes ($p < 0.0001$) differed significantly. The vector difference was calculated for the flow angle (4%), peak systole (8%), end diastole (-27%), and the resistive index (10%). In all Bland-Altman plots zero was within the limits of agreement indicating that the measurements were not biased, but only distributed as expected for biological measurements.

Conclusion

With the vector method, the flow direction did not differ from the conventional, manual angle setting. This means that the manual angle setting can be automated and calculated in the same way for all scans and not depend on the sonographer. The velocities and the resistive indexes did not correspond.

3.2 Study II

Novel flow quantification of the carotid bulb and the common carotid artery with vector flow ultrasound

Further details are found in appendix 2

Aim

The aims of this study were to visualize and calculate the presence of disturbed flow patterns in CCA and CB, and to compare visual evaluation and quantitative calculations using the commercially available ultrasound scanner equipped with the vector velocity technique.

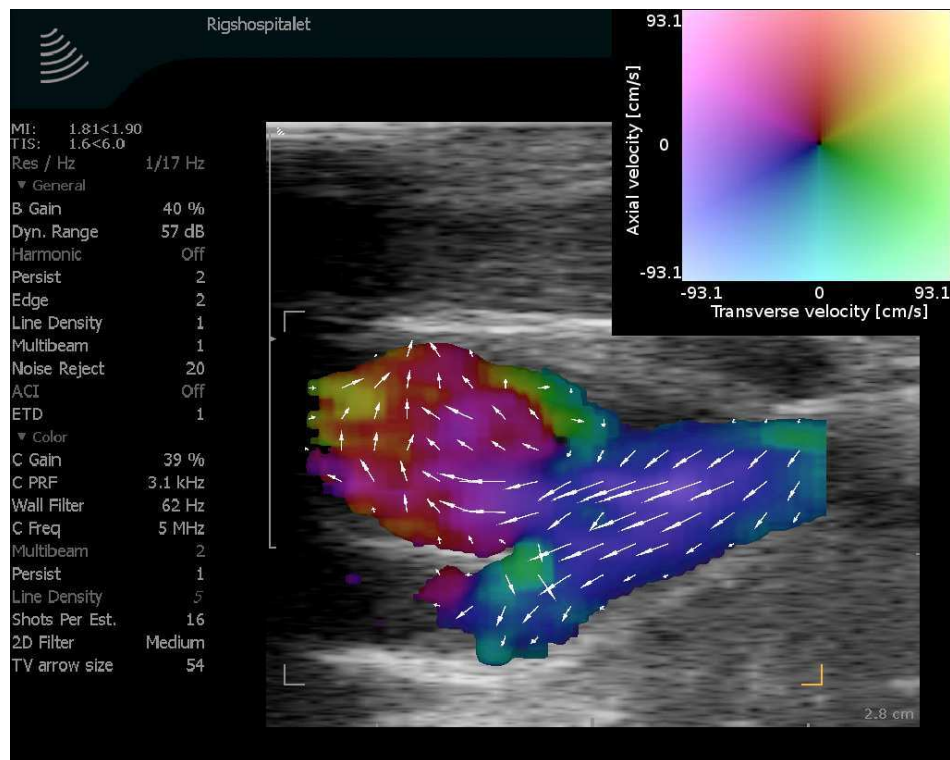


Figure 3.4: *Vector flow ultrasound of the carotid bifurcation including the common carotid artery (right), and the carotid bulb (top left) with clearly different flow patterns.*

Materials and methods

The carotid bifurcation of eight healthy volunteers (5 men, 3 women, age [28 45], median 39.5 years) were scanned in a longitudinal plane with vector flow ultrasound. One

cardiac cycle was obtained for each volunteer. A total of 164 image frames were used in this study where the CCA and CB areas were outlined on every image frame. In random order, each frame was presented to five experienced radiologists individually. They were asked to evaluate if disturbed flow was present in each area or not as shown in Fig. 3.5. For each volunteer the mean expert evaluation value and the standard deviation were calculated for CCA and CB. The vector data of the outlined areas were

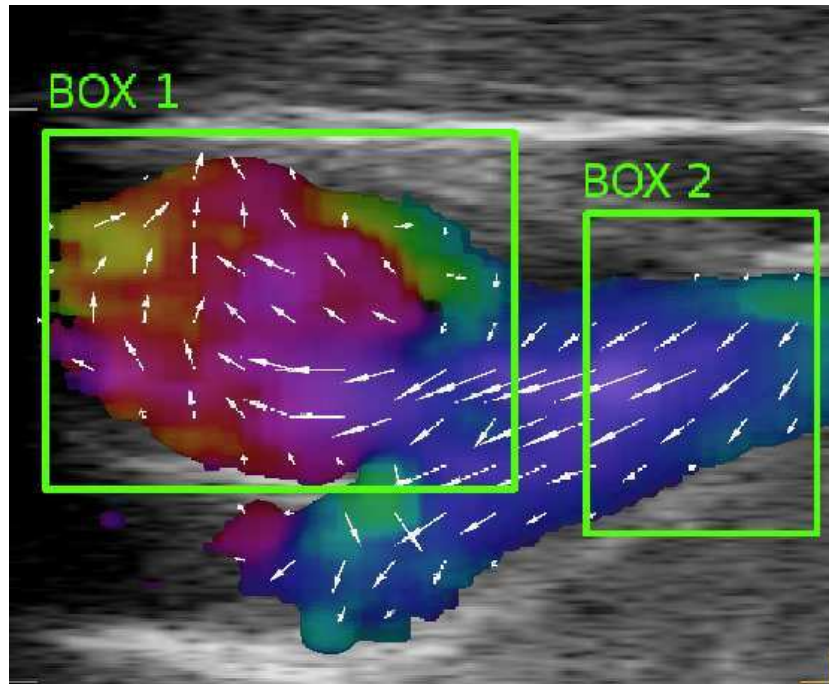


Figure 3.5: *Vector flow ultrasound of the carotid bifurcation where the carotid bulb (box 1) and the common carotid artery (box 2) are outlined.*

used to quantify the flow complexity. The expression, vector concentration, presented by Baschelet calculates a simple number between 0 and 1 for a 2D vector field [65]. For a perfectly laminar flow, the value is 1, whereas the number decreases towards zero with increased amount of complexity as illustrated in Fig. 3.6. In circular statistics the dispersion of the angles, s , is used as an equivalent to the standard deviation of linear statistics [65]. For each volunteer the mean vector concentration and the mean velocity were calculated for each area as shown in Table 3.3.

Statistical analysis

Fleiss Kappa analysis was used to calculate the level of observer agreement, κ , where $\kappa=[0.41\ 0.60]$ was interpreted as moderate agreement. Wilcoxon's matched pair test was used to compare the CCA to the CB. The mean expert evaluations, the mean vector

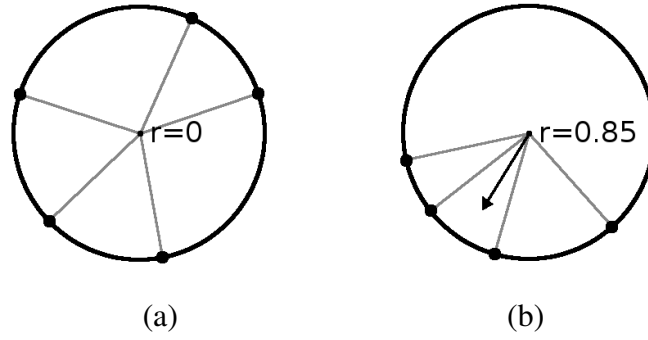


Figure 3.6: The vector angles of two 2D vector fields are plotted on the unit circle. The vector concentration, r , for complex flow (a) and more laminar flow (b). The resulting magnitude expresses how uniform the vector field is.

concentrations, and the mean velocity magnitudes for CCA and CB were tested and the null-hypothesis that there was no difference between CCA and CB was tested. $p < 0.05$ was considered significant, thereby rejecting the null-hypothesis.

Volunteer	$\bar{r} \pm \bar{s}$ [rad]		\bar{v} [cm/s]	
	CCA	CB	CCA	CB
1	0.97 ± 0.22	0.90 ± 0.39	24.6 ± 3.4	8.4 ± 1.6
2	0.96 ± 0.24	0.88 ± 0.46	15.6 ± 2.4	8.3 ± 1.3
3	0.94 ± 0.34	0.67 ± 0.78	13.6 ± 3.1	4.7 ± 1.7
4	0.97 ± 0.22	0.80 ± 0.61	31.2 ± 4.8	11.2 ± 2.1
5	0.96 ± 0.22	0.84 ± 0.56	15.1 ± 3.5	10.4 ± 2.5
6	0.94 ± 0.35	0.83 ± 0.57	17.5 ± 3.7	11.7 ± 1.6
7	0.98 ± 0.17	0.79 ± 0.63	11.3 ± 3.2	9.5 ± 2.2
8	0.98 ± 0.17	0.89 ± 0.43	20.0 ± 4.3	12.3 ± 2.8

Table 3.3: The mean vector concentration, \bar{r} , the mean angular dispersions, \bar{s} , and the mean velocities, \bar{v} , for all image frames from each volunteer in CCA and CB.

Results

The visual evaluations and the vector concentration were both able to separate the flow patterns of CCA from CB significantly and CB also presented significantly lower velocities compared to CCA. Moderate agreement was found between the experts visual evaluations for CCA ($\kappa=0.42$), and for CB ($\kappa=0.52$). With Wilcoxon's matched pair test the null-hypothesis was rejected for the visual evaluation, the mean vector concentration, and the mean vector velocity. Thus, all three methods showed significant differences between CCA and CB. The mean visual evaluations were plotted as a function of

the mean vector concentrations for CCA and CB as shown in Fig. 3.7 and at a mean vector concentration of 0.92 the CCA is separated from CB. This value is suggested as a threshold value to separate the CCA from the CB flow patterns.

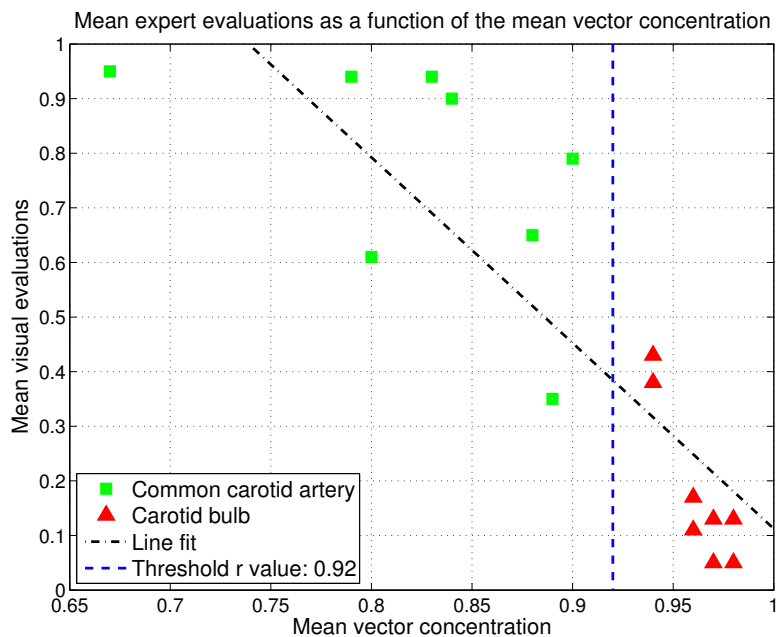


Figure 3.7: The mean visual evaluation as a function of the mean vector concentration illustrates a linear correlation where a mean vector concentration of 0.92 separates the common carotid artery from the carotid bulb measurements.

Conclusion

In conclusion the different flow patterns of CCA and CB can be distinguished with vector flow ultrasound by visual evaluation and by the quantitative measure, vector concentration.

3.3 Study III

Vector flow ultrasound quantification of arterial blood rotations in the cross-sectional plane

Further details are found in appendix 3

Aim

The aim of this study was to visualize and quantify rotational arterial flow patterns in real-time with vector flow ultrasound.

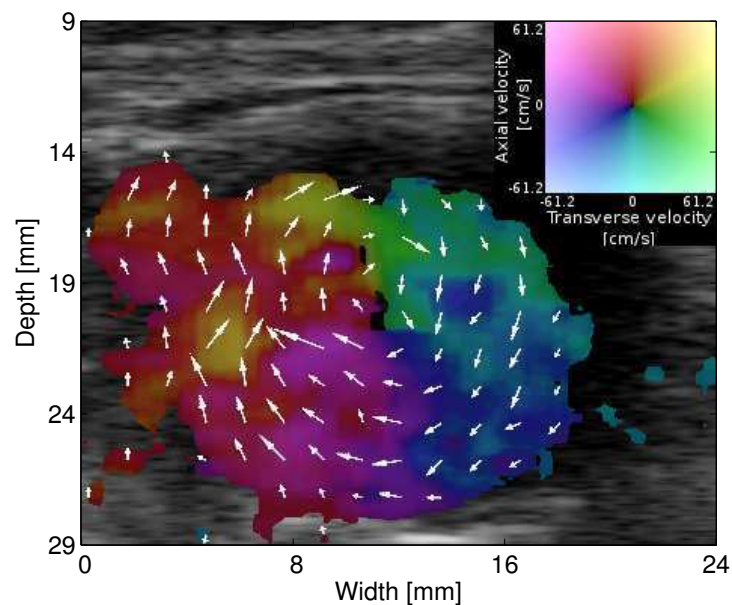


Figure 3.8: *Vector flow ultrasound of the abdominal aorta in the cross-sectional plane. The flow pattern is visualized by the colors and the white vectors providing the magnitude (length) and angle (direction) of the flow.*

Materials and methods

Using vector flow ultrasound, the following three arteries were scanned in the cross-sectional plane on 5 healthy volunteers:

- The abdominal aorta
- The common carotid artery
- The common iliac artery

Each of the 15 scannings consisted of 10 seconds of continuous vector data. For each artery, three data sets were selected, resulting in nine data sets where rotational flow was clearly visible during the cardiac cycles. An example of the real-time color encoded vector data is shown in Fig. 3.8.

Additional data sets of the abdominal aorta for one healthy volunteer were obtained with different settings for the pulse repetition frequency and wall filter settings. All visible rotational flow patterns were calculated and the distance in time from peak systole was calculated for each frame with rotational flow.

Streamline imaging

The 2D vector field of each image frame was visualized with streamlines using an in-house Matlab script. The details of the flow pattern and the flow direction are clearly visible with the lines and the arrows as shown in Fig. 3.9.

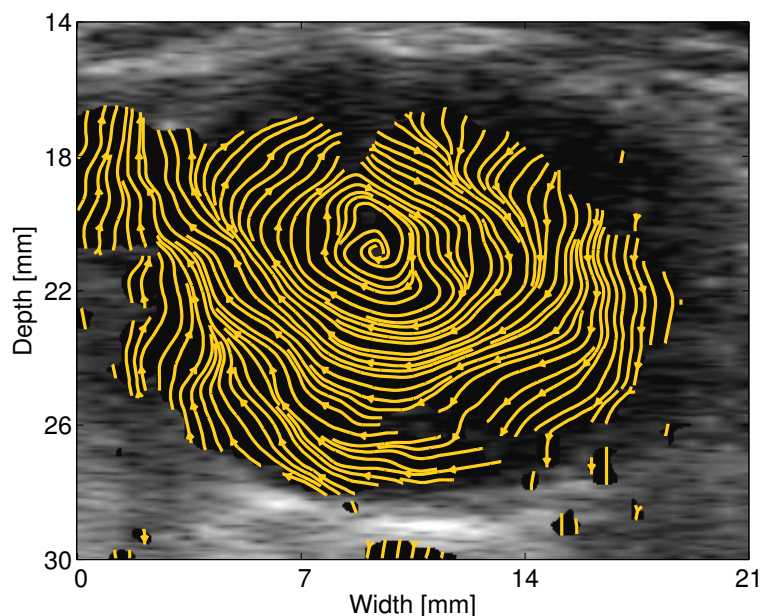


Figure 3.9: *Vector flow data of the abdominal aorta in the cross-sectional plane. The streamlines visualize the rotational flow pattern and the rotation direction.*

Rotational frequency and direction

From the center of the rotational flow pattern, the 2D vector field was divided into squared subareas outlined by grid lines. Each 2D vector field was divided into subareas to fit the center of the rotating flow pattern. For each subarea the z-component of the

curl was calculated as

$$(\nabla \times F)_z = \frac{\partial}{\partial x} F_y - \frac{\partial}{\partial y} F_x, \quad (3.4)$$

where $(\nabla \times F)_z$ is the z component of the curl in a 2D vector field composed of two vector components, $[F_x, F_y]$, as described in [56]. This provides the rotational frequency for each subarea in radians per second. The sign indicates the rotation direction, where a negative sign indicates clockwise rotation, and a positive sign indicates counter clockwise rotation. Dividing this by $2 \cdot \pi$ results in the rotational frequency in rotations per second. The grid size was adjusted according to the size of the vessel and the flow pattern.

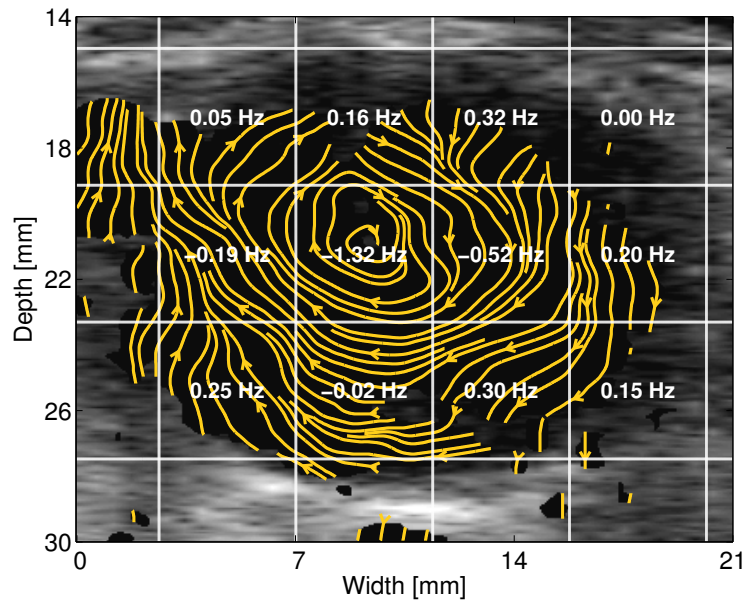


Figure 3.10: *Cross-sectional plane of the abdominal aorta during the diastole. A rotational flow pattern is clearly visualized with streamlines and the subareas and the rotational frequencies are imposed on the image.*

Statistical analysis

Each data set was analyzed for the presence of rotational flow patterns and the rotational frequencies of the rotation center were used to calculate the mean rotational frequency and standard deviation.

For the extended measurements on the abdominal aorta, the distance in time from peak systole was normalized for all cardiac cycles to a heart rate of 1 per second. The purpose was to investigate a possible two-directional rotation during the cardiac cycle in the

abdominal aorta. The rotational frequency was plotted as a function of the cardiac cycle for each artery.

Results

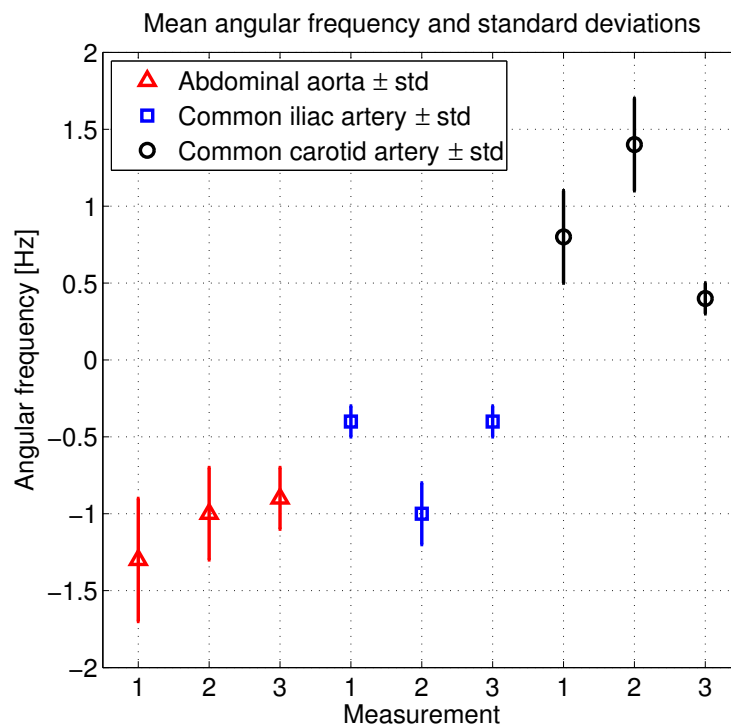


Figure 3.11: *The mean rotational frequency and standard deviation for each data set. The rotation direction is indicated by the sign, which are all identical for each artery. A negative sign indicates clockwise rotation, and a positive sign counter clockwise rotation.*

The rotational directions were unidirectional for all measurements of each artery: clockwise for AA, and CIA, and counter clockwise for CCA. The expanded data set shown in Fig. 3.12 for the abdominal aorta indicates the presence of a two-directional rotation with a counter clockwise rotation appearing in the systole and a clockwise rotation during diastole.

Conclusion

With vector flow ultrasound the rotational flow patterns of three arteries were obtained. The flow pattern and rotational direction and frequency was presented. The secondary flow in AA and CIA rotates clockwise, whereas CCA rotates counter clockwise. Ex-

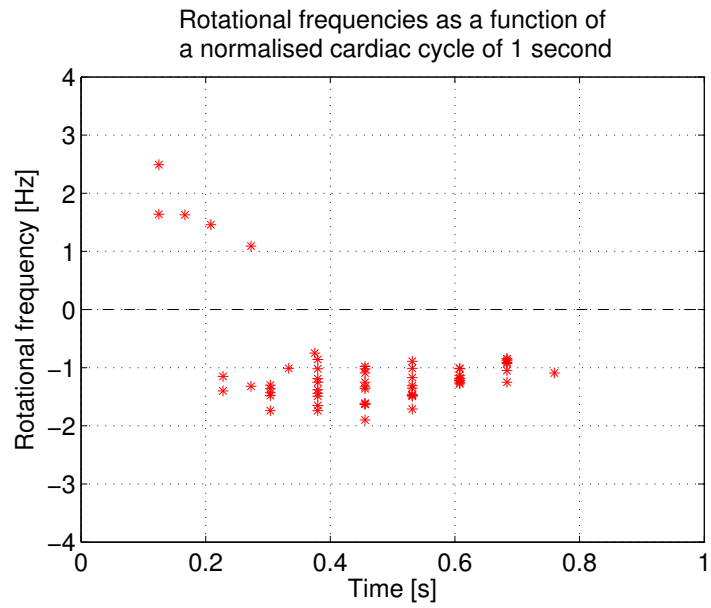


Figure 3.12: *All rotational frequencies of the abdominal aorta as a function of time. The rotation direction is clearly changing from counter clockwise to clockwise during the cardiac cycle.*

panded data sets of AA indicate the presence of a two-directional flow pattern. In conclusion real-time vector flow can visualize and quantify secondary flow patterns of three main arteries which presented constant rotational directions.

Discussion

New achievements with vector flow

This thesis presents the first *in vivo* studies on the commercial implementation of TO. The simultaneous data acquisition of spectral velocity estimation and vector flow data in study I has not been obtained before. It makes it possible to compare the methods with no delay which is often difficult in comparison studies. The post processing of the vector data made it possible to calculate the clinical parameters PS, ED, RI, and flow angle.

In study II the complex flow patterns of the carotid bulb and the common carotid artery were visualized and for the first time a quantitative measure of complexity was suggested – the vector concentration. Simultaneous data from the two areas with different flow patterns were compared visually and quantitatively and a threshold value was suggested that separates the two areas. The simple calculation of the vector concentration does not require much extra processing power in a future implementation into the commercial scanner software. Moreover, this vector calculation method can be tested with other vector methods such as MRI and echo PIV in future studies.

Vector flow ultrasound images of secondary flow patterns in the cross-sectional plane of human arteries were presented in study III. Studies with MR and Doppler ultrasound has previously confirmed the existence of such flow patterns and with study III these patterns were illustrated and quantified with vector flow ultrasound for the first time. The processing of the 2D vector fields data sets are simple and should be implemented for further clinical testing in future scanner software.

4.1 Study I - blood velocity estimation

4.1.1 Flow angle

The direction of blood is essential in spectral velocity estimation. Assuming that the blood flows in one direction at all times and everywhere in the vessel, the direction is defined manually by the operator. The method works within an angle between the ultrasound beam and the blood direction of $[0\ 60]^\circ$ and is thus, limited in the clinical use, as many blood vessels run along the skin surface. Nevertheless, this method is presently the only commercially available ultrasound blood velocity estimation method.

The scanner setup for study I was optimized for the spectral velocity estimation and the vector data were obtained with these settings. The mean flow angle in the central half of the vessel diameter corresponded to the manually set spectral angle and this finding means that an automated angle setting is possible. With slight modification of the spectral velocity method, the vector flow method can provide the mean flow angle within the range gate area and thus, eliminate the manual angle setting. In contrast to the manual setting, this automated method uses the same algorithm for all measurements. With conventional spectral estimation only one line in the vessel is measured. In the 2D vector field it is possible to obtain vector data from multiple areas simultaneously. Measurements upstream, over, and downstream of a plaque in the common carotid artery makes it possible to create a velocity profile over time and space which is not possible with the conventional method. It also makes it possible to measure multiple areas in a twisting vessel. Thus, further details can be obtained of the movement and velocity of the blood in the carotid bulb, the abdominal aorta, and in conditions such as carotid artery stenosis, and renal artery stenosis, also where the velocity magnitude and direction changes as a function of space and time.

4.1.2 Temporal information

The vector data was calculated and displayed in real-time on the scanner display as for normal color flow mode. However, the frame rate of the obtained data sets were limited to 14.8 frames per second. This is caused by two main effects: The triplex mode and the vector data estimation. The triplex mode requires spectral data, vector velocity, and the B-mode data to be received before the image data are calculated. With vector flow 16 shots are used per estimate, which also contributes to a lower temporal resolution. However, the aliasing limit for vector flow is higher than with spectral estimation. Thus, in the transverse direction higher velocities can be estimated at a lower pulse repetition frequency with vector flow than with spectral estimation. However, the scanner software

seems to limit the frame rate of the AVI files further as the newest software update has increased the frame rate of a new study to 60 frames per second.

4.1.3 Velocity tracking

The spectral velocity estimation was set to track the maximum velocity as a function of time, and the peak velocities for the past 8 seconds were used for continuous calculation of the peak systole velocity and the scanner software calculates the end diastole velocity as the lowest velocity between two peak systole velocities.

For comparison, the maximum vector velocity for each frame was plotted as a function of time, and with an in-house Matlab script, the peak systole velocities were tracked as illustrated in Fig. 4.1. From the results, the peak systole velocities for the two methods

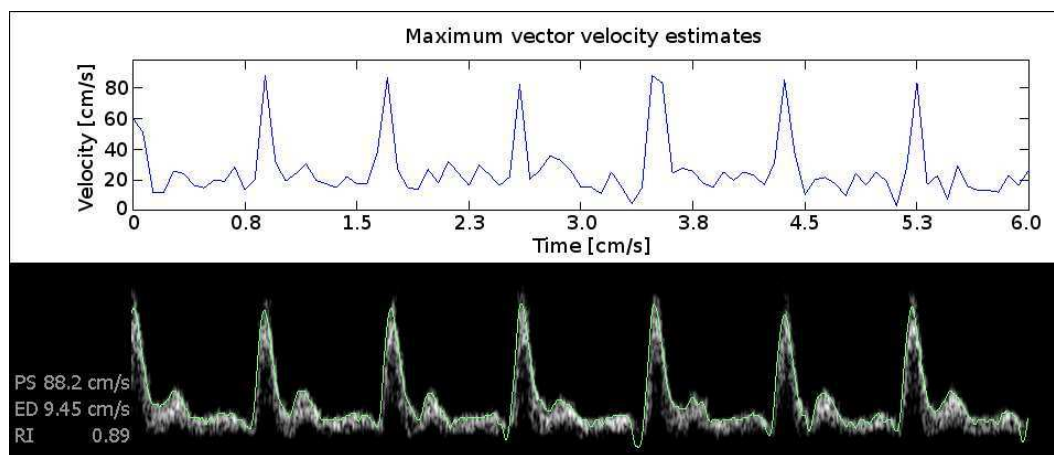


Figure 4.1: *Velocity estimation of the common carotid artery during 10 seconds of continuous data plotted by conventional spectrogram (bottom), and by vector flow data (top). Notice the similarity in the velocity profile.*

differed significantly, as the vector difference of 8% indicates that the spectral velocity magnitudes were higher compared to the vector method. This may be caused by the low frame rate, where the true peak velocity is missed between two frames.

The script tracked the end diastole vector velocities as the lowest velocities just before each peak systole as illustrated in Fig. 3.3. The end diastole vector difference of -27% indicates that the spectral velocity magnitudes were lower compared to the vector method. This may be caused partly by the low frame rate. However, the difference in the tracking by the two methods can also explain the difference, as the lowest velocity between two peaks may be found just after peak systole just after closure of the aortic valve. The PRF of the vector flow was set identical to the spectral estimation and the

setting was adjusted to avoid aliasing during peak systole. Thus, it may have impaired the measurements of the low velocities. Furthermore, due to the echo canceling filter, the error on low velocities with vector flow estimation is higher than the error at high velocities [14] and this was not accounted for.

4.1.4 Clinical use

The investigated vector flow implementation supports one, linear array transducer, thus, limiting the maximum depth to 4-5 cm. Support of a curved array transducer with a lower center frequency will increase the maximum depth and thus, make measurements of abdominal vessels such as the portal vein, and the renal arteries available. However, with the current implementation it is possible to measure the blood movements at any direction and this is very useful. In combination with an automatic angle setting it is potentially a less operator-dependent alternative for velocity estimation on arteries such as the common carotid artery. The examination time may also be shorter with fewer tasks required and less cumbersome to learn for the untrained operator.

4.2 Study II - complex flow patterns

4.2.1 The role of complex flow patterns

Disturbed flow may be physiological as suggested with study II. In theory the flow should occur at a changing diameter as in the carotid bulb or at branching such as the subclavian artery [66]. The complex flow patterns are also present in the venous system and was demonstrated with PW in the femoral and jugular veins [67]. Though disturbed flow is present in healthy volunteers, it may also be present as a sign of atherosclerotic progression. Most commonly the changes in flow velocity are used to quantify stenosis [35]. Impaired vessel compliance and increased plaque formation may be a result of disturbed flow and a final stage is seen with massive connective tissue remodeling in the aortic aneurysms.

Further characterization of the complex flow patterns should be investigated as it may hold prognostic and diagnostic information about cardiovascular disease. With study II the first quantification of the complex flow patterns with vector flow was presented.

4.2.2 Outlining the common carotid artery and the carotid bulb

The common carotid artery and the carotid bulb were outlined visually allowing an area of any size. The carotid bulb was larger in the image compared to the smaller imaged part of the common carotid artery and this may have favored the carotid bulb in the visual evaluation. This could have been avoided with images presenting areas of equal sizes of the two structures. However, the acquired images did not include a large enough area of the common carotid artery. For the vector concentration calculation this was accounted for by dividing the mean values by the number of pixels, n , as shown in (4.1) and (4.2).

$$\bar{x} = \frac{1}{n} \cdot \sum_{i=1}^n \cos(t_i) \quad (4.1)$$

$$\bar{y} = \frac{1}{n} \cdot \sum_{i=1}^n \sin(t_i) \quad (4.2)$$

4.2.3 The amount of vector data depends on the scanner settings

During the cardiac cycle the outlined areas were not filled out with vector color information. At decreasing velocities during the diastole, the scanner setup did not allow for optimal data acquisition as illustrated in Fig. 4.2. This was caused by the setup avoiding aliasing during peak systole and was primarily affected by the pulse repetition

frequency, the echo canceling filter, and the wall filter. Separate setups for systolic complexity measurements and diastolic complexity measurements are suggested in future studies to avoid this compromised data acquisition during diastole.

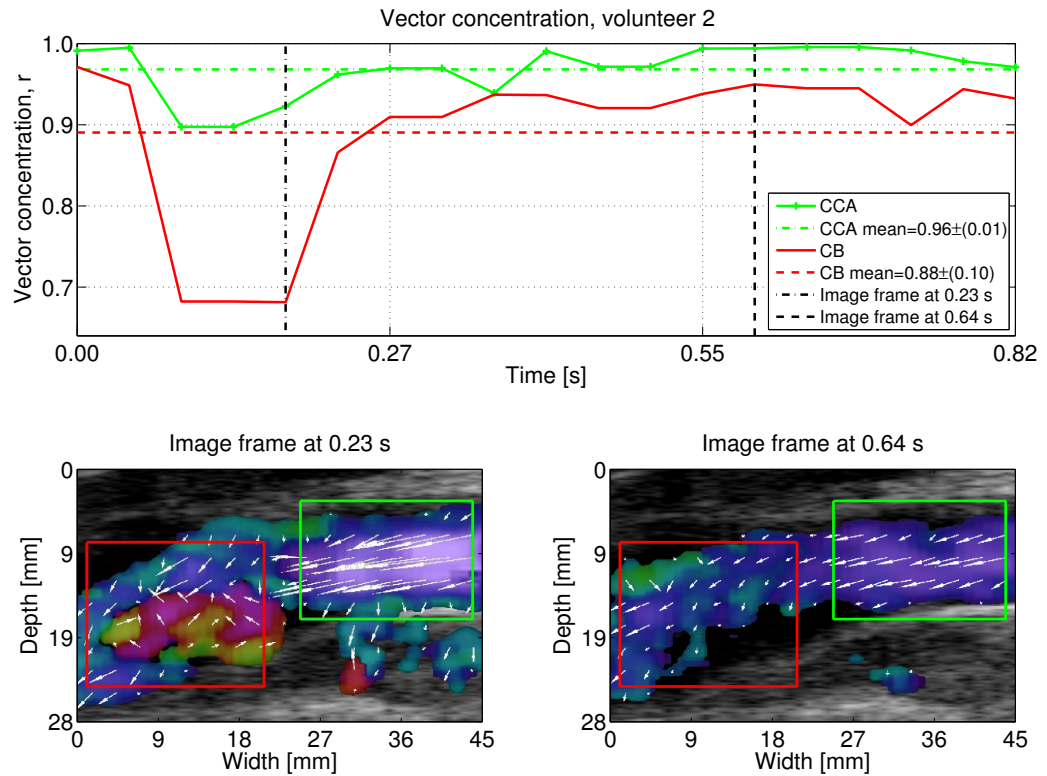


Figure 4.2: *Vector flow ultrasound of the carotid bulb (red) and the common carotid artery (green) in a longitudinal plane during systole (bottom left), and diastole (bottom right). The vector concentration as a function of time during one cardiac cycle is shown in the top. The diastolic image frame shows less colored pixels compared to systole.*

4.2.4 Visual evaluation of complex flow

The Fleiss-Kappa analysis of the inter-observer agreement showed only moderate agreement between the experts. The experts are not using the vector visualization clinically and therefore the moderate agreement may be caused by a different learning curve for each expert. This could have been avoided by introducing a learning series of vector flow images before starting the visual evaluation. The moderate agreement may also be caused by the fact, that each expert percept the flow patterns differently. This only stresses the need for an objective, quantitative method such as the vector concentration

to measure flow complexity. With such method the expert would only be required to locate and select the areas presenting the carotid bulb and the common carotid artery.

4.2.5 Quantitative flow information

Disturbed flow was defined as a more than 90 degree change in vector angle in part of the cardiac cycle. A disturbed flow pattern was demonstrated in the CB of all healthy volunteers and the vector concentration discriminated between disturbed flow and laminar flow equally good as the experts. The vector concentration is a simple method that can be applied on 2D vector fields obtained with any modality and thus, makes further evaluation possible. The result provides a value between 0 and 1 which is applicable for clinical use. A study comparing the flow complexity in the carotid bulb of healthy volunteers with cardiovascular patients should investigate the diagnostic value of the vector concentration.

4.2.6 Prognostic and diagnostic parameters

Conventional ultrasound methods are being used to estimate the prognosis of arterial atherosclerosis by detection of the vessel wall, the plaque formation and the flow characteristics. An increased stress caused by cardiovascular disease can modulate the vessel tone and function. The frictional tangential forces on the endothelium, described by shear stress, is a physiological process. However, increased shear stress causes vasodilatation and flow disturbances with altered shear stress can cause endothelial injury and thus, subsequent deposition of lipids. With a quantitative method which describes the disturbed flow patterns of the carotid bulb, the prognostic and diagnostic potential value should be investigated further.

4.2.7 Vector velocity as an additive to describe rotational flow

Additional to the vector concentration, the mean velocity was shown to correlate well with the visual presence of complex flow. However, low mean velocities are not directly an indication of complex flow but low velocities are present at disturbed flow. Thus, a combination of the flow directions by the vector concentration, and the mean velocities may strengthen the ability to discriminate the flow patterns of CCA and CB quantitatively and should be considered in future studies.

4.3 Study III - rotational flow patterns

4.3.1 Locating the rotational flow pattern

For study III a considerable number of data sets were discarded due to limited visualization of a rotational flow pattern or a limited amount of vector color. A rotational flow pattern seems to require scanning in the exact cross-sectional plane of the vessel and can be difficult with a 1D array. Furthermore, the adjustment of the PRF and the wall filter may vary for each person. The heart rate directly affects the length of the diastolic phase and thus, an increased heart rate makes it more difficult to visualize the diastolic, secondary flow pattern. Therefore, the setup used in study III is not ready for clinical testing. The scan depth is limited by the transducer, which requires the subjects to be slim and to have patience when the exact cross-sectional plane is located. A wider, convex array would allow vector flow ultrasound of deeper structures such as the portal vein and the renal arteries. Using a 2D transducer would make it possible to visualize the flow pattern in 3D and select the exact cross-sectional scan plane during post processing. Implementation on a phased array will provide the option of scanning the heart with vector flow and characterize the flow around the heart valves in more details compared to present Doppler based methods.

However, the main result of the study was to present a new method to visualize and quantify the secondary flow with vector flow for the first time. Future studies should consider a more practical method for obtaining the data in a clinical environment.

4.3.2 Temporal resolution limitation

The study was limited in the frame rate of the AVI files obtained with the prototype software. The recent development on the system has included a software update where an increase in frame rate from about 20 Hz to 60 Hz has been observed in a pilot phantom study. The new update is able to store the frames from the cine loop shown immediately after storage at 60 Hz, whereas storage as AVI files is still cut down to 20 Hz.

The secondary flow patterns occur in very short intervals during the cardiac cycle and the acquisition of the flow patterns is thus, depending on the maximum frame rate. Measurements such as the two-directional rotation in the abdominal aorta would benefit from such an increase in frame rate. The length of one data sequence allowed by the scanner was about 10 seconds. An increase to 120 seconds would allow averaging and thus improve the estimates for flow direction and velocity. With CFM and B-mode imaging several minutes of storage are allowed.

The scanner has a research interface where pre-processed data is available with higher

spatial and temporal resolution. This system was recently presented in a working state and is now being used for vector flow studies. The methods presented in study III should be investigated further with this setup.

4.3.3 Subarea grid size

The visualization of the rotational flow pattern with streamlines makes it possible to find the center of the rotation. The in-house Matlab script used for study III required manual setting of the rotation center and definition of the grid size around the rotation. However, the influence of the grid size was not tested. A constant grid size was used for each data set that matched the rotation center. This leaves a question on how robust the method is to different grid sizes and how the grid size should be defined in future studies. The

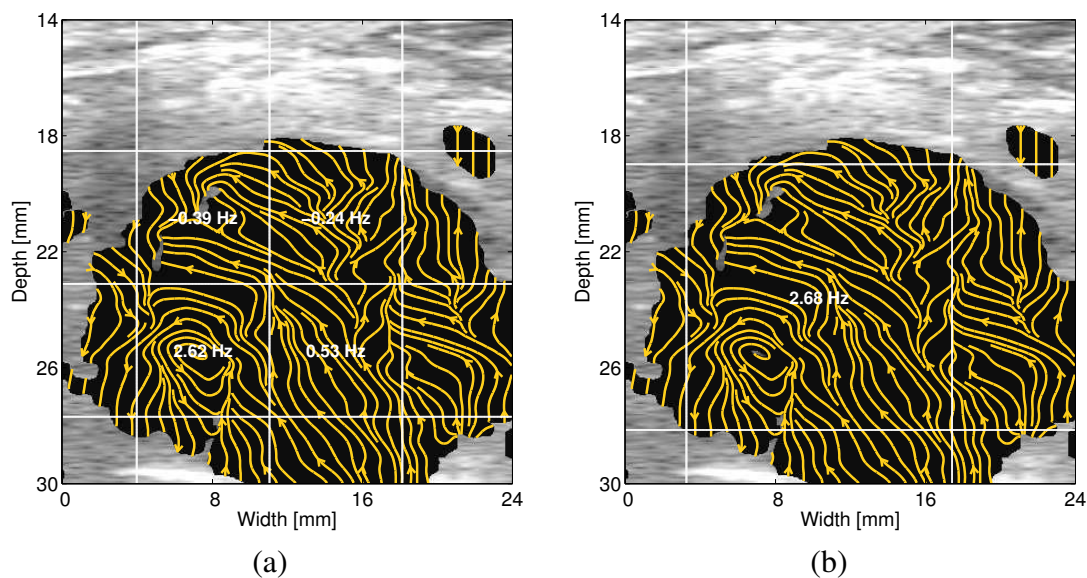


Figure 4.3: *Rotational flow pattern of the abdominal aorta in the cross-sectional plane. The calculated rotational frequency of the rotation center in the lower left subarea in (a) is almost identical to the frequency of a larger grid size shown in (b).*

rotational frequency was calculated by the z-component of the curl. The calculation is robust as long as the center of the rotation is within the grid. Two rotations of opposite rotation direction will cancel out, and two identical rotations of same direction will increase the frequency by a factor of two. Thus, it is suggested that the grid size is set to include the center of one rotation. The effect of different grid size is illustrated in Fig. 4.3, where the rotational frequency of one rotation is only slightly affected by the size.

4.3.4 Constant rotation direction

In study III the measurements showed the same rotation direction for each vessel during diastole. This indicates that the method is stable, however, the number of subjects in the study was insufficient for statistical analysis. Further measurements on more subjects would improve the suggestion that the rotation is constant for all healthy volunteers. Another study could correlate the blood pressure to the change in rotational frequency by comparing the rotation before and after intervention such as intravenous methoxedrine or norepinephrine. A comparison study on the rotational frequencies of healthy volunteers and cardiovascular patients should also be considered.

4.3.5 Two-directional rotation in the abdominal aorta

The extended measurements on the abdominal aorta showed a two-directional flow pattern of the abdominal aorta consistent with previous models suggested by Doppler [44], MR [48] studies. Using similar 2D vector fields obtained with MR the wall shear stress (WSS) was previously calculated [60]. WSS is believed to be important in the development of arterial atherosclerosis and thus, should be included in a revised version of study III. As the shear stress against the vessel wall is believed to be an important factor in the development of arterial atherosclerosis [68], the ability to obtain such data with ultrasound makes way for future studies on the flow patterns in the abdominal aneurysms where the clinical criteria for intervention are still very sparse.

Another important physical force, the torque of the rotation, should also be considered as it is theoretically possible to be calculated for a rotation in a 2D vector field.

4.3.6 Clinical use

Conventional ultrasound techniques do not allow visualization or quantification of secondary flow in the cross-sectional plane of arteries. These secondary flow patterns are well investigated and have been predicted in previous studies with MR and CFD in different vessels [30, 69–71] and with the ultrasound method, Plane Wave, Hansen et al showed secondary flow patterns for the first time with ultrasound [43]. With further studies on values of the physiological rotational frequencies and the wall shear stress in healthy volunteers, these parameters are potential diagnostic and prognostic clinical tools. Especially in the characterization of the abdominal aneurysms there is a need for more parameters to indicate the risk of a rupture. The calculations are simple and thus, do not require heavy processing power. Furthermore, the results are simple values that are preferred in the clinical setting.

Conclusion

This thesis has focused on quantification of a new implementation of the vector flow ultrasound technique, Transverse Oscillation, and with study I-III it has been shown that the theoretical advantages of the technique are also beneficial in practical comparisons to conventional ultrasound methods. In study I it was shown that the direction of the blood in the common carotid artery was equally good compared to the manual angle setting used for conventional spectral velocity estimation. An objective calculation of the angle for angle correction was suggested and is believed to be simple to implement in the scanner software. The study also suggested how to calculate the peak systole and end diastole velocities and visualized the velocity as a function of time equal to the conventional spectrogram.

Study II presented the quantitative measure of blood complexity, the vector concentration of the carotid bulb. In comparison to visual evaluation by ultrasound experts no statistical difference was found and thus, the vector concentration is suggested to quantify the level of complex flow. Furthermore, the flow velocities correlated well with the presence of complex flow and were suggested to be combined with the vector concentration.

The secondary flow patterns of the cross-sectional plane in three arteries were investigated in study III. With the 2D vector field the z-component of the curl was used to calculate the rotational frequencies and a stable rotational direction was found for the common carotid artery and the common iliac artery. Extended measurements on the abdominal aorta showed a two-directional rotation which corresponds to previous studies with other modalities.

With study I-III a number of simple quantitative methods have been presented and investigated in comparison to conventional methods. The vector flow method has the main advantage of being angle-independent and able to obtain 2D vector fields in real-time. Velocities in the entire field can be calculated, the flow complexity calculated,

and the flow patterns visualized and quantified. The suggested quantitative measures do not require heavy processing and should be possible to implement in future software updates in the ultrasound scanner. In a clinical perspective the suggested methods all provide simple results. In spectral velocity estimation the operator would be relieved from manually angle setting. The vector concentration provides a value between 0 and 1 as an expression of the flow complexity, and the rotational frequency also provides direct quantification of rotations per second.

Perspectives

Suggestions for future studies:

- Flow phantom study where the correlation between the vector flow pulse repetition frequency and the flow angle is investigated.
- *In vivo* study on the the complex flow of the carotid bulb in patients with arterial atherosclerosis in comparison with healthy volunteers.
- Software development of spectral velocity estimation using vector flow data for automatic angle calculation. A 'click-and-scan' application should be tested by experienced radiologists in comparison to conventional, manual angle setting.
- 3T phase contrast MR of cross-sectional planes of the abdominal aorta followed by vector flow ultrasound. Calculation of rotational frequency and wall shear stress for both methods and statistical comparison.
- Software development that implements automatic tracking of rotation flow patterns and calculates the rotational frequencies in real-time. Evaluation in simulation, flow phantom, and finally *in vivo*.
- Study on the effect of increased blood pressure with noradrenaline on the rotational frequency in the abdominal aorta in healthy volunteers.

BIBLIOGRAPHY

- [1] Munk P. Estimation of the 2-D flow vector in ultrasonic imaging: a new approach. Master's thesis, Department of Information Technology, Technical University of Denmark, 1996.
- [2] Jensen JA and Munk P. A New Method for Estimation of Velocity Vectors. *IEEE Trans. Ultrason., Ferroelec., Freq. Contr.*, 45:837–851, 1998.
- [3] Munk P. *Estimation of blood velocity vectors using ultrasound*. PhD thesis, Department of Information Technology, Technical University of Denmark, Lyngby, Denmark, 2000.
- [4] Jensen JA. Algorithms for estimating blood velocities using ultrasound. *Ultrasonics*, 38(1-8):358–362, 2000.
- [5] Jensen JA. A New Estimator for Vector Velocity Estimation. *IEEE Trans. Ultrason., Ferroelec., Freq. Contr.*, 48(4):886–894, 2001.
- [6] Udesen J and Jensen JA. Investigation of Transverse Oscillation Method. *IEEE Trans. Ultrason., Ferroelec., Freq. Contr.*, 53:959–971, 2006.
- [7] Udesen J, Nielsen MB, Nielsen KR, and Jensen JA. Examples of in-vivo blood vector velocity estimation. *Ultrasound Med. Biol.*, 33:541–548, 2007.
- [8] Hansen KL, Udesen J, Oddershede N, Henze L, Thomsen C, Jensen JA, and Nielsen MB. In vivo comparison of three ultrasound vector velocity techniques to mr phase contrast angiography. *Ultrasonics*, 49:659–667, 2009.
- [9] Pedersen MM, Pihl MJ, Haugaard P, Hansen JM, Hansen KL, Nielsen MB, and Jensen JA. Comparison of real-time in-vivo spectral and vector velocity estimation. *Ultrasound in Med. Biol.*, 38(1):145–151, 2012.

- [10] Pedersen MM, Pihl MJ, Haugaard P, Hansen KL, Lange T, Lönn L, Nielsen MB, and Jensen JA. Novel flow quantification of the carotid bulb and the common carotid artery with vector flow ultrasound. *Ultraschall in der Medizin/European Journal of Ultrasound*, Submitted 2011.
- [11] Pedersen MM, Pihl MJ, Hansen JM, Haugaard P, Hansen PM, Nielsen MB, and Jensen JA. Rotational flow patterns in the arterial blood stream with vector flow ultrasound. *Ultrasonics*, Submitted 2011.
- [12] Starr I, Ambrosi C, Manchester JH, and Shelburne JC. Disturbed blood flow in the carotid artery: its physiological and clinical significance. *Am Heart J*, 5(86):644–50, 1973.
- [13] Jonkman EJ, Tans JT, and Mosmans PC. Doppler flow velocity measurements in patients with intracranial hypertension. *J Neurol*, 3(218):157–69, 1978.
- [14] Jensen JA. *Estimation of blood velocities using ultrasound: A signal processing approach*. Cambridge Univ Pr, 1996.
- [15] Evans DH, McDicken WN, Skidmore R, and Woodcock JP. *Doppler Ultrasound, Physics, Instrumentation, and Clinical Applications*. John Wiley & Sons, New York, 1989.
- [16] Radermacher J, Chavan A, Bleck J, Vitzthum A, Stoess B, Gebel MJ, Galanski M, Koch KM, and Haller H. Use of Doppler ultrasonography to predict the outcome of therapy for renal-artery stenosis. *N Engl J Med*, 344(6):410–7, 2001.
- [17] Krumme B. Renal Doppler sonography—update in clinical nephrology. *Nephron Clin Pract*, 103(2):c24–8, 2006.
- [18] Lanzarini L, Fontana A, Campana C, and Klersy C. Two simple echo-Doppler measurements can accurately identify pulmonary hypertension in the large majority of patients with chronic heart failure. *J Heart Lung Transplant*, 24(6):745–54, 2005.
- [19] Görg C, Riera-Knorrenschild J, and Dietrich J. Pictorial review: Colour Doppler ultrasound flow patterns in the portal venous system. *Br J Radiol*, 75(899):919–29, 2002.
- [20] Westra SJ, Zaninovic AC, Vargas J, Hall TR, Boechat MI, and Busuttill RW. The value of portal vein pulsatility on duplex sonograms as a sign of portal hypertension in children with liver disease. *AJR Am J Roentgenol*, 165(1):167–72, 1995.

- [21] O'Boyle MK, Vibhakar NI, Chung J, Keen WD, and Gosink BB. Duplex sonography of the carotid arteries in patients with isolated aortic stenosis: imaging findings and relation to severity of stenosis. *AJR Am J Roentgenol*, 166(1):197–202, 1996.
- [22] Jassal DS, Tam JW, Dumesnil JG, Giannoccaro PJ, Jue J, Pandey AS, Joyner CD, Teo KK, and Chan KL. Clinical usefulness of tissue Doppler imaging in patients with mild to moderate aortic stenosis: a substudy of the aortic stenosis progression observation measuring effects of rosuvastatin study. *J Am Soc Echocardiogr*, 21(9):1023–7, 2008.
- [23] Wood MM, Romine LE, Lee YK, Richman KM, O'Boyle MK, Paz DA, Chu PK, and Pretorius DH. Spectral Doppler signature waveforms in ultrasonography: a review of normal and abnormal waveforms. *Ultrasound Q*, 26(2):83–99, 2010.
- [24] Hansen KL, Pedersen MM, Jensen JA, and Nielsen MB. In-vivo studies of new vector velocity and adaptive spectral estimators in medical ultrasound. *Danish Medical Bulletin*, Accepted for publication 2011.
- [25] Hoskins P and Thrush A. *Diagnostic ultrasound: physics and equipment*. Cambridge Univ Pr, 2003.
- [26] Kruskal JB, Newman PA, Sammons LG, and Kane RA. Optimizing Doppler and color flow us: application to hepatic sonography. *Radiographics*, 24(3):657–75, 2004.
- [27] Lin PH, Dake MC, Veith FJ, and Krajcer Z. *Advanced Therapy in Endovascular Interventions*. B.C. Decker, 2008.
- [28] Cuhlmann S, Van der Heiden K, Saliba D, Tremoleda JL, Khalil M, Zakkar M, Chaudhury H, Luong le A, Mason JC, Udalova I, Gsell W, Jones H, Haskard DO, Krams R, and Evans PC. Disturbed blood flow induces *rela* expression via *c-jun* n-terminal kinase 1: a novel mode of *nf-b* regulation that promotes arterial inflammation. *Circ Res*, 8(108):950–959, 2011.
- [29] Schuierer G and Huk WJ. Diagnostic significance of flow separation within the carotid bifurcation demonstrated by digital subtraction angiography. *Stroke*, 21(12):1674–1679, 1990.
- [30] Zhao SZ, Xu XY, Hughes AD, Thom SA, Stanton AV, Ariff B, and Long Q. Blood flow and vessel mechanics in a physiologically realistic model of a human carotid arterial bifurcation. *J Biomech*, 33(8):975984, 2000.

- [31] Stokholm R, Oyre S, Ringgaard S, Flaagoy H, Paaske W, and Pedersen EM. Determination of wall shear rate in the human carotid artery by magnetic resonance techniques. *Eur J Vasc Endovasc surg*, 20(5):427–433, 2000.
- [32] Xue YJ, Gao PY, Duan Q, Lin Y, and Dai CB. Preliminary study of hemodynamic distribution in patient-specific stenotic carotid bifurcation by image-based computational fluid dynamics. *Acad Radiol*, 49(5):558–565, 2008.
- [33] Kassam MS, Cobbold RS, Johnston KW, and Graham CM. Method for estimating the doppler mean velocity waveform. *Ultrasound Med Biol*, 8(5):537–44, 1982.
- [34] Phillips DJ, Greene FM, Langlois Y, Roederer GO, and Strandness DE. Flow velocity patterns in the carotid bifurcations of young, presumed normal subjects. *Ultrasound Med Biol*, 9(1):39–49, 1983.
- [35] Arning C, Widder B, von Reutern GM, Stiegler H, and Görtler M. Ultraschallkriterien zur graduierung von stenosen der a. carotis interna - revision der degumkriterien und transfer in nascet-stenosierungsgrade. *Ultraschall in der Medizin*, 31(3):251–257, 2010.
- [36] Samuel KC. Atherosclerosis and occlusion of the internal carotid artery. *J Pathol Bacteriol*, 71(2):391–401, 1956.
- [37] Peterson RE, Livingston KE, and Escobar A. Development and distribution of gross atherosclerotic lesions at cervical carotid bifurcation. *Neurology*, 10:955–959, 1960.
- [38] Hugh AE and Fox JA. The precise localisation of atheroma and its association with stasis at the origin of the internal carotid artery – a radiographic investigation. *Br J Radiol*, 510(43):377–83, 1970.
- [39] Fuster V, Stein B, Ambrose JA, Badimon L, Badimon JJ, and Chesebro JH. Atherosclerotic plaque rupture and thrombosis. evolving concepts. *Circulation*, 82(3 Suppl):II47–59, 1990.
- [40] Bergan JJ and Yao JST. *Cerebrovascular insufficiency*. New York: Grune and Stratton, 1983.
- [41] Oddershede N, Hansen KL, Nielsen MB, and Jensen JA. In-vivo examples of synthetic aperture vector flow imaging. In *Proc. SPIE - Medical Imaging 2007: Ultrasound Imaging and Signal Processing*, volume 6513, 2007.

- [42] Hansen PM, Pedersen MM, Hansen KL, Nielsen MB, and Jensen JA. New technology - demonstration of a vector velocity technique. *Ultraschall in der Medizin/European Journal of Ultrasound*, 32:213–5, 2011.
- [43] Hansen KL, Udesen J, Gran F, Jensen JA, and Nielsen MB. In-vivo examples of flow patterns with the fast vector velocity ultrasound method. *Ultraschall Med*, 30(5):471–7, 2009.
- [44] Frazin LJ, Lanza G, Vonesh M, Khasho F, Spitzzeri C, McGee S, Chandran KB, Mehlman D, Talano J, and McPherson D. Functional chiral asymmetry in descending thoracic aorta. *Circulation*, 82(6):1985–1994, 1990.
- [45] Thomas JD. Flow in the descending aorta. a turn of the screw or a sideways glance? *Circulation*, 82(6):2263–2265, 1990.
- [46] Li C, Zhang J, Li X, Zhou C, Li H, Tang H, and Rao L. Quantification of chronic aortic regurgitation by vector flow mapping: a novel echocardiographic method. *Eur J Echocardiogr*, 2(11):119–124, 2010.
- [47] Swillens A, Segers P, Torp H, and Løvstakken L. Two-dimensional blood velocity estimation with ultrasound: speckle tracking versus crossed-beam vector doppler based on flow simulations in a carotid bifurcation model. *IEEE Trans Ultrason Ferroelectr Freq Control*, 2(57):327–339, 2010.
- [48] Kilner PJ, Yang GZ, Mohiaddin RH, Firmin DN, and Longmore DB. Helical and retrograde secondary flow patterns in the aortic arch studied by three-directional magnetic resonance velocity mapping. *Circulation*, 88(5 Pt 1):2235–47, 1993.
- [49] Suo J, Oshinski J, and Giddens DP. Effects of wall motion and compliance on flow patterns in the ascending aorta. *J Biomech Eng*, 3(125):347–354, 2003.
- [50] Muzzarelli S, Ordovas KG, Hope MD, Meadows JJ, Higgins CB, and Meadows AK. Diagnostic value of the flow profile in the distal descending aorta by phase-contrast magnetic resonance for predicting severe coarctation of the aorta. *J Magn Reson Imaging*, 6(33):1440–1146, 2011.
- [51] Adrian RJ. Particle-imaging techniques for experimental fluid mechanics. *Annu. Rev. Fluid Mech.*, 23:261–304, 1991.
- [52] Hong GR, Pedrizzetti G, Tonti G, Li P, Wei Z, Kim JK, Baweja A, Liu S, Chung N, Houle H, Narula J, and Vannan MA. Characterization and quantification of vortex

- flow in the human left ventricle by contrast echocardiography using vector particle image velocimetry. *JACC Cardiovasc Imaging*, 1(6):705–717, 2008.
- [53] Zhang F, Lanning C, Mazzaro L, Barker AJ, Gates PE, Strain WD, Fulford J, Gosling OE, Shore AC, Bellenger NG, Rech B, Chen J, Chen J, and Shandas R. In vitro and preliminary in vivo validation of echo particle velocimetry in carotid vascular imaging. *Ultrasound Med. Biol.*, 37(3):450–464, 2011.
- [54] Shipkowitz T, Rodgers VGJ, Frazin LJ, and Chandran KB. Numerical study on the effect of secondary flow in the human aorta on local shear stresses in abdominal aortic branches. *J Biomech*, 33(6):717–728, 2000.
- [55] Hugh AE and Fox JA. The precise localisation of atheroma and its association with stasis at the origin of the internal carotid artery—a radiographic investigation. *Br J Radiol*, 43(510):377–83, 1970.
- [56] Lautrup B. *Physics of continuous matter: Exotic and everyday phenomena in the macroscopic world*. Taylor & Francis, 2005.
- [57] Papathanasopoulou P, Zhao SZ, Kohler U, Robertson MB, Long Q, and Hoskins P. Mri measurement of time-resolved wall shear stress vectors in a carotid bifurcation model, and comparison with cfd predictions. *J Magn Reson Imaging*, 17(2):153–162, 2003.
- [58] Marshall I, Papathanasopoulou P, and Wartolowska K. Carotid flow rates and flow division at the bifurcation in healthy volunteers. *Physiological Measurement*, 25:691–697, 2004.
- [59] Markl M, Wallis W, and Harloff A. Reproducibility of flow and wall shear stress analysis using flow-sensitive four-dimensional mri. *J Magn Reson Imaging*, 33(4):988–94, 2011.
- [60] Biegling ET, Frydrychowicz A, Wentland A, Landgraf BR, Johnson KM, Wieben O, and Francois CJ. In vivo three-dimensional mr wall shear stress estimation in ascending aortic dilatation. *J Magn Reson Imaging*, 33(3):589–97, 2011.
- [61] Liu L, Zheng H, Williams L, Zhang F, Wang R, Hertzberg J, and Shandas R. Development of a custom-designed echo particle image velocimetry system for multi-component hemodynamic measurements: system characterization and initial experimental results. *Phys. Med. Biol.*, 5(53):1397–1412, 2008.

- [62] Niu L, Qian M, Wan K, Yu W, Jin Q, Ling T, Gao S, and Zheng H. Ultrasonic particle image velocimetry for improved flow gradient imaging: algorithms, methodology and validation. *Phys. Med. Biol.*, 7(55):2103–2120, 2010.
- [63] Tublin ME, Bude RO, and Platt JF. Review. The resistive index in renal Doppler sonography: Where do we stand? *AJR Am J Roentgenol*, 180(4):885–92, 2003.
- [64] Bland JM and Altman DB. Comparing methods of measurement: why plotting difference against standard method is misleading. *Lancet*, 346(8982):1085–1087, 1995.
- [65] Baschelet E. *Circular statistics in biology*. London: Academic Press, 1981.
- [66] Kristoffer L. Hansen. *In-vivo studies of new vector velocity and adaptive spectral estimators in medical ultrasound*. PhD thesis, department of Radiology, Rigshospitalet, Denmark, 2009.
- [67] Hansen KL, Udesen J, Gran F, Jensen JA, and Nielsen MB. In-vivo examples of complex flow patterns with a fast vector velocity method. *Ultraschall in der Medizin/European Journal of Ultrasound*, 30:471–476, 2009.
- [68] Cheng C, Tempel D, Haperen RV, Baan AVD, Grosveld F, Daemen MJ, Krams R, and Crom RD. Atherosclerotic lesion size and vulnerability are determined by patterns of fluid shear stress. *Circulation*, 23(113):2744–2753, 2006.
- [69] Lee KL, Doorly DJ, and Firmin DN. Numerical simulations of phase contrast velocity mapping of complex flows in an anatomically realistic bypass graft geometry. *Med Phys*, 33(7):2621–2631, 2006.
- [70] Steinman DA, Thomas JB, Ladak HM, Milner JS, Rutt BK, and Spence JD. Reconstruction of carotid bifurcation hemodynamics and wall thickness using computational fluid dynamics and mri. *Magnet Reson Med*, 49(1):149–159, 2002.
- [71] Zhao SZ, Papathanasopoulou P, Long Q, Marshall I, and Xu XY. Comparative study of magnetic resonance imaging and image-based computational fluid dynamics for quantification of pulsatile flow in a carotid bifurcation phantom. *Ann Biomed Eng*, 31(8):962–971, 2003.

Appendix 1: Journal paper I

● *Original Contribution*

COMPARISON OF REAL-TIME *IN VIVO* SPECTRAL AND VECTOR VELOCITY ESTIMATION

MADS MØLLER PEDERSEN,^{*†} MICHAEL JOHANNES PIHL,[†] PER HAUGAARD,[‡] JENS MUNK HANSEN,[†]
KRISTOFFER LINDSKOV HANSEN,^{*} MICHAEL BACHMANN NIELSEN,^{*} and JØRGEN ARENDT JENSEN[†]

^{*}Department of Radiology, Rigshospitalet, Copenhagen, Denmark; [†]Center for Fast Ultrasound Imaging,
Department of Electrical Engineering, Technical University of Denmark, Lyngby, Denmark;
and [‡]B-K Medical A/S, Herlev, Denmark

(Received 15 June 2011; revised 23 August 2011; in final form 9 October 2011)

Abstract—The purpose of this study is to show whether a newly introduced vector flow method is equal to conventional spectral estimation. Thirty-two common carotid arteries of 16 healthy volunteers were scanned using a BK Medical ProFocus scanner (DK-2730, Herlev, Denmark) and a linear transducer at 5 MHz. A triplex imaging sequence yields both the conventional velocity spectrum and a two-dimensional vector velocity image. Several clinical parameters were estimated and compared for the two methods: Flow angle, peak systole velocity (PS), end diastole velocity (ED) and resistive index (RI). With a paired *t*-test, the spectral and vector angles did not differ significantly ($p = 0.658$), whereas PS ($p = 0.034$), ED ($p = 0.004$) and RI ($p < 0.0001$) differed significantly. Vector flow can measure the angle for spectral angle correction, thus eliminating the bias from the radiologist performing the angle setting with spectral estimation. The flow angle limitation in velocity estimation is also eliminated, so that flow at any angle can be measured. (E-mail: mmp@elektro.dtu.dk) © 2012 World Federation for Ultrasound in Medicine & Biology.

Key Words: Transverse oscillation, Blood velocity estimation, Vector flow, Real-time, Spectral estimation, *In vivo*.

INTRODUCTION

Spectral velocity estimation

Estimation of blood velocities with ultrasound is widely used for clinical evaluation. Investigation of the systemic arteries are performed during several cardiac cycles to form the spectrogram as shown in Figure 1, where the temporal evolution of the blood velocity distribution is depicted (Jensen 1996). The scanner software tracks the maximum velocities and finds the velocity at peak systole (PS) and at end diastole (ED) for every cardiac cycle (Evans et al. 1989). Using the estimates from the past 8 s of data, the average PS velocity and the average ED velocity are found and updated continuously as shown in Figure 2. From the axial velocities at PS and ED, the resistive index (RI) is calculated using (Tublin et al. 2003):

$$RI_{To} = \frac{PS_{To} - ED_{To}}{PS_{To}} \quad (1)$$

Thus, conventional spectral RI is calculated without angle correction.

Clinical use

The PS, ED and RI are used to diagnose several haemodynamic diseases. In renal artery stenosis (Radermacher et al. 2001), both PS and RI are increased and the spectrogram waveform is changed (Radermacher et al. 2001; Krumme, 2006). The spectral estimation is also used as a tool to diagnose conditions such as pulmonary hypertension (Lanzarini et al. 2005), restrictive liver conditions (Görg et al. 2002; Westra et al. 1995), pressure gradients of the aortic valve (O'Boyle et al. 1996; Jassal et al. 2008) and increased resistance in the umbilical artery (Wood et al. 2010) among many other applications.

Angle correction

All of the methods assume reliable velocity estimates at proper angles of insonation. However, the spectral estimation only estimates velocities for blood moving toward or away from the transducer surface along the ultrasound beam (Jensen 1996). As only velocities

Address correspondence to: Mads Møller Pedersen, Department of Radiology X-2023, Blegdamsvej 9, 2100 Copenhagen, Rigshospitalet, Denmark. E-mail: mmp@elektro.dtu.dk

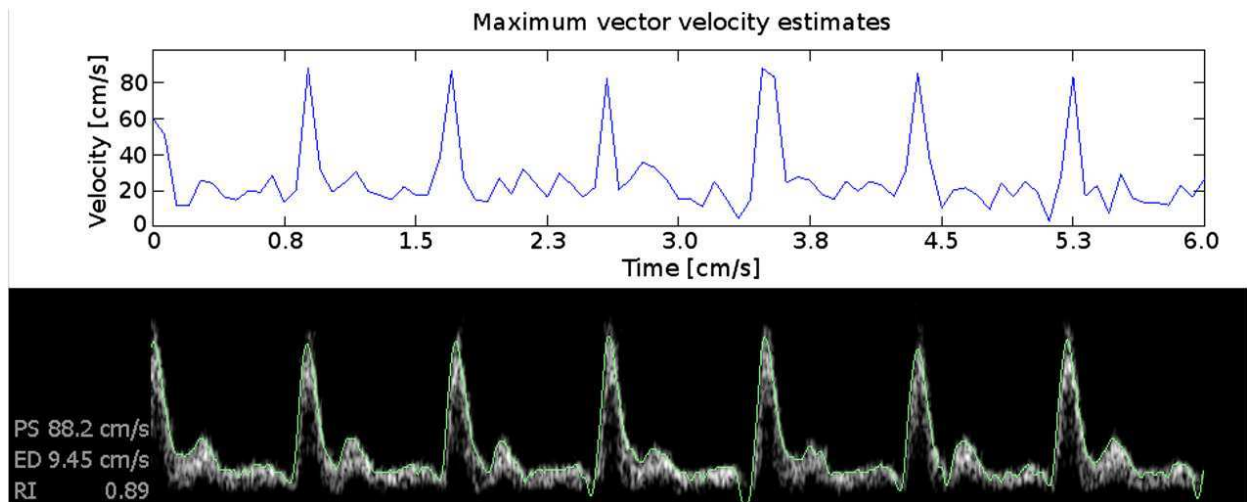


Fig. 1. Spectrogram (bottom) shows the spectral data over time. The maximum value is traced by the scanner software (green line) and used to estimate the peak systole (PS) velocity and end diastole (ED) velocity. From simultaneously obtained vector data, the “vectogram” (top) shows the maximum vector velocity estimate over time.

directly along the ultrasound beam, v_z , are measured, the true velocity has to be angle corrected. The true velocity magnitude of the blood, $|v|$, is estimated using the angle correction:

$$|v| = \frac{v_z}{\cos \theta} = \frac{f_{pd}c}{2f_0 \cos \theta} \quad (2)$$

where θ is the flow angle between the ultrasound beam and the blood velocity direction, f_p is the estimated frequency, f_0 is the center frequency of the emitted ultrasound pulse and c is the speed of sound (Jensen 1996; Evans et al. 1989).

The accuracy of the angle correction depends on the actual angle. For angles above 60° , even a slight error in

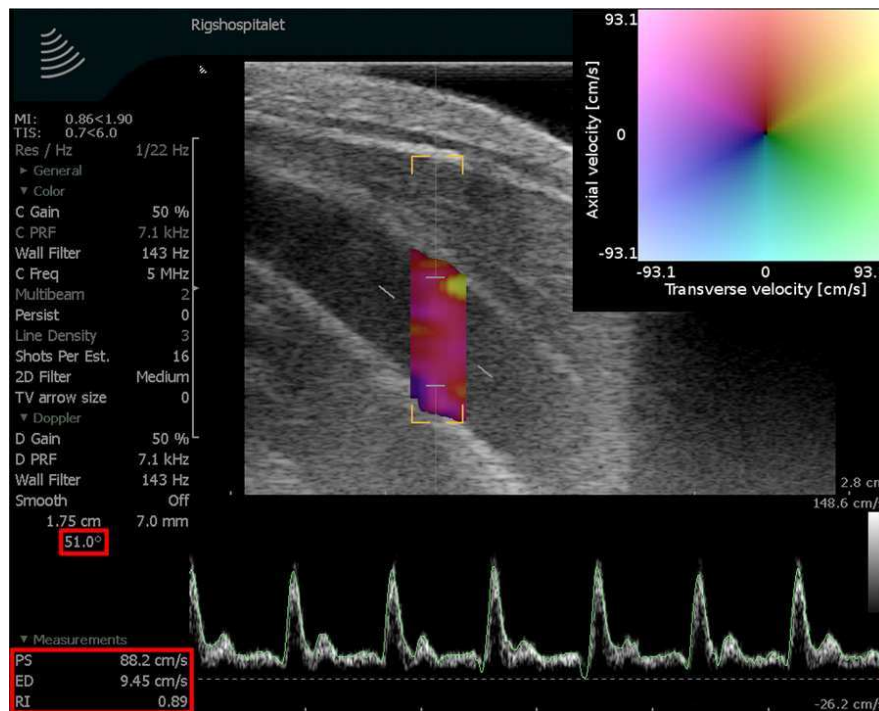


Fig. 2. Simultaneous data acquisition using spectral estimation and transverse oscillation. The manually set flow angle and the spectral estimation results are marked in red at the lower left of the image. The color encoded vector values are decoded using the color map shown in the top, right corner as explained in Figure 3.

the assumed angle can give rise to large velocity errors (Hoskins and Thrush 2003). Thus, the operator is encouraged to visualize the vessel of interest at a flow angle within 60° (Kruskal *et al.* 2004). Moreover, estimating velocities at 90° is not possible with spectral velocity estimation, as no useful signal is received at this angle where $\cos(90^\circ) = 0$. Current spectral velocity estimation, thus, assumes that a fixed angle exists and the transducer and imaging direction can be manipulated to yield an acceptable angle. In many cases, this is not true as the angle will vary with spatial position and over the cardiac cycle (Udesen *et al.* 2007) for complex geometries like bifurcations or valves and for affected vessels containing *e.g.*, atherosclerosis. There is, thus, a need for methods, which are angle independent and can yield correct velocities for any angle as a function of time.

Transverse oscillation

The ultrasound vector technique, transverse oscillation (TO), can yield both the axial and transverse velocity components at the same time. Here, a conventional Doppler ultrasound pulse is transmitted (Jensen and Munk 1998). The received echos are beamformed with special processing to yield three beams in parallel. One uses conventional beamforming and is used for estimating the axial velocity, v_z , and the other two beams are used for estimating the transverse velocity component, v_x . Thus, the two-dimensional (2-D) velocity vector is determined and, from this, the velocity angle, θ , and magnitude, $|v|$, can be determined by:

$$\theta = \arctan(v_x, v_z) \quad (3)$$

$$|v| = \sqrt{v_x^2 + v_z^2}. \quad (4)$$

The approach relies on creating a double oscillating field during the receive beamforming as well as two dedicated estimators for determining the two velocity components. It is further described in (Jensen and Munk 1998; Jensen 2000). Further details on the application and accuracy of the approach are given by Udesen and Jensen (2006) and Udesen *et al.* (2007).

Purpose

The purpose is to show whether vector velocity imaging gives correct angles and velocities *in vivo* and whether the approach, therefore, can supplement or substitute spectral estimation. Two methods for blood velocity estimation are compared: Spectral velocity estimation and the vector technique, TO. The set-up is optimized for the conventional method (spectral velocity estimation).

Whether the flow angle, PS velocity, ED velocity and the RI are estimated equally well for the two tech-

niques were investigated. This study is the first performed with the commercial implementation of the TO technique.

MATERIALS AND METHODS

Data acquisition

Sixteen healthy volunteers, aged 24 to 47, years participated in this study (5 men and 11 women) and both of their common carotid arteries were scanned. This prospective study was performed after approval by The Danish National Committee on Biomedical Research Ethics (J.nr: [KF]07307579) and informed consent was received from each participant in the study. A commercial ultrasound scanner (ProFocus Ultraview; BK Medical, DK-2730, Herlev, Denmark) and a multifrequency imaging transducer was used at 5 MHz (Type: 8670; BK Medical). Prototype software on the scanner was used. Simultaneous data acquisition with spectral velocity estimation and vector flow were selected in the scanner software for triplex imaging. The scan settings were optimized for spectral velocity estimation: The right common carotid artery of each volunteer was scanned longitudinally, the center of the artery was located and the flow angle was kept below 60° . Tilting of the ultrasound beam was not available with the prototype software. Instead, the transducer was tilted on the skin surface to obtain this blood flow angle. As seen in Figure 2, only the part of the transducer still in contact with the skin was used to obtain data. In some cases, the gel layer was visible.

The entire vessel diameter was covered by the range gate area as shown in Figure 2. A maximum scan depth of 2.8 cm was selected. The maximum temporal resolution allowed by the scanner was 14.8 frames per second. For each volunteer, an AVI video sequence of 166 frames covering 11.2 s was obtained. All image frames were used for TO postprocessing to obtain the axial and transverse velocity components.

Velocity data

Identical settings of the pulse repetition frequency (PRF), the wall filter, the gain and smoothing filter were used for spectral and vector estimation and the settings are listed in Table 1. For each volunteer, the PRF was adjusted manually to avoid aliasing.

Just prior to data acquisition, the spectrogram was used to monitor PW aliasing. Color mixtures representing opposite directed vectors were used to indicate TO aliasing. Data was only obtained when both methods did not indicate aliasing. Furthermore, postprocessing of the axial and the transverse TO velocity components were used for plotting each component over time. A sudden change in sign indicates aliasing and was not found in any of the datasets.

Table 1. Scan parameters set for both spectral and vector estimation

Scan parameters	Values
Pulse repetition frequency	7.1, 9.2 kHz
Wall filter	143, 184 Hz
Gain	50%
Shots per estimate (TO)	16
Range gate diameter	7, 8 mm
Scan depth	[1.43, 2.27] cm

The wall filter was adjusted manually to avoid artifacts from movements of the surrounding tissue. The blood flow angle for spectral estimation was set visually by the radiologist as in a routine examination. The spectral PS velocity, ED velocity and RI were calculated in real-time by the scanner software.

The color box for vector flow data acquisition was set to cover the range gate area. The height of the color box was not allowed smaller than shown in Figure 2 by the prototype software. Only vector data within the vessel were used.

Velocity estimation

The maximum spectral velocity estimates are used by the scanner software to calculate the PS, ED and RI continuously based on the past 8 s of axial velocity estimates, v_z (Tublin et al. 2003). Vector flow data was encoded as coloured pixels. With an in-house Matlab script and a circular color map, the color data was decoded into vector data as shown in Figure 3 from the AVI data. Thus, each coloured pixel was represented by a vector with an axial and a transverse component. The flow angle, θ , and the velocity magnitude, $|v|$, are calculated using the axial, v_z , and transverse, v_x , vector components shown in eqn (3) and eqn (4). Vector flow data from the center part of the vessels (50% of their diameter) were used in calculating the values to avoid effects introduced by the echo canceling at the vessel boundary. The maximum velocity within the vessel for each frame shown in Figure 4 was selected for further analysis. The average peak value was calculated as the vector flow peak systole (PS_{TO}) value for each volunteer. Before each peak, the lowest velocity was found. The mean of all the low velocities was calculated for each volunteer as the vector flow end diastole (ED_{TO}) velocity. The vector flow resistive index (RI_{TO}) was calculated by eqn (1).

Statistical analysis

The two methods were compared on each of the four parameters using paired t -test analysis and Bland-Altman analysis and plots. The null-hypothesis tested with the paired t -test states that the mean difference between the two methods does not differ from a normal distribution

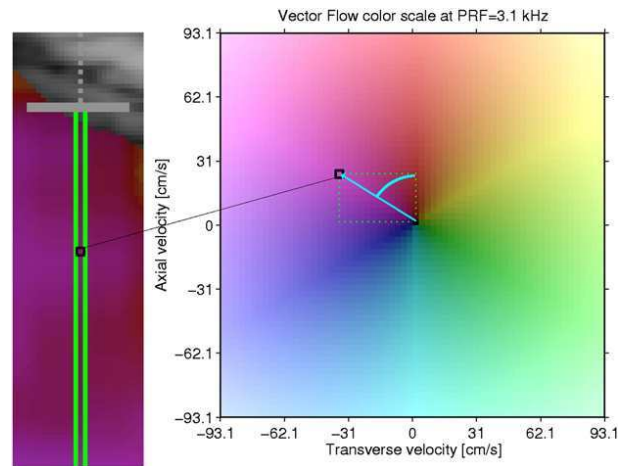


Fig. 3. The range gate covering the whole vessel diameter is shown in the right graph. The pixel values of the central line are used for the vector flow estimates. The color values of each pixel contain the encoded vector information used for the vector flow method.

with a mean of zero. For each parameter, a p value, the confidence interval at 95% significance level and the standard deviation was calculated; $p < 0.05$ was considered significant, meaning that the two methods differs significantly.

The difference between the two methods as a function of the average estimate was calculated for each parameter and a Bland-Altman plot was made for each parameter as shown in Figure 5. In all the plots, zero is within the limits of agreement indicating that the measurements were not biased but only distributed as expected for biologic measurements.

The amount that the vector velocity deviates from the spectral velocity, dif_{vector} , was calculated as:

$$dif_{vector} = \left(1 - \frac{v_{vector}}{v_{spectral}} \right) * 100, \quad (5)$$

where $v_{vectorPS}$ is the vector PS velocity and $v_{spectralPS}$ is the spectral PS velocity.

Statistical analysis was performed with the program Matlab (ver. R2010a; MathWorks, Natick, MA, USA).

RESULTS

Simultaneous data acquisition with spectral velocity estimation and vector flow estimation were performed on 32 common carotid arteries. The clinical parameters for both methods were calculated: Flow angle, PS, ED and RI. All vector datasets were analysed for aliasing in the axial and the transverse velocity components and no change in sign was seen as an indication of no aliasing.

With Bland-Altman analysis the average difference, the limits of agreement and vector difference were

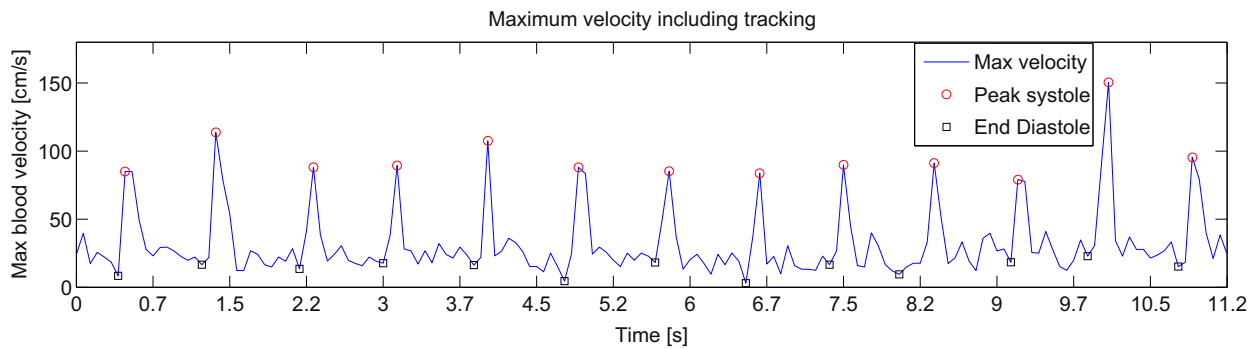


Fig. 4. The maximum vector flow velocity estimate for each frame plotted over time. The peak systole and end diastole are marked.

calculated as shown in Table 2. The Bland-Altman plot for each parameter is shown in Figure 5.

The paired *t*-tests of the difference between the two methods have been performed for each of the four parameters as shown in Table 3. The flow angle was not significantly different for the two methods ($p = 0.658$), whereas the PS velocity ($p = 0.034$), ED velocity ($p = 0.004$) and RI ($p < 0.0001$) differed significantly. The 95% confidence interval and the standard deviation for each parameter calculated for the flow angle PS velocity, at ED velocity and for the RI and are shown in Table 3.

DISCUSSION

Flow angle

The flow angle did not differ significantly for the two methods and the average vector angle was 4% lower compared with the spectral angle as seen in Table 2. Thus, vector flow can be used to calculate the flow angle instead of the manually set angle by a radiologist with the conventional spectral estimation. The main advantage of the vector method is the independence of the flow direction, where the radiologist is no longer needed to set an angle used for angle correction.

As the movement in any direction can be measured, the shape of the vessel is no longer required to be a straight tube containing blood that moves in only one direction at any time during the cardiac cycle. The velocity and direction of the blood can be measured on non-straight vessels

and the spatial and temporal velocity profile can be obtained. Thus, further details can be obtained of the movement and velocity of the blood in the carotid bulb, the abdominal aorta, and in conditions such as carotid artery stenosis and renal artery stenosis, and, also, where the velocity magnitude and direction changes as a function of space and time.

Temporal information

In this study, the vector data was calculated and displayed in real-time as in normal color flow mode. The temporal resolution was, however, limited from the triplex imaging showing 14.8 frames per second. This is caused by two main effects: The triplex mode and the vector data estimation. The triplex mode requires spectral, vector velocity and the B-mode data to be received before the image data are calculated. With vector flow 16 shots are used per estimate, which also contributes to a lower temporal resolution. However, the aliasing limit for vector flow is higher than with spectral estimation. Thus, higher velocities can be estimated at a lower pulse repetition frequency with vector flow than with spectral estimation.

Peak systole velocities

Tracking of the PS was performed with Matlab and the peaks are clearly distinct in the signal (Fig. 4). However, the true peaks may be located between two measurements at a low temporal resolution, leading to

Table 2. Bland Altman analysis of the clinical parameters: Flow angle, peak systole (PS), end diastole (ED) and resistive index (RI)

Parameter	Angle	PS	ED	RI
Average difference	2.1°	6.9 cm/s	-3.3 cm/s	0.1
Limits of agreement	[-10.2, 14.4]°	[-27.6, 41.5] cm/s	[-12.2, 5.6] cm/s	[-0.1, 0.2]
Vector difference	4%	8%	-27%	10%

The vector difference is the average difference divided by the average spectral estimate times 100. The limits of agreement are shown in absolute numbers.

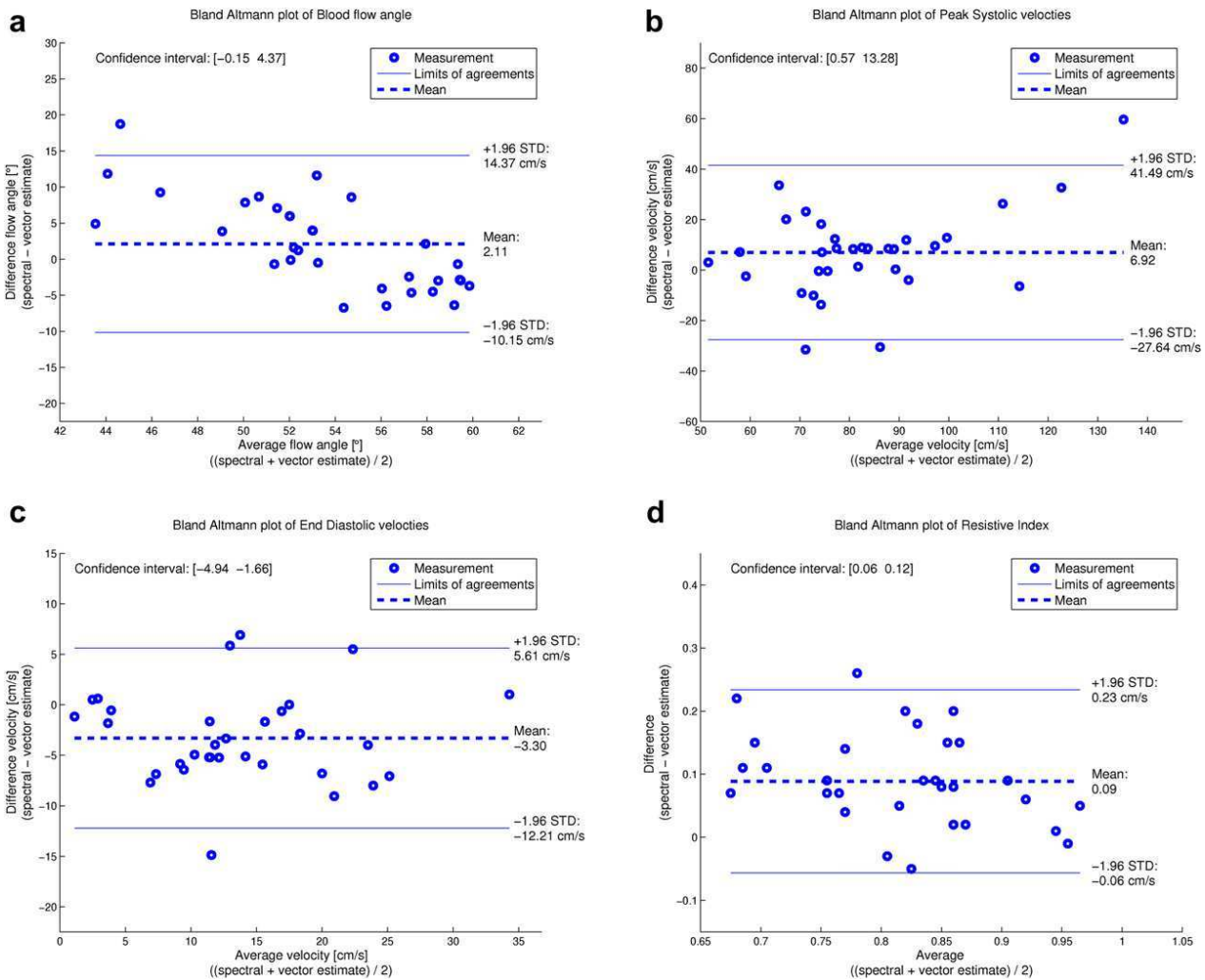


Fig. 5. Bland-Altman plots for 32 measurements of the common carotid artery. The flow angle (a), peak systole velocity (b), end diastole velocity (c) and the resistive index (d) are illustrated.

a lower peak velocity. Thus, the “true” average PS may be higher than estimated with this study and may have contributed to the difference of 8% as shown in Table 3 between the vector and the spectral estimates. It should also be noted that finding the peak velocity in the spectrum depends on a number of choices for defining what the peak value is in a spectrum. The TO estimator finds the mean velocity within a pulse length and then finds the peak values over the range gate. This is slightly different than finding the peak value in the spectrum calculated over the range gate.

End diastole velocities

The ED velocities differed significantly and the vector flow is on average 27% higher than the spectral estimates. The limited temporal resolution may also have caused the true ED velocities to be missed in between two frames as mentioned for the PS velocities.

The PRF was optimised to allow peak velocities with no aliasing, thus, impairing the measurement of the low velocities. The error of vector flow estimates at low velocity is higher than the error at high velocity due to the echo canceling filter (Jensen 1996). This was

Table 3. Paired *t*-test of the hypothesis that the spectral and vector data came from the same distribution

Parameter	Angle	PS	ED	RI
P	0.658	0.034*	0.0004*	<0.0001*
Confidence interval	[-0.2, 4.4]°	[0.6, 13.3] cm/s	[-4.9, -1.7] cm/s	[0.06, 0.12]
Std of the difference	6.26°	17.64 cm/s	4.55 cm/s	0.07

Each parameter was tested and a *p* < 0.05 was considered significant and marked with*.

not adjusted for in this study. Thus, the flow angle calculation and the velocity estimation of areas with low velocity may have influenced the result too much. A weighting according to the error size might decrease the standard deviation of the velocity estimates. Also, the calculation of the minimum value is different for the two methods as the ED is calculated as the lowest value between two peaks, whereas the ED_{TO} is tracked as the lowest value before each peak.

Vector flow limitations

At present, the prototype scanner software only supports the multifrequency imaging transducer (Type: 8670; BK Medical) used for this study. Thus, the system is currently limited to a scan depth of 4–5 cm. The AVI files are limited in frame rate and length and, thus, not suitable for clinical studies where more detailed data over a longer period is needed. The system is at present also being developed to support curved array and phased array transducers for abdominal imaging.

Clinical use

The clinical use of velocity estimates today is limited by the angle correction $<60^\circ$ and influenced by the manual angle setting by the radiologist. With an equally good method without these limitations, the clinical velocity estimation is possible at any angle. The radiologist will also be able to scan at locations where the flow angle is $>60^\circ$ such as perpendicular to the carotid artery. With vector flow, the clinical examination of the blood velocity may only require the radiologist to locate the vessel as there is no need for manual angle setting and there is no angle limitation. In a clinical perspective, this may provide more accurate measurements as the bias from the angle setting is eliminated. The examination time may also be shorter as the radiologist must perform fewer tasks.

CONCLUSIONS

The absolute velocities and angles are directly available with vector flow. Statistical analysis of simultaneously acquired spectral and vector data has been performed on the clinical parameters: Flow angle, PS, ED and RI. The flow angle does not differ significantly and may consequently be estimated using vector flow instead of a manual setting by the radiologist.

In conclusion, vector flow is comparable to spectral velocity estimation regarding the flow angle on the

common carotid artery and, thus, a potential better angle setting alternative for such velocity estimation.

Acknowledgments—The authors would like to thank M.D. Søren Heerwagen (Department of Radiology, Rigshospitalet, Denmark) for useful discussions about the statistical methods used for this study.

REFERENCES

- Evans D, McDicken WN, Skidmore R, Woodcock JP. Doppler ultrasound: Physics, instrumentation, and clinical applications. Chichester, UK: John Wiley & Sons; 1989.
- Görg C, Riera-Knorrenschild J, Dietrich J. Pictorial review: Colour Doppler ultrasound flow patterns in the portal venous system. *Br J Radiol* 2002;75:919–929.
- Hoskins P, Thrush A. Diagnostic ultrasound: Physics and equipment. New York: Cambridge University Press; 2003.
- Jassal DS, Tam JW, Dumesnil JG, Giannoccaro PJ, Jue J, Pandey AS, Joyner CD, Teo KK, Chan KL. Clinical usefulness of tissue Doppler imaging in patients with mild to moderate aortic stenosis: A sub-study of the aortic stenosis progression observation measuring effects of rosuvastatin study. *J Am Soc Echocardiogr* 2008;21:1023–1027.
- Jensen JA. Estimation of blood velocities using ultrasound: A signal processing approach. New York: Cambridge University Press; 1996.
- Jensen JA. Algorithms for estimating blood velocities using ultrasound. *Ultrasonics* 2000;38:358–362.
- Jensen JA, Munk P. A new method for estimation of velocity vectors. *IEEE Trans Ultrason Ferroelectr Freq Control* 1998;45:837–851.
- Krumme B. Renal Doppler sonography—Update in clinical nephrology. *Nephron Clin Pract* 2006;103:c24–c28.
- Kruskal JB, Newman PA, Sammons LG, Kane RA. Optimizing Doppler and color flow us: Application to hepatic sonography. *Radiographics* 2004;24:657–675.
- Lanzarini L, Fontana A, Campana C, Klersy C. Two simple echo-Doppler measurements can accurately identify pulmonary hypertension in the large majority of patients with chronic heart failure. *J Heart Lung Transplant* 2005;24:745–754.
- O'Boyle MK, Vibhakar NI, Chung J, Keen WD, Gosink BB. Duplex sonography of the carotid arteries in patients with isolated aortic stenosis: Imaging findings and relation to severity of stenosis. *AJR Am J Roentgenol* 1996;166:197–202.
- Radermacher J, Chavan A, Bleck J, Vitzthum A, Stoess B, Gebel MJ, Galanski M, Koch KM, Haller H. Use of Doppler ultrasonography to predict the outcome of therapy for renal-artery stenosis. *N Engl J Med* 2001;344:410–417.
- Tublin ME, Bude RO, Platt JF. Review. The resistive index in renal Doppler sonography: Where do we stand? *AJR Am J Roentgenol* 2003;180:885–892.
- Udesen J, Jensen JA. Investigation of transverse oscillation method. *IEEE Trans Ultrason Ferroelectr Freq Control* 2006;53:959–971.
- Udesen J, Nielsen MB, Nielsen KR, Jensen JA. Examples of *in vivo* blood vector velocity estimation. *Ultrasound Med Biol* 2007;33:541–548.
- Westra SJ, Zaninovic AC, Vargas J, Hall TR, Boechat MI, Busuttill RW. The value of portal vein pulsatility on duplex sonograms as a sign of portal hypertension in children with liver disease. *AJR Am J Roentgenol* 1995;165:167–172.
- Wood MM, Romine LE, Lee YK, Richman KM, O'Boyle MK, Paz DA, Chu PK, Pretorius DH. Spectral Doppler signature waveforms in ultrasonography: A review of normal and abnormal waveforms. *Ultrasound Q* 2010;26:83–99.

Appendix 2: Journal paper II

Novel flow quantification of the carotid bulb and the common carotid artery with vector flow ultrasound

Mads Møller Pedersen¹, Michael Johannes Pihl², Per Haugaard³, Kristoffer Lindskov Hansen¹,
Theis Lange⁴, Lars Lönn¹, Michael Bachmann Nielsen¹, Jørgen Arendt Jensen²

¹Department of Radiology, Rigshospitalet, 2100 Copenhagen, Denmark

²Center for Fast Ultrasound Imaging, Technical University of Denmark, 2800 Lyngby, Denmark

³B-K Medical A/S, Mileparken 34, 2730 Herlev, Denmark

⁴Department of Biostatistics, University of Copenhagen, Denmark

Abstract

Purpose:

With conventional Doppler ultrasound the flow patterns in the blood can be visualised. The laminar flow pattern in the common carotid artery (CCA) differs from the disturbed flow pattern in the carotid bulb (CB). Conventional ultrasound methods can not quantify disturbed flow. This work aims to quantify a threshold value for the flow patterns of the common carotid artery and the carotid bulb with vector ultrasound technique.

Materials and Methods:

With vector flow ultrasound the carotid bifurcation of eight volunteers were scanned. A commercial vector flow ultrasound scanner (ProFocus Ultraview, BK Medical, Denmark) was used with a linear transducer at 5 MHz (8670, BK Medical) and prototype Transverse Oscillation vector flow scanner software. The flow patterns of CCA and CB were visually analysed by experts and by quantitative vector calculations. The correlation between the two methods was shown and a quantitative threshold that separates the flow patterns was suggested.

Results:

Eight carotid bifurcations were investigated with both methods with the following results: 1. Moderate inter observer agreement, 2. Significant difference on CCA and CB with both visual evaluations and quantitative measurements, 3. A correlation between the visual evaluations and the quantitative methods, and a quantitative vector concentration threshold of 0.92 is suggested to separate the two flow patterns.

Conclusion:

With a commercial vector flow ultrasound scanner the visibility of disturbed flow in CCA is significantly lower compared to CB. The vector concentration and the mean velocity magnitudes of the CCA flow patterns are both significantly higher compared to CB. A threshold of 0.92 is suggested to separate the CCA from CB quantitatively.

Introduction

Atherosclerosis poses a public health problem because of its high prevalence and increased risk for cardiovascular disease and death. Atherosclerotic plaques consist of a mixture of cells, connective tissue, calcification, lipids and debris compounds. Atherosclerotic changes in the carotid arteries mirror general atherosclerosis, and earlier stages of carotid disease are associated with the risk of stroke, which is the third leading cause of death worldwide. Atherosclerosis has a complex pathogenesis but carotid artery intima media thickness measured by ultrasound has proven to be a risk marker for preclinical atherosclerosis and can identify incident cardiovascular disease. Lesions are predominantly localised in areas with low shear stress while areas of high shear stress are relatively sparse (Bergan and Yao, 1983). Changes in the vessel wall are typically found in relation to branches, twists and bends. In the initial plaque development there is a compensatory enlargement of the artery to accommodate the plaque while maintaining flow (Lin et al., 2008).

The flow patterns of the common carotid artery (CCA) and carotid bulb (CB) have long been investigated as the bifurcation is one of the most frequent sites for cerebrovascular disease occurrence (Samuel, 1956; Peterson et al., 1960; Hugh and Fox, 1970; Fuster et al., 1990). Morphological criteria have mainly been used, while duplex classification of stenosis and normal vessels are based on the blood flow velocities.

The peak Doppler frequency and spectral broadening index presented by Kassam et al. (1982) have been correlated to the degree of carotid stenosis (Brown et al., 1982) and with Doppler velocity analysis complex flow changes have been located at the carotid bulb (Phillips et al., 1983). However, no quantitative calculations on flow complexity are available with conventional ultrasound systems and thus, complexity is not used for clinical diagnosis or prognosis. Moreover, the conventional methods are not able to visualize movement perpendicular to the ultrasound beam as only the axial velocities are obtained (Jensen, 1996; Evans et al., 1989). Thus, quantitative data such as the flow directions and the transverse velocity magnitudes are not directly available. With the vector ultrasound technique, Transverse Oscillation, the blood velocities of both the axial and the transverse directions are obtained. This technique demonstrates vortex formation in CB during systole in experiment setups (Udesen et al., 2007, Hansen et al., 2009, Hansen et al., 2011).

The aims of this study are to visualize and calculate the presence of disturbed flow patterns in CCA and CB, and to compare visual evaluation and quantitative calculations using a commercially available ultrasound scanner equipped with the vector velocity technique. The null-hypothesis was that the CCA and CB could not be distinguished using the vector technique.

Materials and Methods

Data acquisition

The carotid bifurcation of eight healthy volunteers (5 men, 3 women, age 28-45, median 39.5 years) was scanned in a longitudinal plane with vector flow ultrasound as shown in Fig. 1. At a frame rate of 22 frames per second, one cardiac cycle was obtained for each volunteer covering 17, 19, 22, 22, 20, 19, 22, and 23 image frames respectively. The number of frames fluctuated due to different heart rates. A total of 164 image frames were used in this study where the CCA and CB areas were outlined on every image frame as shown in Fig. 2. These areas were used for expert evaluation and for quantitative vector calculation. A commercial vector flow ultrasound scanner (ProFocus Ultraview, BK Medical, Denmark) was used with a linear transducer at 5 MHz (8670, BK Medical) and prototype Transverse Oscillation vector flow scanner software. The Transverse Oscillation vector technique is described in details by Munk (1996), Munk (2000), Jensen (Priority date: April 2000), Jensen and Munk (1998), Jensen (2001), and Udesen and Jensen (2006).

Expert evaluation

An in-house PHP web interface and a MySQL database were used to present the 164 images in random order and to store the evaluations. The flow directions and velocity magnitudes were presented as the direction and length of the white vectors shown in Fig. 1. Each frame was presented to five ultrasound experts individually evaluating if disturbed flow was present (score 1), or not (score 0) in each of the two areas. An example is shown in Fig. 2. For each volunteer the mean expert evaluation value and the standard deviation were calculated for CCA and CB as shown in Table 1.

Vector data decoding

The axial and transverse vector velocity magnitudes of the image frames were encoded as coloured pixels shown in Fig. 1. The colour data were decoded into the axial velocity magnitudes, v_z , and the transverse velocity magnitudes, v_x , using an in-house Matlab script and a colour map identical to the map used for encoding by the scanner software. A 2D vector field was thus calculated for each of the two areas in each image frame.

Vector concentration of a 2D vector field

For a vector at position i , the flow angle, θ_i , was calculated in degrees as

$$\theta_i = \arctan(v_{x,i}, v_{z,i}). \quad (1)$$

Each vector angle, t_i , is represented on the unit circle as $p_i = (x_i, y_i)$, where $x_i = \cos(t_i)$ and $y_i = \sin(t_i)$. The mean values of all points were calculated for each 2D vector field as

$$\bar{x} = \frac{1}{n} \cdot \sum_{i=1}^n \cos(t_i), \quad (2)$$

$$\bar{y} = \frac{1}{n} \cdot \sum_{i=1}^n \sin(t_i), \quad (3)$$

where n is the total number of vectors in the 2D vector field.

Simple circular statistics was used to determine if the flow pattern was laminar or disturbed. The resulting vector concentration, r , was found using Pythagoras' theorem,

$$r = \sqrt{\bar{x}^2 + \bar{y}^2}, \quad (4)$$

as illustrated in Fig. 3.

For a perfectly laminar blood flow patterns, r equals one, whereas r increases towards a value of zero with increasing complexity as described by Baschelet (1981).

Equivalent to the standard deviation in linear statistics the dispersion, s , is used in circular statistics. The dispersion of the angles is expressed as the mean angular deviation,

$$s = \sqrt{2 \cdot (1 - r)}, \quad (5)$$

where a perfectly laminar flow pattern ($r=1$) will present zero dispersion, while a perfectly disturbed flow pattern ($r=0$) will result in a maximum dispersion. The mean vector concentration and the dispersion were calculated for each volunteer as shown in Table 2.

Statistical analysis

For each image frame the sum of all CCA and CB evaluations were used for Fleiss Kappa analysis to calculate the level of inter observer agreement, κ , where $\kappa = [0.41 \ 0.60]$ was interpreted as moderate agreement. The mean expert evaluations, the mean vector concentrations, and the mean velocity magnitudes for CCA and CB were tested with Wilcoxon's matched pair test and the null-hypothesis that there was no difference between CCA and CB was tested. $p < 0.05$ was considered significant, thereby rejecting the null-hypothesis.

For each volunteer the mean expert evaluation and the mean vector concentration value was calculated for CCA and CB as shown in Tables 1 and 2 respectively. An example is shown in Fig. 4, and an overview of all volunteers is shown in Fig. 5. At the mean vector concentration where the flow patterns of CCA and CB are separated, threshold value was found.

Results

Vector flow ultrasound imaging of CCA and CB were evaluated visually and quantitatively. The Fleiss Kappa test showed moderate agreement between the experts visual evaluations for CCA ($\kappa=0.42$), and for CB ($\kappa=0.52$). The Wilcoxon's matched pair test rejected the null-hypothesis for both visual evaluation ($p=0.0078$), the mean vector concentration ($p=0.0078$), and the mean vector velocity ($p=0.0078$), meaning that all three methods showed significantly different flow patterns between CCA and CB. The mean visual evaluations, the mean vector concentrations, and the mean vector velocities of CCA and CB were calculated for each volunteer as shown in Tables 1 and 2. The mean visual evaluations were plotted as a function of the mean vector concentrations for CCA and CB as shown in Fig. 6. From the fitted line a mean vector concentration of 0.92 separates the CCA from CB. This is suggested as a threshold value to separate the CCA from the CB flow patterns.

Discussion

This is to our knowledge the first in vivo study where the flow patterns in the CCA and CB are compared visually and quantitatively with the vector flow ultrasound technique. When disturbed flow is defined as a more than 90 degree change in vector angle in part of the cardiac cycle, the vector technique demonstrates the vortex formation in the CB in all healthy volunteers. As this disturbed flow pattern can now be quantified, it needs to be addressed further in atherosclerotic patients to appreciate its possible clinical importance.

However, disturbed flow may be physiological as demonstrated in this study. Theoretically it should occur when there is an abrupt change in vessel diameter like the carotid bulb and potentially at branching of large vessels such as explored in the vicinity of the subclavian artery (Hansen KL, 2009). In the venous system, disturbed flow has also been demonstrated in the femoral and jugular veins at the passage of a venous valve (Hansen KL, 2009; Hansen PM, 2011).

Disturbed flow may also be associated with pathology as plaque formation will lead to a change in the flow pattern and an increase in the blood velocities. Flow velocity changes are commonly used to quantify a stenosis (Arning C, 2010). Disturbed flow may impair the vessel compliance and accelerate the plaque formation. Atherosclerotic manifestations are stenosis, ulcers and aneurysms. Aneurysms develop in the degenerated aorta secondary to atherosclerotic affliction, a multifactorial process which leads to remodeling of the connective tissue in the vessel wall.

Traditionally, utilization of conventional ultrasound has been used in the prognosis of arterial atherosclerosis, since it can detect the vessel wall with its plaque formations in combination of flow characteristics. The endothelium is sensitive to flow-induced stress and can modulate vascular tonus and function, i.e. vasodilatation/vasoconstriction. The characterization of shear stress is of greatest importance for regulation of vascular function. Shear stress, defined as the frictional tangential forces applied on the endothelium is a physiologic process to keep vascular homeostasis. However, increase in shear stress have considerably constrain on vessel wall and cause vasodilatation, i.e. "endothelium-dependent flow-mediated dilatation". Low-density lipoproteins can in itself induce endothelial injury. Flow disturbances with altered shear stress can cause endothelial injury and thus subsequent deposition of lipids.

When disturbed flow was assessed visually there was only moderate agreement when studied by different ultrasound experts. The quantitative vector concentration and the dispersion of the angles eliminate many of these errors and provide better reproducibility. The expert would only be required to select the location of the anatomical area of interest. Such quantitative method would be very suitable for further studies.

Another limitation or error may be attributed to the outlined areas not being filled out with colored vector information during the entire cardiac cycle. This is primarily affected by the pulse

repetition frequency, the echo cancelling filter, and the wall filter. To avoid aliasing, the settings had to be optimised to allow correct measurements at peak velocities during systole and thus, measurements of slower flow during the diastole were compromised. Further support for this view is illustrated in Fig. 4, where two image frames are shown at systole (left frame) and diastole (right frame). At diastole, there is a lack of coloured pixels as compared to systole.

The significant discriminative ability of the vector concentration is of great interest as it is quantitative and simple to calculate. Used in combination with the mean vector velocity also it can clearly discriminate between CCA and CB. However, low velocity is not directly an indication of disturbed flow and is thus suggested as an additive measure to the vector concentration.

The anatomical areas used for defining the vessels varied in size, which for the visual evaluations may have favored the judgement in larger areas in respect to the smaller areas. This problem could have been overcome with boxes of equal pixel numbers. However, the acquired images of both the CCA and the CB structures did not allow for boxes of equal size as the imaged part of CCA was not as large as CB. The difference in the number of pixels was accounted for in the vector concentration calculation and the mean vector velocity by dividing with the number of pixels in (2,3). In the future an automated evaluation of flow type can be developed based on this threshold value.

Conclusion

In conclusion, this study has, for the first time, addressed the initial findings for use of a clinical vector flow ultrasound scanner which can distinguish disturbed flow visually or using a quantification method, the latter being superior to the visual interpretation. Further studies to justify its clinical role needs to be addressed.

Tables

Volunteer	Mean visual evaluation \pm one standard deviation	
	Common carotid artery	Carotid bulb
1	0.13 \pm 0.33	0.79 \pm 0.41
2	0.11 \pm 0.31	0.65 \pm 0.48
3	0.43 \pm 0.50	0.95 \pm 0.21
4	0.05 \pm 0.23	0.61 \pm 0.49
5	0.17 \pm 0.38	0.90 \pm 0.30
6	0.38 \pm 0.49	0.94 \pm 0.24
7	0.13 \pm 0.33	0.94 \pm 0.25
8	0.05 \pm 0.22	0.35 \pm 0.48

Table 1: Visual assessment of disturbed flow in the right common carotid artery and carotid bulb in one cardiac cycle of eight healthy volunteers. Five ultrasound experts individually scored all 164 frame separately in random order for the presence (score 1), or absence (score 0) of disturbed flow.

Volunteer	mean r \pm s		mean v [cm/s]	
	Common carotid artery	Carotid bulb	Common carotid artery	Carotid bulb
1	0.97 \pm 0.22	0.90 \pm 0.39	24.6 \pm 3.4	8.4 \pm 1.6
2	0.96 \pm 0.24	0.88 \pm 0.46	15.6 \pm 2.4	8.3 \pm 1.3
3	0.94 \pm 0.34	0.67 \pm 0.78	13.6 \pm 3.1	4.7 \pm 1.7
4	0.97 \pm 0.22	0.80 \pm 0.61	31.2 \pm 4.8	11.2 \pm 2.1
5	0.96 \pm 0.22	0.84 \pm 0.56	15.1 \pm 3.5	10.4 \pm 2.5
6	0.94 \pm 0.35	0.83 \pm 0.57	17.5 \pm 3.7	11.7 \pm 1.6
7	0.98 \pm 0.17	0.79 \pm 0.63	11.3 \pm 3.2	9.5 \pm 2.2
8	0.98 \pm 0.17	0.89 \pm 0.43	20.0 \pm 4.3	12.3 \pm 2.8

Table 2: Quantification of disturbed flow in the right common carotid artery and carotid bulb in one cardiac cycle of eight healthy volunteers. The mean vector concentrations, the dispersions, and the mean velocities were calculated.

Figures

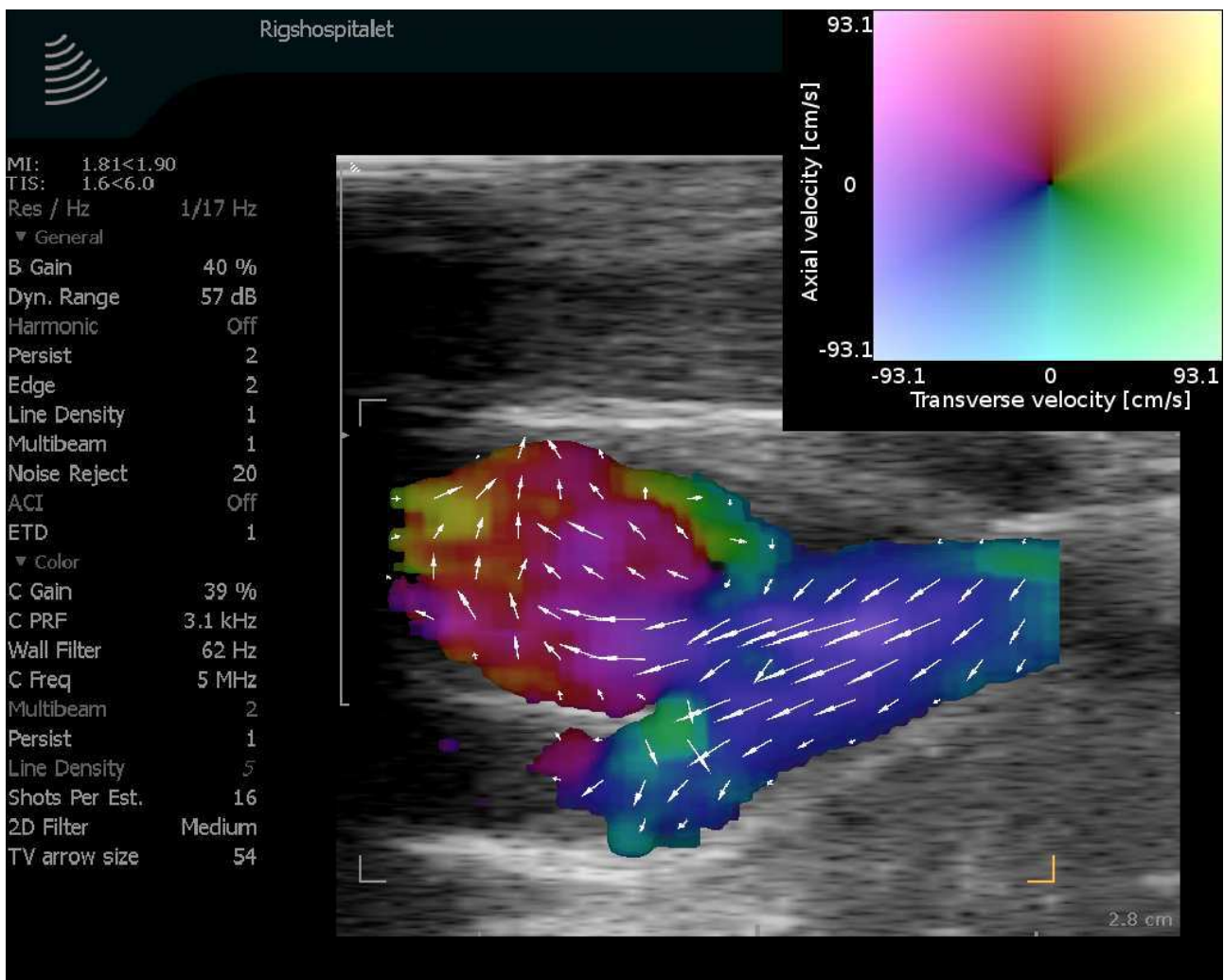


Figure 1: Image frame demonstrating vector flow ultrasound at the carotid bifurcation using a commercial ultrasound scanner. The common carotid artery is to the right, the carotid bulb to the left. The white vectors illustrate the velocity magnitude and direction of the blood. The colour scale used is inserted in the upper right corner for illustration. The vectors were used for the visual assessment method, the coloured pixels for the quantification method.

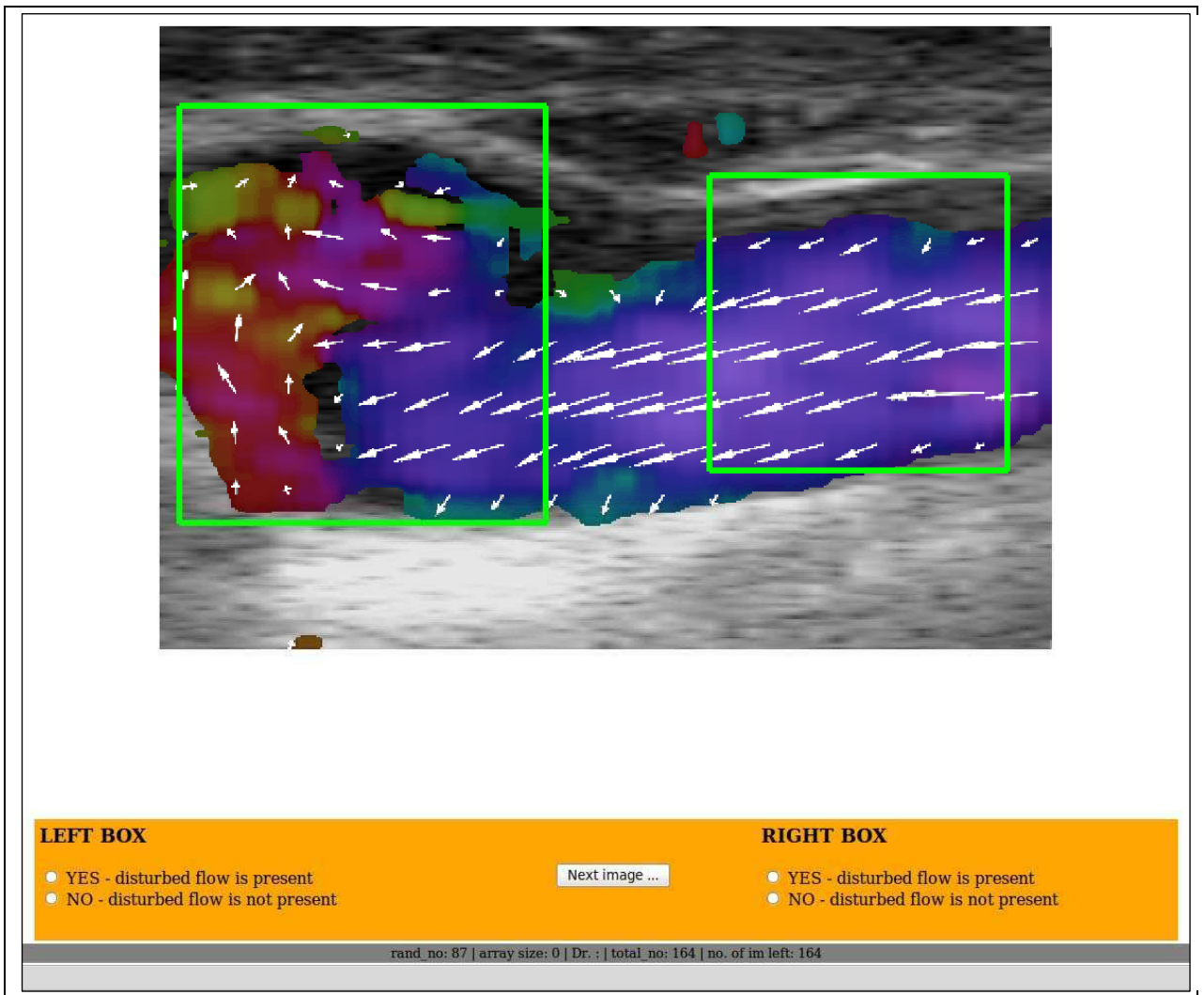


Figure 2: Demonstration of an image frame used for visual assessment by ultrasound experts. The cropped image included two outlined areas. The green boxes define the common carotid area (right) and carotid bulb (left). Each of the 164 frames available from the eight volunteers was presented randomly to the experts using a web interface.

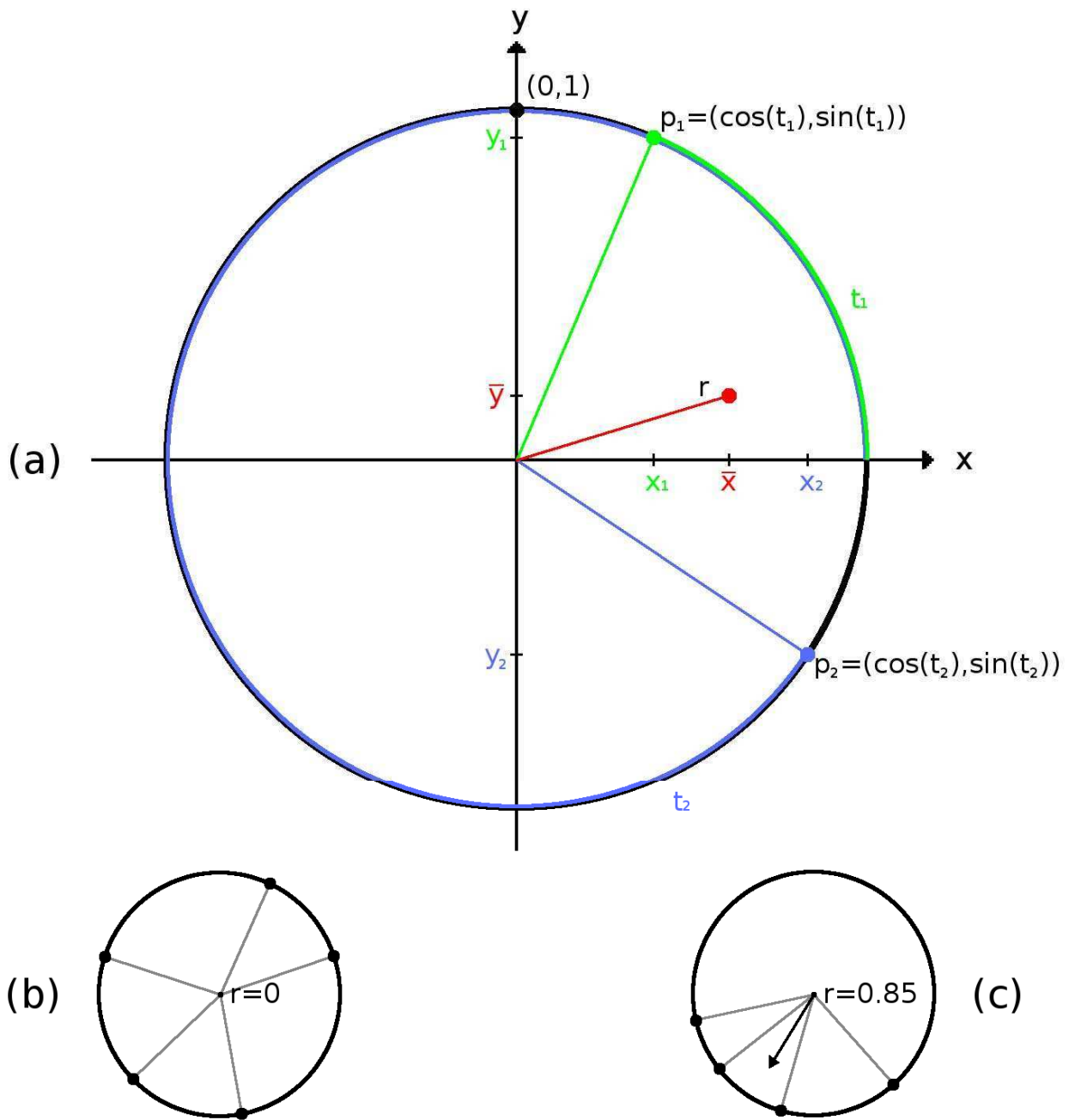


Figure 3: Three unit circle plots. (a): Example, where the vector concentration, r (red line), is calculated for a vector field of two vectors, p_1 (green) and p_2 (blue). The mean x and y values are used to calculate the length which is the vector concentration, r . (b): Perfect dispersion, where $r=0$ for a vector field of five vectors. (c): The vector concentration increases at higher point concentration.

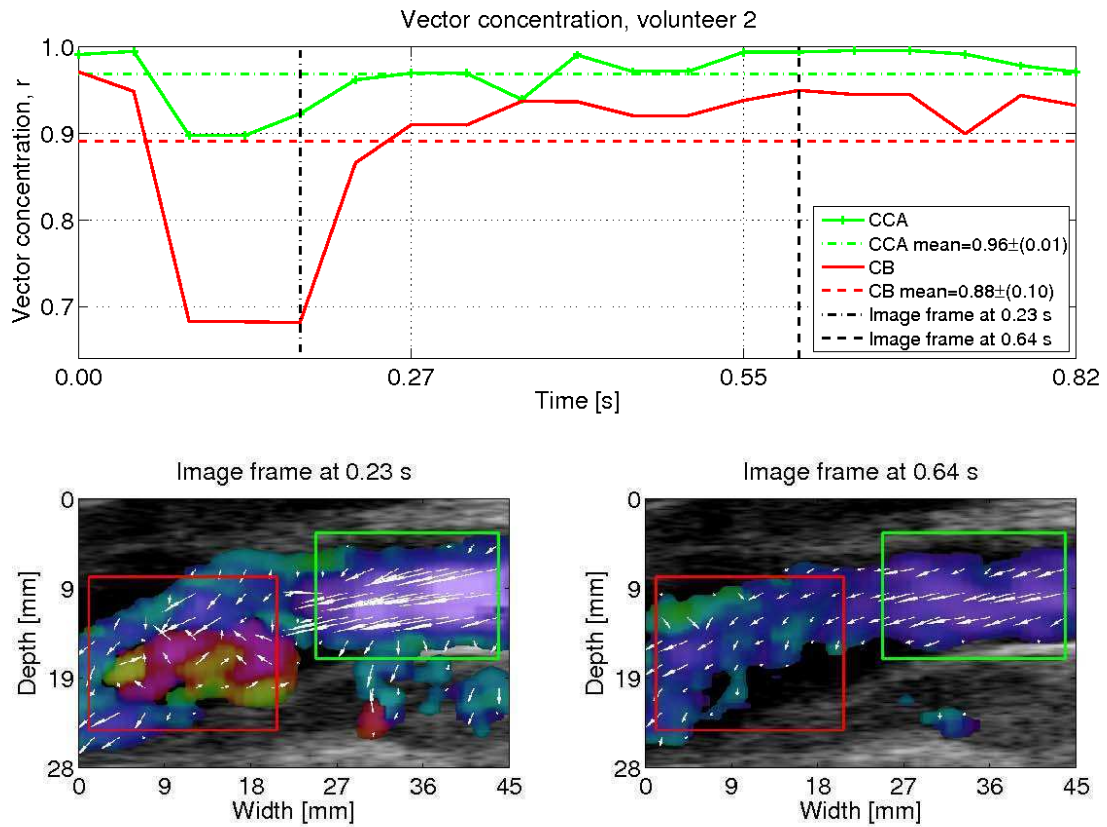


Figure 4: Vector flow data of the carotid bifurcation for volunteer 2. The vector concentration as a function of time (top), and two image frames of different (bottom left), and similar (bottom right) r -values for the common carotid artery (green), and the carotid bulb (red).

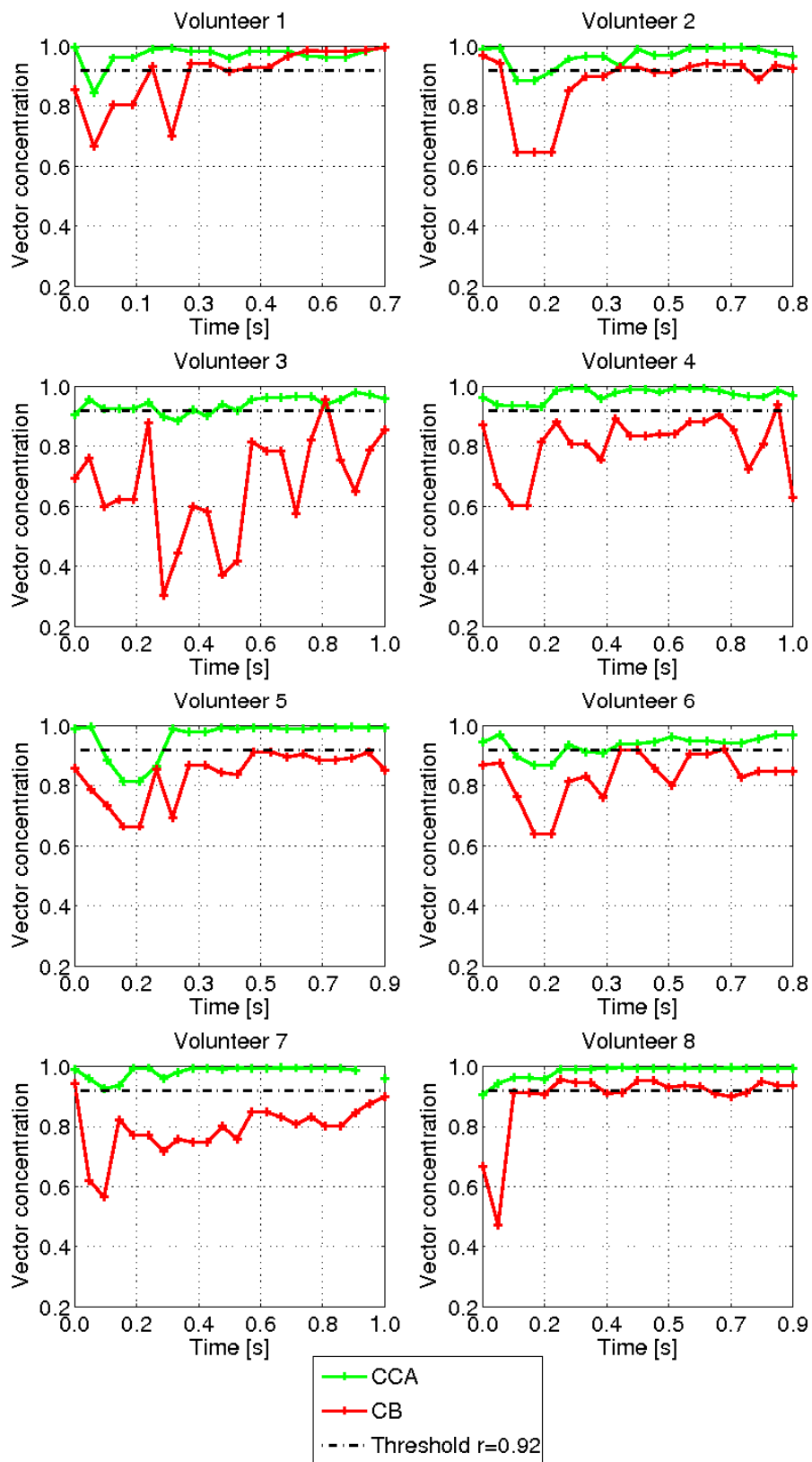


Figure 5: The vector concentration throughout one cardiac cycle for all volunteers. The values of CCA (green) and CB (red), and the threshold value are shown.

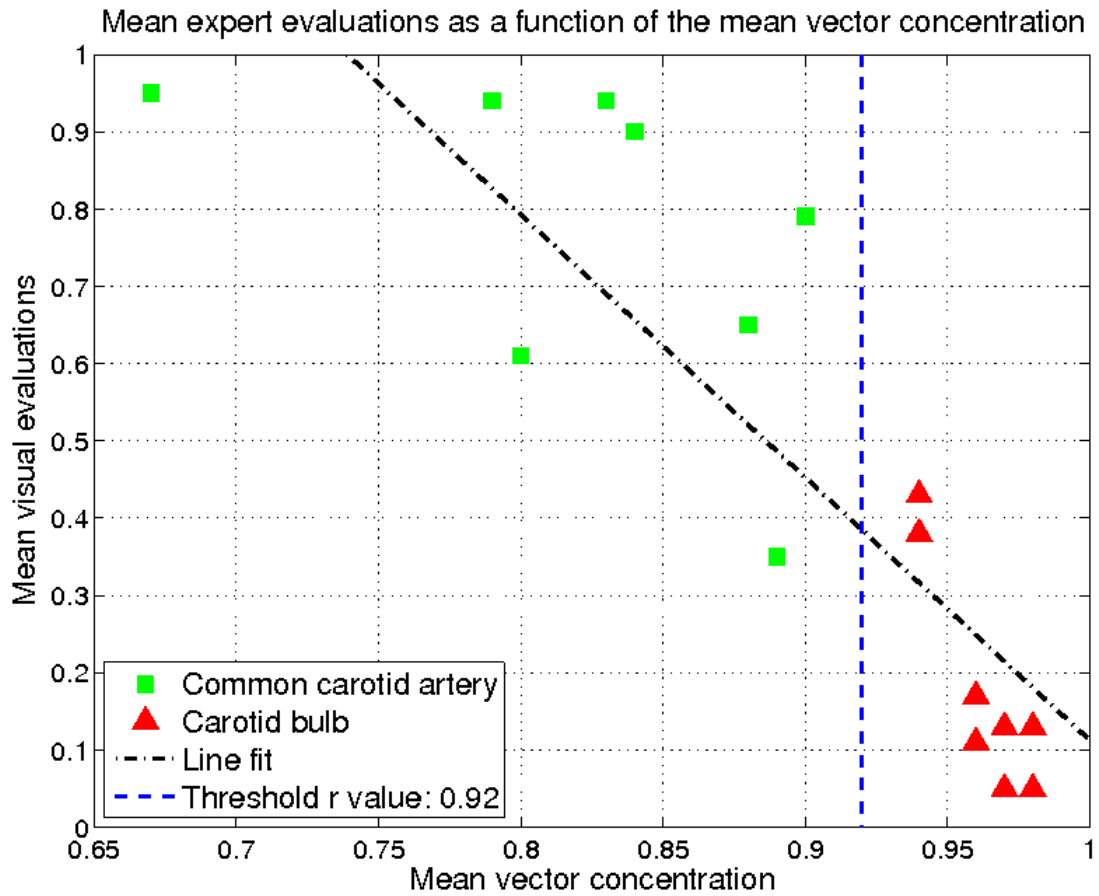


Figure 6: The mean expert evaluation as a function of the mean vector concentration for CCA and CB of all volunteers. A mean vector concentration of 0.92 separates CCA from CB.

References

- 1 Bergan J, Yao J. Cerebrovascular insufficiency. New York: Grune and Stratton, 1983.
- 2 Lin P, Dake M, Veith F, Krajcer Z. Advanced Therapy in Endovascular Interventions. B.C. Decker, 2008.
- 3 Samuel KC. Atherosclerosis and occlusion of the internal carotid artery. *J Pathol Bacteriol* 1956, 71 (2), 391–401.
- 4 Peterson RE, Livingston KE, Escobar A. Development and distribution of gross atherosclerotic lesions at cervical carotid bifurcation. *Neurology* 1960, 10, 955–9.
- 5 Hugh AE, Fox JA. The precise localisation of atheroma and its association with stasis at the origin of the internal carotid artery – a radiographic investigation. *Br J Radiol* 1970, 43 (510), 377–83.
- 6 Fuster V, Stein B, Ambrose JA, Badimon L, Badimon JJ, Chesebro JH. Atherosclerotic plaque rupture and thrombosis. evolving concepts. *Circulation* 1990, 82 (3 Suppl), II47–59.
- 7 Kassam MS, Cobbold RS, Johnston KW, Graham CM. Method for estimating the doppler mean velocity waveform. *Ultrasound Med Biol* 1982, 8 (5), 537–44.
- 8 Brown PM, Johnston KW, Kassam M, Cobbold RS. A critical study of ultrasound doppler spectral analysis for detecting carotid disease. *Ultrasound Med Biol* 1982, 8 (5), 515–23.
- 9 Phillips DJ, Greene FM, Langlois Y, Roederer GO, Strandness DE. Flow velocity patterns in the carotid bifurcations of young, presumed normal subjects. *Ultrasound Med Biol* 1983, 9 (1), 39–49.
- 10 Jensen JA. Estimation of blood velocities using ultrasound: A signal processing approach. Cambridge University Press, 1996
- 11 Evans DH, McDicken WN, Skidmore R, Woodcock JP. Doppler Ultrasound, Physics, Instrumentation, and Clinical Applications. John Wiley & Sons, New York, 1989.
- 12 Udesen J, Nielsen MB, Nielsen KR, Jensen JA, Examples of In Vivo Blood vector velocity Estimation. *Ultrasound Med Biol* 2007, 33 (4), 541-548.
- 13 Hansen KL, Udesen J, Oddershede N, Henze L, Thomsen C, Jensen JA, Nielsen MB. In vivo comparison of three ultrasound vector velocity techniques to MR phase contrast angiography. *Ultrasonics* 2009, 49 (8), 659–67.
- 14 Hansen PM, Pedersen MM, Hansen KL, Nielsen MB, Jensen JA. New technology - demonstration of a vector velocity technique. *Ultraschall in Med* 2011, 32 (2), 213–5.
- 15 Munk P. Estimation of the 2-D flow vector in ultrasonic imaging: A new approach. Master's thesis, Department of Information Technology, Technical University of Denmark, 1996.
- 16 Munk P. Estimation of blood velocity vectors using ultrasound. Ph.D. thesis, Department of Information Technology, Technical University of Denmark, Lyngby, Denmark, 2000.

- 17 Jensen JA, Priority date: April 2000. An estimator for vector velocity estimation, International patent.
- 18 Jensen JA, Munk, P. A new method for estimation of velocity vectors. IEEE Trans Ultrason Ferroelectr Freq Control 1998, 45 (3), 837–51.
- 19 Jensen JA. A New Estimator for Vector Velocity Estimation. IEEE Trans. Ultrason., Ferroelec., Freq. Contr. 2001, 48 (4), 886–894.
- 20 Udesen J, Jensen JA. Investigation of Transverse Oscillation Method. IEEE Trans. Ultrason., Ferroelec., Freq. Contr. 2006, 53, 959–971.
- 21 Baschelet E. Circular statistics in biology. London: Academic Press, 1981.
- 22 Arning C, Widder B, von Reutern G M, Stiegler H, Görtler M. Ultraschallkriterien zur Graduierung von Stenosen der A. carotis interna - Revision der DEGUM-Kriterien und Transfer in NASCET-Stenosierungsgrade. Ultraschall in Med 2010, 31(3), 251-257.

Appendix 3: Journal paper III

Rotational flow patterns in the arterial blood stream with vector flow ultrasound.

Mads Møller Pedersen^{1,2}, Michael Johannes Pihl², Jens Munk Hansen²,

Peter Møller Hansen^{1,2}, Per Haugaard³, Michael Bachmann Nielsen¹ and Jørgen Arendt Jensen²

¹Dept. of Radiology, Copenhagen University Hospital, Rigshospitalet, DK-2100 Copenhagen, Denmark

²Center for Fast Ultrasound Imaging, Dept. of Elec. Eng., Bldg. 349

Technical University of Denmark, DK-2800 Lyngby, Denmark

³R&D Applications & Technologies, BK Medical, DK-2730 Herlev, Denmark

Abstract

This study presents the first quantification and visualization of secondary flow patterns with Transverse Oscillation vector flow ultrasound. The first commercial implementation of Transverse Oscillation was used to obtain *in vivo*, 2D vector fields in real-time. The hypothesis of this study was that the rotational direction is constant within each artery. Three data sets of 10 seconds were obtained from three main arteries in healthy volunteers.

For each data set the rotational flow patterns were identified during diastole. Rotational flow patterns in the abdominal aorta during systole were also identified. Each data set contains a 2D vector field over time using the vector angles and velocity magnitudes the blood flow patterns were visualized using streamlines in Matlab (Mathworks, Natick, MA, USA). The rotational flow during diastole was quantified by the angular frequency for each cardiac cycle, and the mean rotational frequencies and standard deviations were calculated for the abdominal aorta $\{-1.3\pm 0.4; -1.0\pm 0.3; -0.9\pm 0.2\}$ Hz, the common iliac artery $\{-0.4\pm 0.1; -1.0\pm 0.2; -0.4\pm 0.1\}$ Hz, and the common carotid artery $\{0.8\pm 0.3; 1.4\pm 0.3; 0.4\pm 0.1\}$ Hz. A positive sign indicates an anti-clockwise rotation, and a negative sign indicates clockwise rotation. The sign of the rotational directions within each artery were constant during diastole. In the abdominal aorta the flow pattern was counter clockwise during systole and clockwise during diastole.

I. INTRODUCTION

The vector flow technique, Transverse Oscillation (TO), has been investigated thoroughly since the first presentations in 1996 [1], [2], [3], [4]. The method has been tested in simulation [5], by *in vivo* studies with the experimental scanner, RASMUS [6], and in comparison with magnetic resonance (MR) angiography [7]. In contrast to conventional Doppler techniques, TO directly provides the absolute velocities and flow angles of blood at any angle in a 2D vector field. The method is non-invasive, as it does not require contrast agents.

Measurement of the transverse velocity component has been investigated with several other techniques. Particle-image velocimetry (PIV) obtains the velocity of moving particles using an optical system, where the particles are illuminated with pulsed light. The movement of the speckles are tracked to form a vector field [8]. Replacing the light and photo equipment with

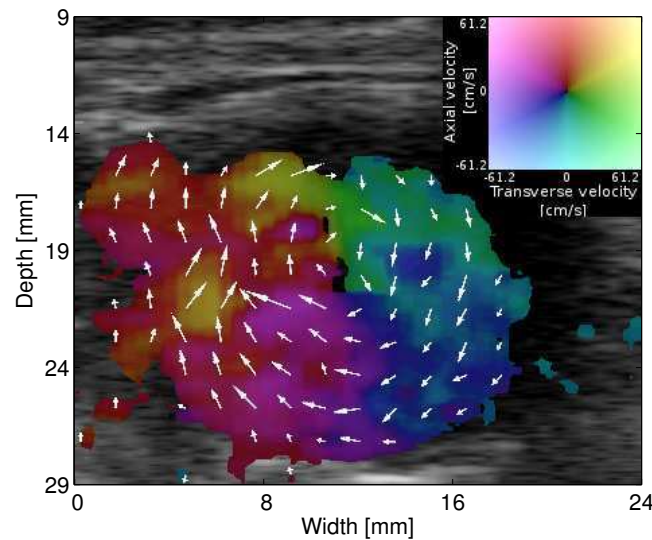


Fig. 1: Real-time, *in vivo* TO ultrasound image of the abdominal aorta in the transverse plane. The vector velocity color map is shown in the upper right corner.

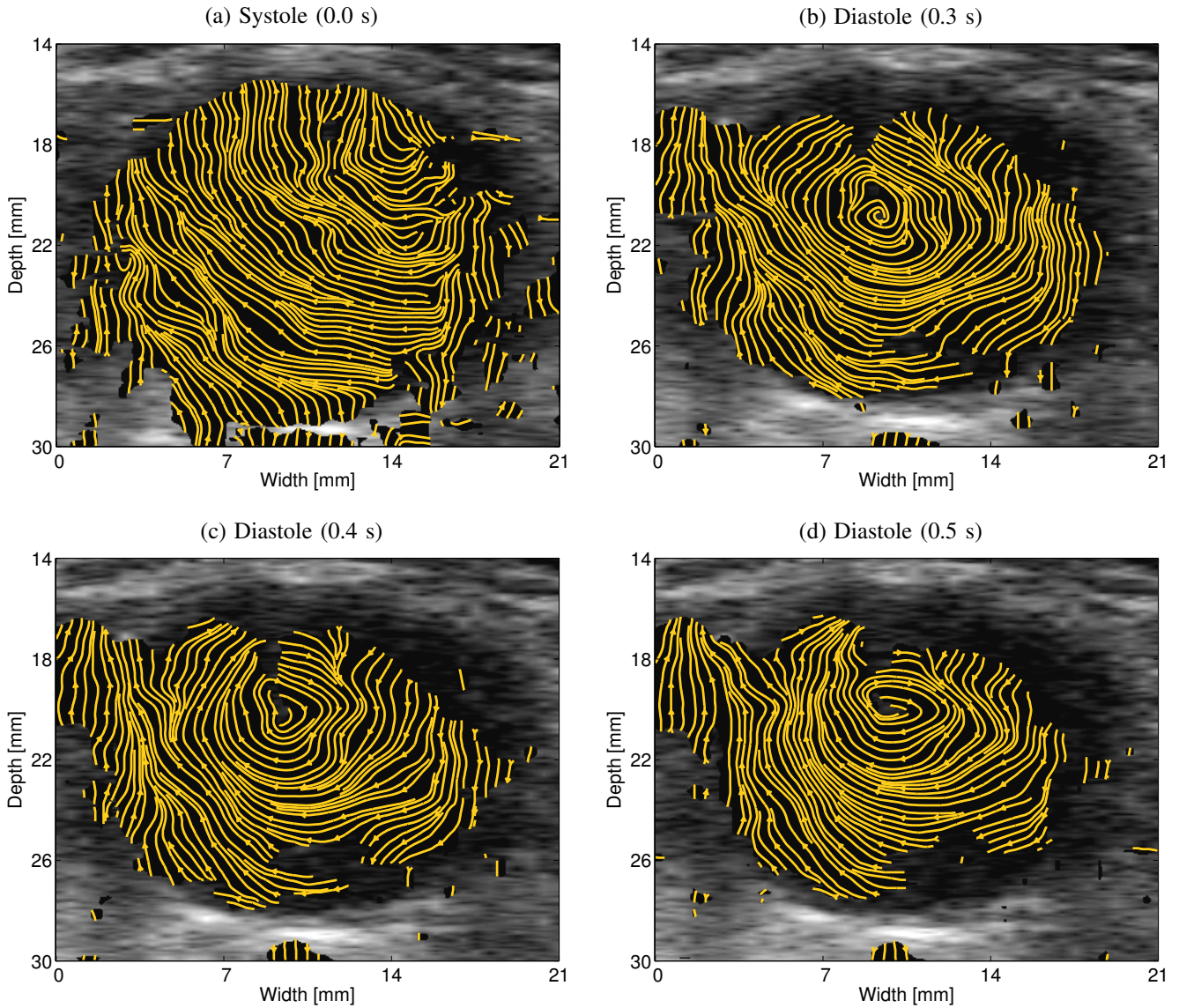


Fig. 2: TO ultrasound of the abdominal aorta in the transverse plane. The streamlines through one cardiac cycle illustrate a systolic flow pattern (a) with no secondary flow, whereas the pattern is fully developed during the diastole (b-c).

ultrasound, the technique echo PIV uses micro bubbles as contrast agent. In a phantom study the flow patterns in stenosis and aneurysm phantoms clearly illustrates the flow patterns [9]. The velocity estimation of echo PIV was recently correlated with phase contrast magnetic resonance (PCMRI) with good agreement in a phantom study [10]. An *in vivo* study of the carotid artery in live rats, showed a deviation of 15% from the Doppler-measured peak velocities [11]. The vortex flow of the human heart was quantified with PIV using micro bubbles as contrast agent [12].

Color Doppler has been used to illustrate the flow patterns in the aorta. Based on the color patterns of *in vivo* transesophageal ultrasound, it was concluded that blood rotates anticlockwise in the diastole as a result of backflow [13]. A comment on this finding suggested that such color patterns might simply be a result of a 20° misalignment of the transverse plane [14], as only the axial velocities were measured.

PCMRI techniques are able to visualize and quantify secondary flow patterns [15]. The MR vector information makes it possible to estimate physiological forces, such as wall shear stress [16], [17].

The experimental ultrasound method, Plane Wave, showed the secondary flow patterns during systole with ultrasound for the first time [28].

With the recent implementation of TO in a commercial scanner, detailed real-time blood velocity magnitudes and flow directions have been illustrated *in vivo* [18], and have been compared to spectral velocity estimation [19]. The presence of disturbed flow patterns in the carotid bifurcation have been confirmed visually and quantitatively [7], [6]. Thus, rotational flow patterns are visualized and can be obtained in real-time for further analysis. Previous studies have indicated that rotational flow

patterns may play a role in the pathogenesis of atherosclerosis [20], [21].

With this study the rotational flow patterns are visualized with *in vivo*, real-time TO ultrasound for the first time. Furthermore, a quantitative method is presented which calculates the rotational frequency.

II. METHODS

A. Data acquisition

Five healthy volunteers participated in this study. For each volunteer the transverse plane of three arteries were scanned with TO ultrasound: The abdominal aorta (AA), the common carotid artery (CCA), and the common iliac artery (CIA). A commercial TO ultrasound scanner (ProFocus Ultraview, BK Medical, Denmark) was used with a 5 MHz linear array (type: 8670, BK Medical, Denmark) and prototype scanner software. Ten seconds of data were obtained as AVI files with a mean frame rate of 21 ± 5 Hz with a range of [13 28] Hz. Three data sets for each artery, which presented a rotational flow pattern, were selected, resulting in nine data sets. A frame example of the real-time colour encoded vector data is shown in Fig. 1.

Extra measurements of the flow in the abdominal aorta was obtained with different settings of the PRF and wall-filter to obtain the flow patterns of different velocities. These measurements were processed separately as described in the result section.

B. Real-time vector data

The real-time vector information is displayed as colours and by post processing the axial, v_z , and transverse, v_x , vector velocity magnitudes were obtained through time in 2D vector fields. Further details on data processing of the colour encoded vector information is provided in [22].

C. Streamline imaging

Streamlines were used to visualize the blood flow patterns for every frame. The line density was set low to make the visual impression as clear as possible. In Fig. 2 the development of a secondary flow pattern through the cardiac cycle is shown for the abdominal aorta.

D. Angular speed and frequency of a 2D vector field

A grid defining subareas in the 2D vector field is set from the center of the rotation and the rotational frequency of each subarea is calculated [23] by

$$(\nabla \times F)_z = \frac{\partial}{\partial x} F_y - \frac{\partial}{\partial y} F_x. \quad (1)$$

For each data set, the frequencies during each diastolic phase were found and a mean rotational frequencies and a standard deviation was calculated for each dataset. The frequencies were calculated using Matlab.

III. RESULTS

Nine data sets were post processed to calculate the mean angular frequencies and standard deviations of each data set. The results are shown in Fig. 4.

All frequencies of AA and CIA were negative, indicating a unidirectional, clockwise rotation. All CCA frequencies were positive, indicating a unidirectional, anticlockwise rotation.

The extra measurements of the abdominal aorta of one of the subjects were post processed separately. The peak systole was identified visually as illustrated in Fig. 2(a) and the time from peak systole to the appearance of a rotational flow pattern was calculated for all cardiac cycles. All measurements were normalised and are shown in Fig. 5. An example of the counter clockwise rotational flow during systole in the abdominal aorta is shown in Fig. 6.

The angular frequencies and streamlines imposed on the B-mode image are shown for one image frame of the abdominal aorta in Fig. 3. The center of the rotation represents the maximum angular frequency of -1.32 Hz, whereas the peripheral magnitudes are lower. If the image represented a water tank, a paddle placed in a peripheral subarea would rotate at a lower frequency compared to a paddle placed in the center. The streamlines in combination with the angular frequencies and the B-mode image are suggested for clinical imaging of rotational flow with TO.

IV. DISCUSSION

A. Scanner setting

The TO method depends on the pulse repetition frequency and wall filter settings. The scanner was adjusted to obtain the low velocities present at the secondary flow patterns in the cross-sectional plane and further adjustments for extra data sets of the abdominal aorta made it possible to measure a two-directional flow pattern during the cardiac cycle. The non-rotational flow shown during systole in Fig. 2(a) can illustrate that the scan plane was not perfectly cross-sectional. It does not, however, exclude that the true flow is laminar during peak systole.

With the present setup, the mean frame rate was limited to 21 Hz. An increase in the temporal resolution would provide further details on the development of the rotational flow patterns and the peak frequencies during the cardiac cycle.

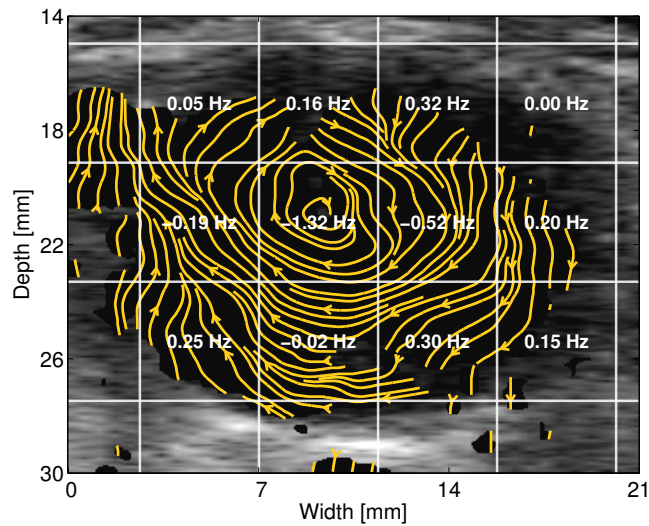


Fig. 3: In a transverse section of the abdominal aorta, the angular frequency of each subarea are imposed on the streamlines and the B-mode image.

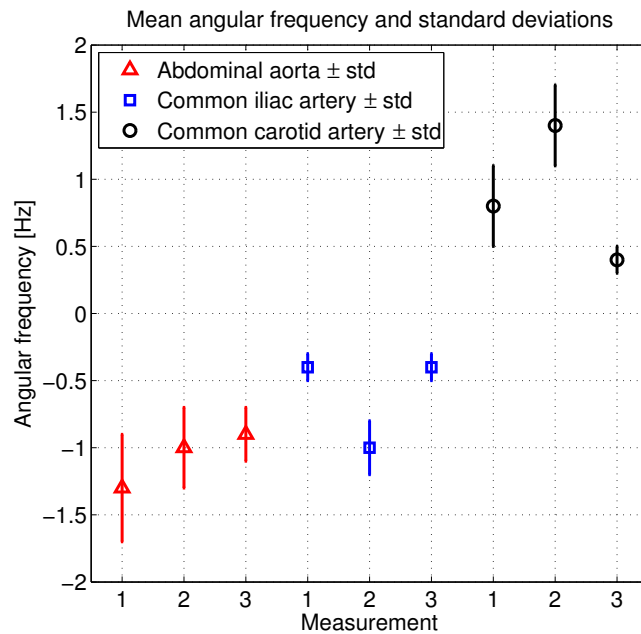


Fig. 4: The angular frequencies, mean values, and standard deviations for all measurements. The direction is given by the sign, which is identical for all measurements of each artery.

B. Clinical use

The measurements with the present implementation of the vector flow technique is not yet ready for quick-and-easy clinical use. The linear transducer available limits the maximum scan depth to about 4 cm and thus, scanning of deep structures, such as the abdominal aorta, the renal artery, and the portal vein, are only possible on slim subjects. Furthermore, the rotational flow pattern is only visible in the exact cross-sectional plane and it took up to 15 minutes to find the plane and obtain the flow pattern. Future implementations on 2D array transducers and wider, convex arrays, is believed to make it easier to obtain the secondary cross-sectional flow pattern.

C. Clinical importance

To our knowledge, this is the first study to present quantification of the secondary flow patterns *in vivo* with a commercial ultrasound scanner. The role of secondary flow patterns have been investigated thoroughly with MR and CFD [24], [25], [26],

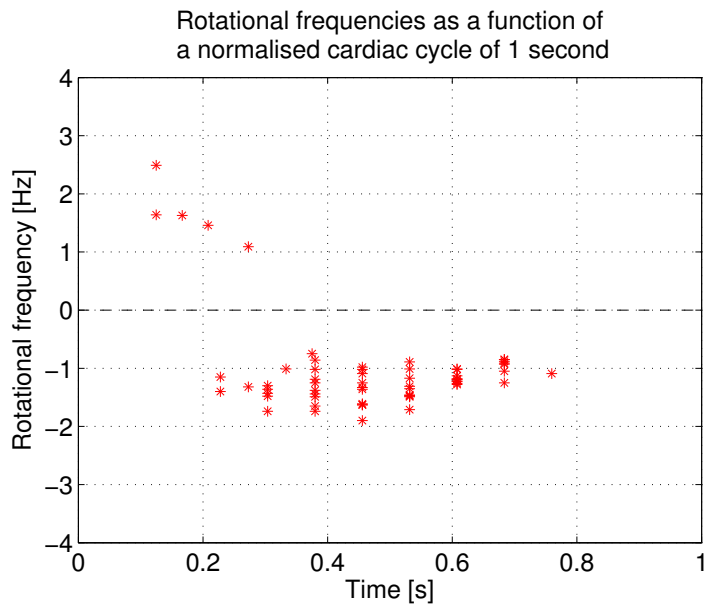


Fig. 5: All rotational frequencies of the abdominal aorta as a function of time. The direction of direction is clearly changing from counter clockwise to clockwise during the cardiac cycle.

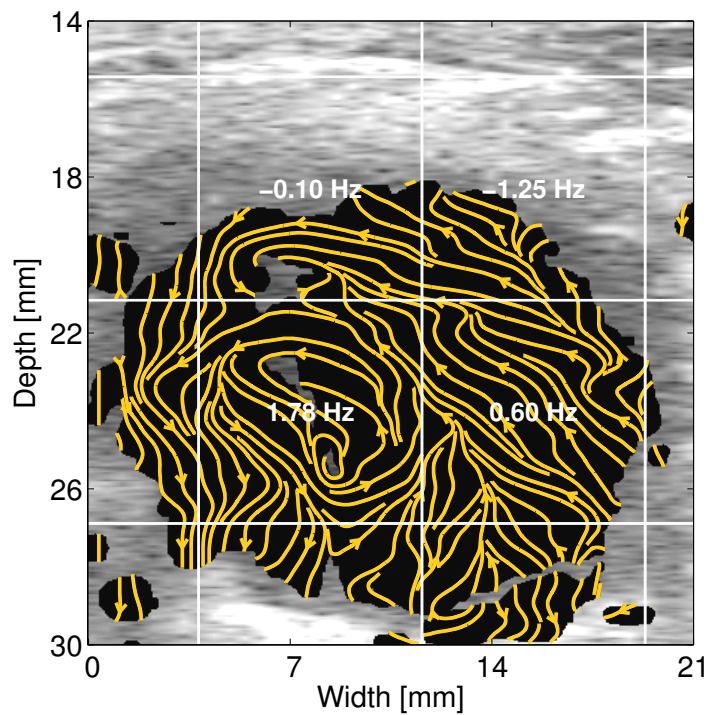


Fig. 6: Example of counter clockwise rotation in the abdominal aorta during systole.

[27], and shown with Plane Wave ultrasound [28].

Previous studies have indicated that rotational flow patterns may play a role in the pathogenesis of atherosclerosis. Both MR [15] and color flow studies [13] have illustrated a rotational flow during systole and several studies have suggested that secondary flow plays an important role in the development of atherosclerosis [29], [20], [21].

With the vector flow ultrasound scanner a new tool is available that is ready for in-hospital use. Thus, rotational flow patterns during systole should be addressed in future TO studies.

V. CONCLUSION

With the commercial real-time vector flow ultrasound scanner, *in vivo* data can be used to calculate the angular frequencies. Secondary flow patterns have been measured in diastole in the AA, CIA, and CCA. The diastolic secondary flow in AA and CIA rotates clockwise, whereas CCA rotates anticlockwise. Additional investigation of the systolic flow pattern of AA shows a two-directional flow pattern during the cardiac cycle. A new plot presenting both the flow streamlines, the angular frequencies, and the B-mode image was suggested for clinical use. In conclusion real-time vector flow can visualize and quantify secondary flow patterns of three main arteries and the rotational directions were constant within each artery.

ACKNOWLEDGEMENTS

This work was supported by grant 26-04-0024 from the Danish Science Foundation and by BK Medical Aps, Denmark.

REFERENCES

- [1] P. Munk. Estimation of the 2-D flow vector in ultrasonic imaging: a new approach. Master's thesis, Department of Information Technology, Technical University of Denmark, 1996.
- [2] J. A. Jensen and P. Munk. A New Method for Estimation of Velocity Vectors. *IEEE Trans. Ultrason., Ferroelec., Freq. Contr.*, 45:837–851, 1998.
- [3] P. Munk. *Estimation of blood velocity vectors using ultrasound*. PhD thesis, Department of Information Technology, Technical University of Denmark, Lyngby, Denmark, 2000.
- [4] J. A. Jensen. A New Estimator for Vector Velocity Estimation. *IEEE Trans. Ultrason., Ferroelec., Freq. Contr.*, 48(4):886–894, 2001.
- [5] J. Udesen and J. A. Jensen. Investigation of Transverse Oscillation Method. *IEEE Trans. Ultrason., Ferroelec., Freq. Contr.*, 53:959–971, 2006.
- [6] J. Udesen, M. B. Nielsen, K. R. Nielsen, and J. A. Jensen. Examples of in-vivo blood vector velocity estimation. *Ultrasound Med. Biol.*, 33:541–548, 2007.
- [7] K. L. Hansen, J. Udesen, N. Oddershede, L. Henze, C. Thomsen, J. A. Jensen, and M. B. Nielsen. In vivo comparison of three ultrasound vector velocity techniques to mr phase contrast angiography. *Ultrasonics*, 49:659–667, 2009.
- [8] R. J. Adrian. Particle-imaging techniques for experimental fluid mechanics. *Annu. Rev. Fluid Mech.*, 23:261–304, 1991.
- [9] L. Liu, H. Zheng, L. Williams, F. Zhang, R. Wang, J. Hertzberg, and R. Shandas. Development of a custom-designed echo particle image velocimetry system for multi-component hemodynamic measurements: system characterization and initial experimental results. *Phys. Med. Biol.*, 5(53):1397–1412, 2008.
- [10] F. Zhang, C. Lanning, L. Mazzaro, A. J. Barker, P. E. Gates, W. D. Strain, J. Fulford, O. E. Gosling, A. C. Shore, N. G. Bellenger, B. Rech, J. Chen, J. Chen, and R. Shandas. In vitro and preliminary in vivo validation of echo particle velocimetry in carotid vascular imaging. *Ultrasound Med. Biol.*, 37(3):450–464, 2011.
- [11] L. Niu, M. Qian, K. Wan, W. Yu, Q. Jin, T. Ling, S. Gao, and H. Zheng. Ultrasonic particle image velocimetry for improved flow gradient imaging: algorithms, methodology and validation. *Phys. Med. Biol.*, 7(55):2103–2120, 2010.
- [12] G. R. Hong, G. Pedrizzetti, G. Tonti, P. Li, Z. Wei, J. K. Kim, A. Baweja, S. Liu, N. Chung, H. Houle, J. Narula, and M. A. Vannan. Characterization and quantification of vortex flow in the human left ventricle by contrast echocardiography using vector particle image velocimetry. *JACC Cardiovasc Imaging*, 1(6):705–717, 2008.
- [13] L. J. Frazin, G. Lanza, M. Vonesh, F. Khasho, C. Spitzzeri, S. McGee, K. B. Chandran D. Mehlman, J. Talano, and D. McPherson. Functional chiral asymmetry in descending thoracic aorta. *Circulation*, 82(6):1985–1994, 1990.
- [14] J. D. Thomas. Flow in the descending aorta. a turn of the screw or a sideways glance? *Circulation*, 82(6):2263–2265, 1990.
- [15] P. J. Kilner, G. Z. Yang, R. H. Mohiaddin, D. N. Firmin, and D. B. Longmore. Helical and retrograde secondary flow patterns in the aortic arch studied by three-directional magnetic resonance velocity mapping. *Circulation*, 88(5 Pt 1):2235–47, November 1993.
- [16] Biegling ET, Frydrychowicz A, Wentland A, Landgraf BR, Johnson KM, Wieben O, and Francois CJ. In vivo three-dimensional mr wall shear stress estimation in ascending aortic dilatation. *J Magn Reson Imaging*, 33(3):589–97, March 2011.
- [17] M. Markl, W. Wallis, and A. Harloff. Reproducibility of flow and wall shear stress analysis using flow-sensitive four-dimensional mri. *J Magn Reson Imaging*, 33(4):988–94, April 2011.
- [18] P. M. Hansen, M. M. Pedersen, K. L. Hansen, M. B. Nielsen, and J. A. Jensen. New technology - demonstration of a vector velocity technique. *Ultraschall in der Medizin/European Journal of Ultrasound*, 32:213–5, 2011.
- [19] Pedersen MM, Pihl MJ, Haugaard P, Hansen JM, Hansen KL, Nielsen MB, and Jensen JA. Comparison of real-time in-vivo spectral and vector velocity estimation. *Ultrasound Med. Biol.*, page Accepted, 2011.
- [20] Hugh AE and Fox JA. The precise localisation of atheroma and its association with stasis at the origin of the internal carotid artery—a radiographic investigation. *Br J Radiol*, 43(510):377–83, 1970.
- [21] V. Fuster, B. Stein, J. A. Ambrose, L. Badimon, J. J. Badimon, and J. H. Chesebro. Atherosclerotic plaque rupture and thrombosis. evolving concepts. *Circulation*, 82(3 Suppl):II47–59, 1990.
- [22] Pedersen MM, Pihl MJ, Haugaard P, Nielsen MB, and Jensen JA. Preliminary quantification of complex blood flow using real-time in vivo vector flow ultrasound. In *IEEE Proc.*, pages 1088–1091, 2010.
- [23] B. Lautrup. *Physics of continuous matter: Exotic and everyday phenomena in the macroscopic world*. Taylor & Francis, 2005.
- [24] Lee KL, Doorly DJ, and Firmin DN. Numerical simulations of phase contrast velocity mapping of complex flows in an anatomically realistic bypass graft geometry. *Med Phys*, 33(7):2621–2631, 2006.
- [25] Steinman DA, Thomas JB, Ladak HM, Milner JS, Rutt BK, and Spence JD. Reconstruction of carotid bifurcation hemodynamics and wall thickness using computational fluid dynamics and mri. *Magnet Reson Med*, 49(1):149–159, 2002.
- [26] Zhao SZ, Xu XY, Hughes AD, Thom SA, Stanton AV, Ariff B, and Long Q. Blood flow and vessel mechanics in a physiologically realistic model of a human carotid arterial bifurcation. *J Biomech*, 33(8):975984, 2000.
- [27] Zhao SZ, Papatheanopoulos P, Long Q, Marshall I, and Xu XY. Comparative study of magnetic resonance imaging and image-based computational fluid dynamics for quantification of pulsatile flow in a carotid bifurcation phantom. *Ann Biomed Eng*, 31(8):962–971, 2003.
- [28] K L Hansen, J Udesen, F Gran, J A Jensen, and M Bachmann Nielsen. In-vivo examples of flow patterns with the fast vector velocity ultrasound method. *Ultraschall Med*, 30(5):471–7, October 2009.
- [29] Shipkowitz T, Rodgers VGJ, Frazin LJ, and Chandran KB. Numerical study on the effect of secondary flow in the human aorta on local shear stresses in abdominal aortic branches. *J Biomech*, 33(6):717–728, 2000.